12-2003

Modeling of Corrugated Graphite Foam Heat Exchangers

Timothy Henry Norton Jr.
University of Tennessee - Knoxville

To the Graduate Council:

I am submitting herewith a thesis written by Timothy Henry Norton Jr. entitled "Modeling of Corrugated Graphite Foam Heat Exchangers." I have examined the final electronic copy of this thesis for form and content and recommend that it be accepted in partial fulfillment of the requirements for the degree of Master of Science, with a major in Mechanical Engineering.

Rao V. Arimilli, Major Professor

We have read this thesis and recommend its acceptance:

Masood Parang, Leon M. Tolbert

Accepted for the Council:
Carolyn R. Hodges

Vice Provost and Dean of the Graduate School

(Original signatures are on file with official student records.)

To the Graduate Council:

I am submitting herewith a thesis written by Timothy Henry Norton, Jr., entitled, "Modeling of Corrugated Graphite Foam Heat Exchangers." I have examined the final electronic copy of this thesis for form and content and recommend that it be accepted in partial fulfillment of the requirements for the degree of Master of Science, with a major in Mechanical Engineering.

Rao V. Arimilli
Major Professor

We have read this thesis
and recommend its acceptance:

Masood Parang

Leon M. Tolbert

Accepted for the Council:

Anne Mayhew
Vice Provost and
Dean of Graduate Studies

(Original signatures are on file with official student records.)

Modeling of Corrugated Graphite Foam Heat Exchangers

A Thesis

Presented for the

Master of Science

Degree

The University of Tennessee, Knoxville

Timothy H. Norton, Jr.

December 2003

Dedication

This thesis is dedicated to my parents,

Tim and Debra Norton

for the wonderful education they have provided me,

and to my best friend,

Cathy

for her endless love and support.

Acknowledgements

I would like to acknowledge all those who helped me complete my Master of Science degree in Mechanical Engineering at the University of Tennessee, Knoxville.

I would especially like to thank Dr. Rao V. Arimilli, who has been a devoted teacher and advisor during both my undergraduate and graduate studies. I also want to thank Dr. Jeffrey Hodgson for the opportunity he has given me to enhance my education at the University of Tennessee through his involvement with the FutureTruck and GATE programs. In addition, I want to thank Dr. Masood Parang and Dr. Leon Tolbert for their participation on my advisory committee.

Finally, I want to express my dearest appreciation to the members of the Oak Ridge National Laboratory, especially Dr. James Klett, Dr. Nidia Gallego, and Dr. Dave Stinton for their exceptional support.

This research was jointly funded by DOE Office of FreedomCAR and Vehicle Technologies and DOE Office of Distributed Energy and Electricity Reliability through Oak Ridge National Laboratory, Oak Ridge, Tennessee.

Abstract

A new manufacturing process was recently developed by the Oak Ridge National Laboratory for the production of graphite foam. The high thermal conductivity and heat transfer area of the foam make it desirable for thermal management applications such as compact heat exchangers. The heat transfer capabilities of the foam are especially useful in internal forced convection applications. However, due to the very low permeability of graphite foam, pressure-drop is very high compared to other porous media, and pressure-drop reduction schemes are necessary to ensure its practical application. Pressure-drop reduction can be achieved through the strategic machining of graphite foam into complex geometries. In this study, a corrugated configuration is analyzed. Computational methods are employed to determine optimal geometric parameters of corrugated graphite foam heat exchangers that result in a significant reduction in pressure-drop without severely affecting heat transfer performance. The results indicate that pressure-drop in optimal corrugated configurations is reduced by nearly two orders of magnitude when compared to a full graphite foam block of the same overall size. These optimal cases are characterized by relatively uniform flow in the transverse direction across the foam, and this uniformity is reduced by slot widths that are too long and narrow and by flowrates that are too high. These optimal configurations decrease the heat transfer coefficients by nearly fifty percent when compared to a full block, but the reduction of pressure-drop is much more significant. Therefore, corrugating the foam is shown to be an effective method to significantly reduce the pressure-drop without severely affecting the heat transfer performance of graphite foam heat exchangers.

Table of Contents

Chapter		Page
1.	Introduction…….	1
	1.1 Background……..	1
	1.2 Scope……	2
2.	Literature Review……	3
	2.1 Graphite Foam…….	3
	2.2 Forced Convection in Channels Filled with Porous Media…….	5
	2.2.1 Porous Media Momentum Equation…….	6
	2.2.2 Porous Media Energy Equation(s)……	8
	2.2.3 Related Topics……..	16
	2.3 FEA and CFD Software……...	17
3.	Problem Statement……..	19
	3.1 Introduction……..	19
	3.1.1 Heat Transfer Enhancement with Graphite Foam…….……..	20
	3.1.2 Pressure-drop Reduction Technique: Corrugated Foam…….	21
	3.2 Modeling Considerations…….	24
	3.2.1 Geometric Simplifications……..	24
	3.2.2 Thermophysical Assumptions…….…….	28
4.	Equations…….	31
	4.1 Introduction…….….	31
	4.2 Background of Porous Media Momentum Equation……..	31

4.2.1 Viscous Drag (Darcy) Term……. 32

4.2.2 Form Drag (Forchheimer) Term…….. 33

4.2.3 Viscous Shear (Brinkman) Term…….. 35

4.2.4 Advective (Convective) Inertial Term…….. 36

4.2.5 General and Applicable Porous Media Momentum Equations 37

4.2.6 Porous Media Reynolds Number…….. 38

4.3 Background of Porous Media Energy Equation…….. 41

4.3.1 Local Thermal Equilibrium…….. 41

4.3.2 Thermal Dispersion…….. 44

4.4 Height Estimation of the Corrugated Foam……. 44

4.5 Dimensionless Performance Parameters ……... 47

4.5.1 Porous Media Friction Factor…….……. 47

4.5.2 Heat Transfer Coefficient…… 47

4.5.3 Compact Heat Exchangers…….……. 49

5. Software Implementation…… 50

5.1 Introduction…….. 50

5.1.1 Governing Equations…… 50

5.1.2 Boundary Conditions…… 50

5.2 FEMLAB® Model…… 51

5.2.1 Governing Equations…… 51

5.2.2 Boundary Conditions…… 53

5.2.3 Grid Considerations…..…… 54

5.3 STAR-CD® Model……. 55

5.3.1 Governing Equations…… 55

5.3.2 Boundary Conditions…… 58

5.3.3 Grid Considerations……..… 59

6. Results……. 60

6.1 Two-dimensional Hydrodynamic Results ……..…. 60

6.1.1 Effect of L/S ……... 67

6.1.2 Effect of C/S…… 69

6.1.3 Reynolds Number Effect ..…….. 72

6.2 Three-dimensional Results …….. 75

6.2.1 3D Pressure Distributions……. 76

6.2.2 Effectiveness of Corrugations……... 76

6.2.3 3D Temperature Distributions……... 78

6.2.4 Heat Transfer Results…… 80

7. Conclusions and Recommendations…….. 84

7.1 Conclusions……. 84

7.2 Recommendations…… 85

References……. 86

Appendices……... 93

Appendix A…… 94

Appendix B……. 98

Vita…… 111

List of Figures

Figure 3.1: Internal forced convection in a conduit exposed to a constant heat flux.…… 19

Figure 3.2: Sketch of internal forced convection in a porous medium-filled channel exposed to a constant heat flux.……... 21

Figure 3.3: Sketch of internal forced convection through a corrugated foam geometry exposed to a constant heat flux.…… 23

Figure 3.4: The Corrugated Unit Cell is shown as one repeatable section of the heat exchanger.…….…… 26

Figure 3.5: A top view (on the x-z plane) of Unit Cell and Half-Unit Cell used for modeling.……...…….. 28

Figure 5.1: The boundary conditions of the FEMLAB® model……. 54

Figure 5.2: Example of mesh in the FEMLAB® model……. 55

Figure 5.3: The boundary conditions of the STAR-CD® model…… 58

Figure 6.1: Porous media friction factor variation with L/S for several values of C/S, for (a) Re_K^* =0.1 and (b) Re_K^* =1 …….. 61

Figure 6.2: The velocity vectors and pressure contours (a) and the slot static pressure (b) for L=0.05 m, L/S=5, C/S=0.1, Re_K^* =0.1…… 65

Figure 6.3: Static pressure along inlet and outlet slots for L=0.05m, Re_K^* =0.1, C/S=0.1……. 68

Figure 6.4: Effect of L/S on velocity vectors, pressure contours, and ΔP_T for L=0.05m, Re_K^* =0.1, C/S=0.1…….. 70

Figure 6.5: Effect of C/S on static pressure along inlet and outlet slots for L=0.05m, Re_K^* =0.1, L/S=5…….. 71

Figure 6.6: Effect of C/S on velocity vectors, pressure contours, and ΔP_T for L=0.05m, Re_K^* =0.1, L/S=5……..……. 73

Figure 6.7: Effect of Re_K^* on velocity vectors, pressure contours, and ΔP_T for L=0.05m, L/S=5, C/S=0.1…… 74

Figure 6.8: Three-dimensional static pressure for L=0.05m, C/S=0.100, L/S=5.00, and Re_K^* =0.10 (a) and Re_K^* =0.50 (b)……. 77

Figure 6.9: Comparison of friction factors for optimal corrugated geometries to an uncorrugated (full) block of graphite foam …… 78

Figure 6.10: Three-dimensional temperature contours for L=0.05m, C/S=0.100, L/S=5.00, Re_K^* =0.10 (a) and Re_K^* =0.50 (b)…….……... 79

Figure 6.11: Nusselt number as a function of Reynolds number for optimal cases 82

Figure 6.12: Colburn-j and friction factor as a function of Reynolds number for optimal cases …….. 82

Figure 6.13: Colburn-j vs. friction factor for optimal cases…….. 83

Nomenclature

A_{cs}	Cross-sectional area of flow passage
a_{sf}	Specific surface area
C	Cut width or slot width
c	Dimensionless constant from Ward (1964)
C_F	Form Coefficient $= c_F / \sqrt{K}$, from Lage (1998)
c_F	Form (Forchheimer) coefficient
C_{p_f}	Specific heat of fluid
$(c_p)_f$	Specific heat of fluid
Da	Darcy number
D_h	Hydraulic diameter $= 2SH/(S+2H)$
d_p	Pore diameter
e	Porous flow length
F	Body force
f	Friction factor $= \Delta P_T D_h / L\rho U_o^2$
$F_{h_t,j}$	Diffusional thermal energy flux in direction x_j
f_K	Friction factor for porous media $= \Delta P_T \sqrt{K} / L\rho U_o^2$
H	Height of heat exchanger
$\bar{h}$	Average heat transfer coefficient
h_{sf}	Interstitial convection coefficient per unit volume

h_t	Thermal enthalpy
j	Index of cell number
j_H	Colburn-j factor $= \bar{h}\,\mathrm{Pr}_f^{2/3} \big/ \left((\rho c_p)_f U_o\right)$
K	Permeability
k	Specific permeability
k_m	Effective thermal conductivity of the matrix
k_f	Thermal conductivity of fluid
k_H	Hydraulic conductivity
K_i	Permeability
k_1	Darcian permeability
k_2	Non-Darcian permeability
L	Length
l	length
$\dot{m}$	Mass flow rate
$\overline{Nu}_{D_h}$	Nusselt number $= \bar{h} D_h \big/ k_f$
P	Pressure
p	Pressure
p_p	Piezometric pressure = $p_s - \rho_0 g_m x_m$ where p_s is static pressure, ρ_0 is reference density, the g_m are gravitational field components and the x_m are coordinates from a datum, where ρ_0 is defined.

P_w	Wetted perimeter of flow passage
Pe_x	Peclet number
Pr_f	Fluid Prandtl number
q''	Heat flux
Re	Reynolds number
Re_{D_h}	Reynolds number based on hydraulic diameter $= \rho U_o D_h / \mu$
Re_K	Porous Media Reynolds number $= \rho U_o \sqrt{K} / \mu$
Re_K^*	Modified Porous Media Reynolds number $= \rho U_o \sqrt{K} c_F / \mu$
S	Spacing of unit cells
s_{ij}	Rate of strain tensor
t	Thickness of foam
t	Time
$T_{b,in}$	Inlet bulk temperature
$T_{b,out}$	Outlet bulk temperature
T_s	Temperature of heated surface
T_W	Temperature of the heated wall
$\overline{T}_W$	Average heated wall temperature
$\langle T \rangle$	Local-volume-averaged temperature
$\langle T \rangle^g (x)$	Local-volume-averaged temperature of gas

$\langle T \rangle^l(x)$	Local-volume-averaged temperature of liquid
$\langle T \rangle^s(x)$	Local-volume-averaged temperature of solid
T_∞	Temperature of matrix far from surface
u	Velocity vector
u_i	Fluid velocity component in direction x_i or ζ_i
$\tilde{u}_j$	$u_j - u_{cj}$, relative velocity between fluid and local (moving) coordinate frame that moves with velocity u_{cj}
u_p	Pore velocity
U_0	Frontal velocity
u_∞	Frontal velocity
V	system volume
v	Velocity vector
v	macroscopic velocity
W	Width of heat exchanger
x_i	Cartesian coordinate (i=1,2,3)
α	Coefficient of linear term in pressure-drop equation
α_i	Coefficient of quadratic term in STAR-CD® distributed resistance equation
α_m	Thermal diffusivity of the matrix
β	Coefficient of quadratic term in pressure-drop equation

β_i	Coefficient of linear term in STAR-CD® distributed resistance equation
ΔP_T	Total pressure-drop
ΔT_d	Temperature difference of the particle
ΔT_δ	Temperature difference of the representative elementary volume
ΔT_l	Temperature difference of the system
∂_{ij}	Kronecker delta function
δ_T	Thermal boundary layer thickness
ε	Porosity
ϕ	Porosity
γ	Porous media shape parameter
η	Dynamic (molecular) viscosity
μ	Molecular viscosity of fluid
μ_e	Effective viscosity
μ'	Effective viscosity
$\mathbf{v}$	Kinematic viscosity
ρ	Density of fluid
ρ_f	Density of fluid
$(\rho U \Delta A)_j$	Mass flowrate for each cell
τ_{ij}	Stress tensor components
$\zeta_i (i = 1,2,3)$	The (mutually orthogonal) orthotropic directions

Chapter 1

Introduction

1.1 Background

As the power density of many electronic applications continues to rise, the optimization of thermal management devices has received an increasing amount of attention from researchers. Devices with high power requirements and fixed total volume require sufficient heat transfer enhancement to dissipate excess power within limited space. Therefore, compact heat exchangers, which contain relatively high surface area-to-volume ratios, have been used to alleviate this problem.

The use of thermally conductive porous media for heat transfer enhancement in compact heat exchangers has recently been the focus of several studies. These materials possess excellent heat transfer capabilities due to their high thermal conductivities and heat transfer area-to-volume ratios. In addition, these materials enhance fluid mixing due to the tortuous paths in their interconnected porous structures.

Conductive porous media include sintered metals, metallic packed beds, metallic foams, and recently-developed graphite foams. Recently, a process for making highly conductive graphite foam has been developed at the Oak Ridge National Laboratory (ORNL) that has provided an opportunity for the design of heat transfer enhancement devices composed of this new material.

Although graphite foam is highly conductive, it consists of relatively small pores that make it less permeable to fluids than typical foams used in heat exchangers. Since

graphite foam imposes a substantial flow resistance, the power required to transport the coolant is relatively high, resulting in a high operational cost. Therefore, certain techniques are necessary to reduce the flow resistance of graphite foam without substantially reducing its heat transfer performance. One such technique will be explored in this study.

In order to design heat exchangers, substantial work is necessary in the areas of modeling and simulation, which enable design engineers to make successful performance predictions. Modeling and simulation are important steps in the design cycle because they reduce the costs related to assembly and testing of prototypes. A greater understanding of the heat transfer and flow friction characteristics of graphite foam is necessary to determine its potential for future applications.

1.2 Scope

The current study considers a technique that reduces flow friction without severely reducing the heat transfer in laminar forced convection in a channel fully filled with highly conductive graphite foam subjected to a constant heat flux.

Chapter 2

Literature Review

This review contains three primary sections. In the first section, graphite foam will be introduced. In the next section, the specific problem of forced convection in a channel filled with a porous medium will be reviewed. Finally, the implementation of the software packages used in this study will be discussed.

2.1 Graphite Foam

A novel manufacturing process for making graphite foam has been invented by researchers at the Oak Ridge National Laboratory and has been patented as number 6,033,506 by the United States Patent and Trademark Office (Klett, 2000).

Klett *et al.* (2000) summarized the manufacturing techniques used in producing graphite foam and explained the foam structure characteristics that enable this material to exhibit excellent thermal properties. Several optical methods were employed to describe the size and shape of the pores, and several comparisons were made with reticulated glassy carbon foams. A flash diffusivity method was used to measure the thermal diffusivity of the foam, and the bulk thermal conductivity was subsequently calculated. The results indicated that the thermal conductivity of the foams varied from 40 to 150 W/m·K over a range of foam densities of 0.2 to 0.6 g/cm^3.

Meanwhile, Tee (2000) developed models for determining the effective thermal conductivity and pressure-drop per unit length of graphite foam based on its micro-

structural characteristics. In the model for effective thermal conductivity, the results indicated that a tapered, anisotropic strut model provided the most accurate solution for this type of foam. In addition, a spherical void model was validated for predicting the pressure-drop performance of the foam for low velocity fluid flow.

Osgood (2001) used the software package STAR-CD® to develop a three-dimensional computational model for predicting the heat transfer and pressure-drop performance of confined forced convection through a graphite foam block. The permeability and form-drag coefficient used were 1.4e-10 m^2 and 0.5243, respectively. In the energy equation that was used to predict heat transfer, the effective thermal conductivity was set at 175 W/m·K; also, an enthalpy source term was introduced to reflect the additional heat transfer that graphite foam would impose on the cooling liquid due to its extremely high thermal conductivity. Compared to experimental results, the author reported errors of 12 % and 0.8 % in the predictions of pressure-drop and outlet temperature, respectively.

Focusing on the application of graphite foam as a heat transfer device, Gallego and Klett (2003) experimentally investigated the performance of graphite foam heat sinks shaped in various configurations. The graphite foams under consideration had thermal conductivities of 40 to 180 W/m·K. One focus of their study was the comparison of heat sinks composed of a solid block of foam versus those machined into fins, pin-fins, vertical blind holes, horizontal blind-holes, and corrugations. The effects of air and water as the cooling fluid were also considered. From this initial investigation, the most effective geometry was the corrugated graphite foam heat sink that reduced the pressure-

drop by a factor of 60 while only reducing the overall heat transfer coefficient by a factor of 2. The corrugated shape from this investigation is the primary motivation for the optimization analysis in the present study.

2.2 Forced Convection in Channels Filled with Porous Media

In order to provide a review of the literature regarding confined forced convection in porous media, a few important concepts will be briefly discussed. For a thorough review of these concepts and others regarding convection in porous media, see Kaviany (1995) or Nield and Bejan (1999). For detailed reviews of fluid flow through porous media, see Muskat (1937) and Scheidegger (1974).

Vafai and Amiri (1998) focused on some of the primary issues surrounding confined forced convective flows in porous media. These include the concepts of local volume-averaging, non-Darcian effects, thermal dispersion, and local thermal equilibrium. These concepts will be briefly explained as an introduction to each of the following sections.

Local volume-averaging is a process by which many investigators develop governing equations for heat transfer and fluid flow in porous media. Since the thermal and frictional interactions between the fluid particles and the ligaments of the porous microstructure are complex and difficult to accurately predict, these transport processes are modeled in bulk on the macroscopic scale. The results of the local volume-averaging process are the momentum and energy conservation equations that treat the fluid and porous solid as one continuum.

2.2.1 Porous Media Momentum Equation

The theory of flow through porous media has a long history that is evident in the evolution of the governing momentum equation, which has been reported extensively by Lage (1998). Nield (2002) provided an informative review of modeling saturated porous media in which the individual terms of the modern porous media flow equation are discussed in detail. The porous media momentum equation consists of several "non-Darcian" terms that have been added to the original viscous (Darcian) term to account for effects that had been previously neglected. A more detailed explanation of the history of these non-Darcian effects and their relevance to the present study will be discussed in the body of the thesis. The culmination of the evolution of this equation was reported by Vafai and Tien (1981), who combined the contributions of Brinkman (1947) and Muskat (1937) to establish local volume-averaged differential balance laws. The end result was a widely used porous media momentum equation that included boundary effects through the Brinkman extension and additional terms that consider the so-called inertial effects.

In order to successfully predict the flow friction characteristics of graphite foam, the appropriate form of the momentum equation must be discovered. In order to verify the inclusion of the non-Darcian velocity-squared term into the momentum equation, several investigators performed experiments with media similar to graphite foam.

Ward (1964) experimentally validated the use of a nonlinear equation to describe flow through granular material. The pressure gradient was related to the macroscopic velocity by an equation in the form of

$$\frac{|dp|}{dl} = \frac{\mu v}{k} + \frac{c\rho v^2}{k^{1/2}} \tag{2.1}$$

Here, μ and ρ are the viscosity and density of the fluid, respectively, and k is the permeability of the porous medium. The empirically determined constant for the nonlinear term of the flow equation was set at c=0.550, which was (incorrectly) suggested to be a universal value for all porous media. The Fanning friction factor was plotted as a function of Reynolds number, which is based on a length scale equal to the square root of the permeability, and the results aligned to a single curve. In addition, the transition from a linear to nonlinear relationship between the macroscopic velocity and the pressure gradient was attributed to the onset of turbulence (which has since been highly debated).

Beavers and Sparrow (1969) investigated the friction characteristics of water flow through five different metallic fibrous media. The nonlinear flow equation governing the flow through porous media was rearranged to provide a straightforward method of determining the permeability and form-drag coefficient for each medium. The friction factors for all media under investigation were plotted as a function of Reynolds number, where the square root of the permeability was used as the length scale. The dimensionless results brought together the friction factor curves for all five samples, indicating that this experimental method is applicable to other similar media.

Philipse and Schram (1991) experimentally investigated isothermal airflow through open-cell alumina-silica foams in order to study the non-Darcian effects. Foams with average pore diameters ranging from 0.34 to 2.15 mm were studied. Darcian, k_1,

and non-Darcian, k_2, permeability coefficients were proposed for the momentum equation, which was stated in the form of

$$\frac{|\Delta P|}{\Delta x} = \frac{\mu}{k_1} U + \frac{\rho}{k_2} U^2 \tag{2.2}$$

It was determined that the ratio of these permeability coefficients, (k_1/k_2), is proportional to the average pore size of the ceramic foam. Therefore, this ratio was considered the characteristic length of the Reynolds number, which was used to estimate the range of each flow regime. The authors concluded that the flow through the ceramic foam follows the non-Darcian flow equation.

The primary conclusion drawn from these experiments is that the viscous and form drag effects, represented by the Darcy and Forchheimer terms in the general porous media momentum equation, are indeed dominant for relatively low permeability porous media.

2.2.2 Porous Media Energy Equation(s)

The concept of local thermal equilibrium (LTE) is an assumption that many authors make in order to relate the heat transfer behavior in a fluid/solid matrix to that in pure fluids. It is based on the idea that the temperature of the fluid is locally equal to that of the surrounding solid, but that temperature gradients occur on a macroscopic scale. For a more detailed analysis in which the temperature distributions of both the fluid and solid phases are sought, the local thermal non-equilibrium (LTNE) assumption is made. Here, an energy equation for both the fluid and solid phases is developed and the equations are coupled by a volumetric heat transfer coefficient, which must be

determined experimentally. The literature regarding the use of one or two energy equations in modeling confined forced convection in porous media has been divided into two sections in this review.

Thermal dispersion is a phenomenon that describes mixing where a temperature gradient occurs within the pores of a matrix and yields an increase in heat transfer. This concept has been used frequently in mass transfer studies and has been introduced in the present context in order to more accurately model the heat transfer performance of porous media as fluid velocities are increased.

One-Energy Equation Models

In addition to the establishment of the widely used porous media momentum equation, Vafai and Tien (1981) implemented the local thermal equilibrium (LTE) assumption to derive an energy equation that was applied to the two-dimensional case of flow through a porous medium adjacent to an external boundary held at a fixed temperature. The results indicated that the boundary and inertia effects were more pronounced with high matrix permeabilities, fluid Prandtl numbers, and pressure gradients; and also in the region close to the leading edge of the momentum boundary layer.

Kaviany (1985) studied laminar flow through a porous channel bounded by isothermal parallel plates using the governing equations adopted from Vafai and Tien (1981). A porous media shape parameter was introduced, defined as $\gamma = \left(H^2 \varepsilon / K\right)$, where H, ε, and K are channel height, porosity, and permeability, respectively. The local volume-averaged governing equations neglected the form drag term in the

momentum equation. The LTE assumption was invoked, so heat transfer was modeled with a single energy equation. Furthermore, the axial conduction term in the energy equation was neglected. Numerical and closed form analytical solutions were obtained for the developing and fully-developed regions, respectively. The results indicated an increase in the average wall Nusselt number up to a certain limit as the porous media shape parameter increases.

Kaviany (1987) presented closed-form analytical solutions, using the integral method, to the problem of forced convection from a semi-infinite flat plate embedded in porous media. The results were found to be in good agreement with those from a series expansion method and a finite-difference approximation. One conclusion drawn was that in the Darcian flow regime, the thermal boundary layer is much larger than the momentum boundary layer, while the boundary layers are within the same order of magnitude in the non-Darcian regime.

Poulikakos and Renken (1987) studied the problem of forced convection in a porous medium-filled channel and included the effects of flow inertia, variable porosity, and Brinkman friction. In their study, the bounding walls were held at constant temperature, and the thermal entry region was the primary focus. A general flow model and a one energy equation model were solved by a finite-difference technique. The results indicated that the thermal entry length increased with dimensionless pressure gradient and that the addition of terms to the Darcy equation results in a higher fully-developed Nusselt number.

Hunt and Tien (1988) considered the concept of thermal dispersion in their study of forced convection through fibrous media. Dispersion was included in the energy equation using an additional advective term that includes the dispersion conductivity. A single energy equation was used since the porous matrices in question have effective conductivities proportional to the fluid conductivities. The results showed a sharper increase in Nusselt number versus Peclet number for lower permeability media.

Vafai and Kim (1989) focused on forced convection through a porous medium in a bounded channel exposed to a constant heat flux. The so-called Brinkman-Forchheimer-extended Darcy model derived in Vafai and Tien (1981) was implemented. The energy equation neglected axial conduction and incorporated thermal dispersion in the effective thermal conductivity. The results indicated that as the permeability decreases, the inertia term in the momentum equation becomes less effective on momentum boundary layer thickness and temperature profile. Furthermore, the Nusselt number reaches a maximum value as permeability is decreased because the fluid flow is effectively a slug flow.

Hadim (1994) investigated confined forced convection through discrete blocks of porous media that are positioned in series directly beneath the localized heat sources, which represent electronic equipment. In other words, the fluid flows through one porous block positioned directly beneath a heat source, and it then flows in a non-porous region before entering the next porous block, and so on. The so-called Brinkman-Forchheimer extended Darcy model and a single energy equation were solved using the control volume based finite-difference technique. The results indicated that the heat transfer

enhancement by separate blocks is comparable with that by a full block, yet the pressure drop is substantially lower due to the removal of matrix material between heat sources. This comparison was made for the channel height equal to the block width and spacing. Furthermore, the Nusselt number increases for decreasing Darcy number, and the heat transfer enhancement is more significant at higher Reynolds number and towards the leading edge of each heat source.

Angirasa (2002) numerically investigated forced convection in a channel fully filled with metallic fibrous materials. The momentum equation derived by Vafai and Tien (1981) was invoked, and the energy equation included both stagnant and dispersion conductivities. The results indicated that dispersion is more prominent in high permeability media and that it is only effective at moderate fluid velocities. Furthermore, heat transfer was shown to be more dramatically enhanced by lowering the Darcy number (permeability) than by increasing the fluid velocity.

Two-Energy Equation Models

Schumann (1929) developed the first two-equation model for predicting temperature profiles in both the fluid and solid phases of a porous matrix. The importance of this work would not be realized until many years later.

Koh and Colony (1974) determined the cooling effectiveness of a compact porous heat exchanger used to enhance the cooling of a rocket nozzle. In a strictly thermal analysis, a two-energy equation model was proposed to predict the temperature profile in the solid and fluid phases, and the finite Fourier transform method was used to solve the

system of equations. In all of the cases studied, cooling effectiveness was increased by more than three times over a nonporous channel.

Vafai and Sozen (1990) analyzed the momentum and energy transport in the forced convection of gas through a packed bed of spheres. The local volume-averaging technique was used to derive the governing equations. Local thermal non-equilibrium (LTNE) was assumed, and the classical Schumann (1929) model for two-phase energy transport was invoked. The so called Ergun (1952) correlation was used for the momentum equation, which is applicable to packed beds. The results indicated that the local thermal equilibrium assumption is more justifiable for low Darcy and Reynolds numbers, and that two-dimensional effects are important for high solid-to-gas diffusivity ratios.

Younis and Viskanta (1993) experimentally determined the volumetric heat transfer coefficient between air and high porosity alumina and cordierite foams. A single-blow transient technique with an inverse method was incorporated for foams ranging from 0.29 to 1.52 mm pore diameter, with thermal conductivities of 2.84 to 4.23 W/mK. The two-energy equation model was solved using the control volume, finite-difference technique. Nusselt number was presented as a function of Reynolds number for the entire range of foams. The results indicate that volumetric heat transfer coefficient increases as average pore diameter decreases.

Amiri and Vafai (1994) investigated the effects of including thermal dispersion in non-Darcian flow that is in local thermal non-equilibrium (LTNE). The study incorporated several effects that previous studies had neglected. An error map was

presented so that investigators can determine the applicability of certain simplifying assumptions. The results showed that transverse thermal dispersion is more influential on thermal boundary layer growth than axial (or longitudinal) dispersion. Also, in determining the validity of the local thermal equilibrium assumption, it was found that the Darcy number is the most influential parameter. For decreasing Darcy number, the LTE assumption becomes more valid; however, as the solid-to-fluid thermal diffusivity ratio and the pore Reynolds number increase, the assumption becomes less applicable.

Hwang and Chao (1994) conducted heat transfer experiments on forced convection of air through sintered bronze beads. A two-energy equation model that includes thermal dispersion and neglects axial conduction was solved by the finite-difference method. Much attention was focused on local Nusselt number since excess values of local temperature can result in failure of electronic equipment. The results show that the local distribution of Nusselt number for bronze beads lies between those of glass and stainless steal beads.

Bartlett and Viskanta (1996) investigated forced convection through an asymmetrically heated duct filled with a high conductivity porous medium. Special attention was given to the thermally developing region, which had been neglected in most previous studies. Closed form analytic solutions of the two-energy equation model subject to both constant heat flux and temperature boundary conditions were developed, and the results were compared to the experimental work of Hwang and Chao (1994). The thermal dispersion effect was not explicitly accounted for, so the influence of dispersion

was implicitly handled by the solid-to-fluid convection term. Results showed that heat transfer enhancement is proportional to the ratio of solid-to-fluid thermal conductivity.

Calmidi and Mahajan (2000) analyzed forced convection through aluminum foam with porosity greater than ninety percent. Separate energy equations for the fluid and solid phases were solved numerically under the LTNE assumption. A dispersion conductivity was added to the stagnant conductivity to account for effects at high Peclet number. Nusselt number as a function of pore Reynolds number was determined, and numerical and experimental results were compared to obtain empirical constants in the models for dispersion conductivity and interstitial heat transfer coefficient. The authors emphasized the difficulty in quantifying the dispersion conductivity for high ratios of solid-to-fluid thermal conductivity.

Hwang *et al.* (2002) focused on the influence of foam porosity and Reynolds number (based on pore diameter) on the interstitial heat transfer coefficient and frictional drag of aluminum foam. The samples of foam under consideration consisted of 6101-T6 aluminum, with porosities and their corresponding effective thermal conductivities ranging from 0.70 to 0.95 and 65.4 to 10.9 W/mK, respectively. A transient single-blow technique was utilized along with a model based on thermal non-equilibrium. The equations were solved using a control volume based finite-difference technique. The results indicated that the friction factor decreases with increasing porosity and Reynolds number. Furthermore, the volumetric heat transfer coefficient increases with decreasing porosity and with increasing Reynolds number.

2.2.3 Related Topics

Justifying the Local Thermal Equilibrium Assumption

Kim and Jang (2002) developed a new criterion for the validity of the local thermal equilibrium (LTE) assumption that is especially applicable when forced convection is the primary mode of heat transfer. The LTE condition was presented in terms of Darcy number, Prandtl number, and Reynolds number. The determination of interstitial heat transfer coefficient, among other values, is required to test the criteria. The results indicated that the LTE assumption is valid as Darcy and Reynolds number approach zero.

Experimental Heat Transfer Studies on Metallic Foams

Kim *et al.* (2000) experimentally investigated the influence of porosity and permeability on the friction and heat transfer of air through a porous aluminum fin. Friction factor and modified j-factor were defined and correlations were developed based on Reynolds and Darcy numbers. Comparisons were made with a conventional louvered fin used in compact heat exchangers. Results indicated that the porous fins under investigation behave similar to the louvered fins thermally, but the friction imposed by the foam is greater. In addition, the authors recommend the use of low porosity, high pore density foams (i.e., low permeability) for use in compact heat exchangers.

Kim *et al.* (2001) experimentally investigated the enhancement of heat transfer through aluminum foam in an asymmetrically heated channel. The results indicated that the Nusselt number is increased with Reynolds number, and that enhancement is much more pronounced for low permeability foams. The Nusselt number correlation derived is

independent of the effective thermal conductivity and greatly dependent on the foam permeability. The authors attribute this behavior to the high heat transfer surface area associated with low permeability foams rather than to the conductivity of the solid.

Compact Heat Exchangers

Kays and London (1984) have reported a significant amount of experimental data regarding various surfaces used in compact heat exchangers. The heat transfer results are in the form of j-factor and friction factor, which are defined to encompass the wide variety of fin types. Cowell and Achaichia (1997) have incorporated some of this data intheir study of compact heat exchangers used in the automobile industry. The authors report an improvement of heat transfer coefficients by 50 percent over the past 20 years.

2.3 FEA and CFD Software

In the present study, the 2D and 3D simulations will be handled by the software packages FEMLAB® and STAR-CD®, respectively. FEMLAB® is a finite element analysis (FEA) software based on the MATLAB® programming environment. The fluid flow equations used in this software are stated in the FEMLAB® User's Guide (2002). The specific forms of the equations used were derived by Gresho and Sani (1998). For the present study, the Navier-Stokes and Brinkman equations are invoked for the fluid and porous regions, respectively. More details of the manipulation of the governing equations will be discussed in the next chapter.

The governing mass, momentum, and energy conservation equations in STAR-CD® are stated in the STAR-CD® v3.15 Methodology (2001) and are solved by the

control-volume method. These equations were derived previously by separate authors. The mass and momentum (Navier-Stokes) conservation equations invoked by STAR-CD® were derived by Warsi (1981), and they apply to incompressible and compressible fluid flow on a stationary or moving coordinate frame. Similarly, the energy conservation equation was derived by Jones (1980) and is considered the general form of the enthalpy conservation equation for a fluid mixture by the STAR-CD® v3.15 Methodology (2001).

Chapter 3

Problem Statement

3.1 Introduction

In the design of heat exchangers, a classic problem is internal forced convection of a fluid flowing through a conduit that is subjected to a constant heat flux. Applications such as electronics cooling have been the motivation for the development of heat transfer coefficient and friction factor correlations. Typically, as shown in Figure 3.1, the length, L, is considered to be the dimension of the heat exchanger parallel to the flow direction; the width, W, and height, H, make up the cross-sectional area perpendicular to the flow direction. The exposure of one face to a constant heat flux has traditionally been termed an asymmetric heat flux condition.

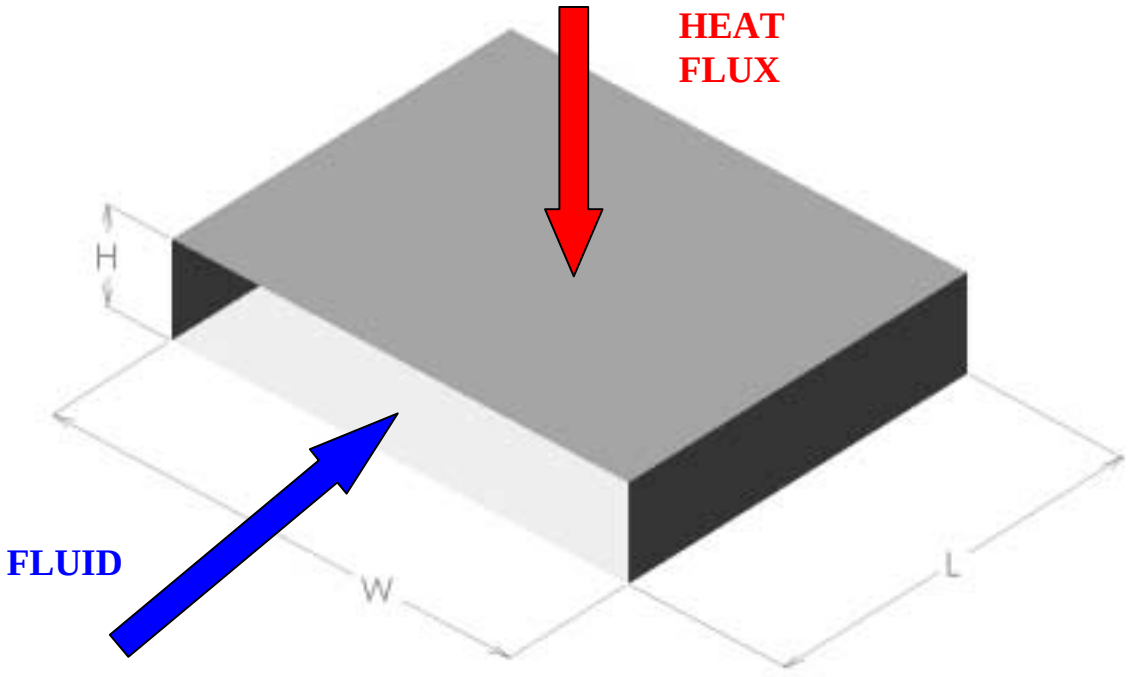

Figure 3.1. Internal forced convection in a conduit exposed to a constant heat flux.

3.1.1 Heat Transfer Enhancement with Graphite Foam

For heat transfer enhancement, heat transfer surfaces extending from each plate into the channel are incorporated in order to increase the heat transfer surface area-to-volume ratio; consequently, high values of this ratio are sought in the design of compact heat exchangers. Extended surfaces usually consist of fins of various shapes, and much has been accomplished in the literature in the development of applicable design correlations (Kays and London, 1984).

In addition to finned surfaces, the use of thermally conductive porous media for heat transfer enhancement in compact heat exchangers has also been the focus of several studies. The focus of the present investigation is the performance prediction of highly conductive graphite foam. In order to take full advantage of the heat transfer properties of graphite foam, the problem of internal forced convection through a graphite foam-filled channel, as shown in Figure 3.2, is adopted here in which the fluid is forced to flow through the foam at some location. Osgood (2001) numerically investigated the problem of a 3D block of graphite foam in a channel exposed to a constant temperature boundary, and the heat transfer performance of the foam was exceptional. However, graphite foam imposes a considerable frictional flow resistance, so certain techniques have been investigated that involve the strategic removal of foam in certain locations in order to reduce this adverse effect. One such method of reducing this resistance to fluid flow was explored in this study, as will be described below.

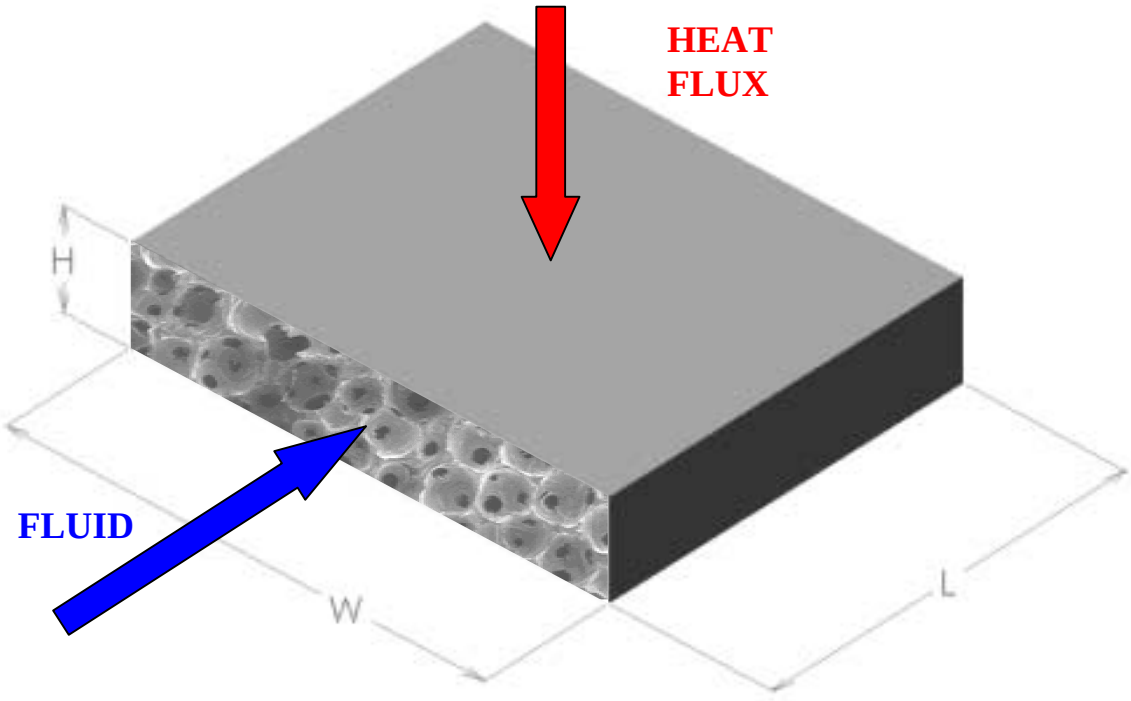

Figure 3.2. Sketch of internal forced convection in a porous medium-filled channel exposed to a constant heat flux.

3.1.2 Pressure-drop Reduction Technique: Corrugated Foam

One of the primary considerations in the selection of thermal management components is the operational cost of transporting the working fluid. This operational cost is a function of the pumping power required, which equals the product of the pressure-drop and the volumetric flowrate across the heat transfer component.

Due to its relatively small pore diameter ($\cong$ 350 microns), graphite foam causes a substantial pressure-drop within the fluid, and thus pressure-drop reduction schemes are necessary in order to utilize the foam in practical applications. Gallego and Klett (2003) experimentally explored several foam geometries that reduced the overall pressure-drop,

and the pressure-drop reduction technique that proved to be most promising is that of a corrugated geometry.

In flow through porous media, the pressure-drop is proportional to the fluid velocity for small flowrates (Darcy flow) and to the square of the fluid velocity for high flowrates (Forchheimer flow); also, it is proportional to the porous path length through which fluid flows. Therefore, corrugated graphite foam heat exchangers can be expected to reduce the overall pressure-drop relative to non-corrugated ones for two important reasons:

1) The length of foam through which most of the fluid flows will be reduced from overall length, L, to thickness, t, of the foam, and this results in a corresponding reduction in pressure-drop.
2) When the lateral flow through the corrugated foam is uniformly distributed, the average velocity of fluid that flows through the foam would be significantly reduced, and this also results in a significant reduction of overall pressure-drop. The uniformity of lateral velocity through foam is very important in providing the reductions in the pressure-drop.

The combination of geometric and flow conditions that result in relatively uniform lateral velocity distribution through the foam can be expected to provide the optimal pressure-drop. So, one the purpose of this research is to find the right combination of these conditions that result in uniformly distributed lateral flow.

The corrugated foam geometry is achieved by machining alternating blind slots into the foam, which are equally spaced along the width of the heat exchanger and

parallel to the flow direction, as shown in Figure 3.3. In this figure, fluid enters the *foam entry area* that consists of the frontal interfaces and the blue faces within the *inlet slot*. After passing through the foam, fluid exits the *foam exit area* that consists of the trailing faces (not shown) and the red faces within the *outlet slot*.

In this configuration, the removal of foam results in a reduction of both the contact area with the surface of the heat source and the interstitial heat transfer area between the porous solid and the fluid. Therefore, the engineering challenge of this design procedure is to significantly reduce pressure-drop across a section of foam without substantially sacrificing heat transfer performance.

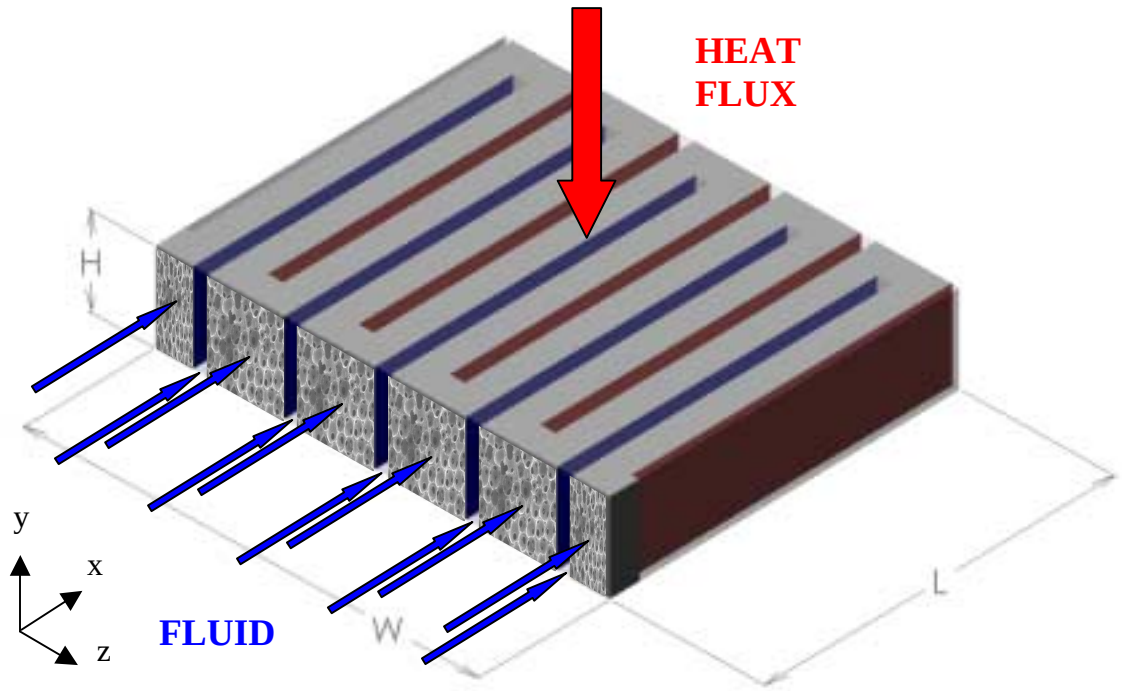

Figure 3.3. Sketch of internal forced convection through a corrugated foam geometry exposed to a constant heat flux.

3.2 Modeling Considerations

3.2.1 Geometric Simplifications

Two-dimensional vs. Three-dimensional

In the configuration shown in Figure 3.2, L, the dimension along which fluid flows, should be shorter than W; this orientation results in higher overall heat transfer coefficients and lower pressure-drop for flow through porous media. In fact, most studies in the literature regarding forced convection through a channel fully filled with porous media focus on the simplified two-dimensional (2D) model in which W >> L, and the problem is defined as flow between two semi-infinite parallel plates. For some applications, a 2D analysis is sufficient. In fact, in this study, the pressure gradients are expected to prevail predominantly in the plane perpendicular to the planes of the slots (i.e., minimal flow in the y-direction is expected), so the total pressure-drop can be calculated with a 2D analysis. This is especially helpful for conducting a parametric study involving a large number of simulations. However, the present problem is rather complex due to its three-dimensional (3D) nature since the predominant direction of heat transfer would be perpendicular to the plane in which the 2D pressure-drop problem is analyzed. Therefore, the pressure-drop problem is 2D in the x-z plane, whereas the heat transfer problem is fully three-dimensional.

In order to solve this problem, a parametric study was done using the software packages FEMLAB® and STAR-CD®, each of which was utilized for its specific advantages. Specifically, the finite element analysis (FEA) software FEMLAB® was used to conduct an extensive 2D parametric study to analyze the fluid flow field and the

resultant pressure-drop across the foam. The results of this portion of the study served as a guideline for selecting the more computationally demanding 3D cases. Consequently, the computational fluid dynamics (CFD) software STAR-CD® was used to analyze a limited number of 3D cases involving the combined effects of pressure-drop and heat transfer across the foam.

Corrugated Unit Cell

The creation of a complex geometry requires the introduction of several geometric parameters that must be varied to produce an optimal design. First, a repeatable shape within the footprint of the heat source was chosen that can be modeled separately and then duplicated as many times as necessary. The repetitive geometry is defined here as the *Corrugated Unit Cell* (CUC), as shown in Figure 3.4. This repeatable unit cell can be optimized for given input parameters and then a specific number of unit cells can be chosen to fill the footprint. In numerical modeling, focusing on a unit cell allows the designer to allocate more computer memory to a smaller geometric section, thereby obtaining more accurate results with reduced computational time.

In a given channel *Width,* W, slots can be machined parallel to the primary fluid flow direction at a certain *Spacing,* S. The width of the slots that are machined into the foam is defined as the *Cut-width,* C. In this study, the slots are cut to a length such that the *Thickness, t,* of the foam in the x-direction equals that in the z-direction. Therefore, in this study, the following relationship holds:

$$S = 2t + 2C\,. \tag{3.1}$$

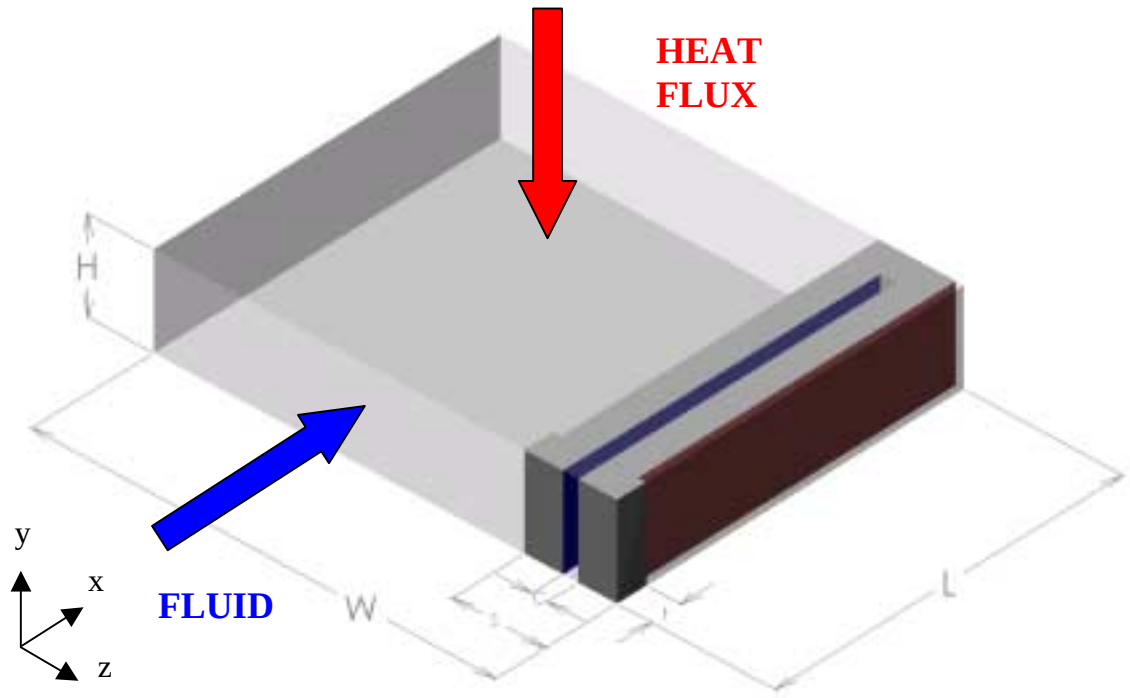

Figure 3.4. The Corrugated Unit Cell is shown as one repeatable section of the heat exchanger.

In addition, it is assumed that the heat exchanger has a pre-determined heated surface area composed of a width and length equal to that of the attached heat source.

Under this assumption, the heat exchanger can be comprised of one row of corrugated foam that extends to the limits of both dimensions. It is possible to incorporate several rows of corrugated foam to fill the same area if the manufacturing limits necessitate such a design; however, the corresponding pressure-drop may be higher since the fluid would permeate each row in series. Therefore, it is advantageous to design one row of corrugated foam; so in this study, the length, L, was held at fixed values of 0.05, 0.075, and 0.10 m for the simulations. For each L value, the dimensionless variables L/S and C/S were varied in order to find the optimal configurations. Specifically, L/S was increased from 2 to 10 by decreasing S in order to examine the

effect of narrowing the unit cell. Also, C/S was increased from 0.075 to 0.175 in increments of 0.025 by increasing C in order to determine the relative importance of the slot width compared to the unit cell spacing.

Corrugated Half-Unit Cell

In order to focus on the detailed flow patterns that contribute to the overall pressure-drop, two additional simplifications were invoked in the models. First, half of the CUC was modeled under the assumption that a symmetry axis (2D) or plane (3D) separates two identical regions on either side of the inlet slot. The region defined as the *Corrugated Half-Unit Cell* (CHUC) is shown in comparison with the CUC in Figure 3.5. Also, though the fluid region upstream of the CHUC was included in the models to encompass the flow effects that occur in this region, the downstream region of the CHUC was neglected by setting the pressure to zero at the trailing edge of the foam. This approach allows for mesh refinement in crucial areas where large pressure and velocity gradients are present. An improved mesh quality provides the opportunity for a more stable and accurate solution.

In summary, a list of the geometric simplifications that were made in the development of the appropriate model is as follows:

1. A two-dimensional (2D) analysis can be used to predict the pressure-drop performance since negligible flow and pressure gradients are expected in the y-direction.

2. A single row of corrugated foam is used in the heat exchanger that extends the full length and width of the heat source.

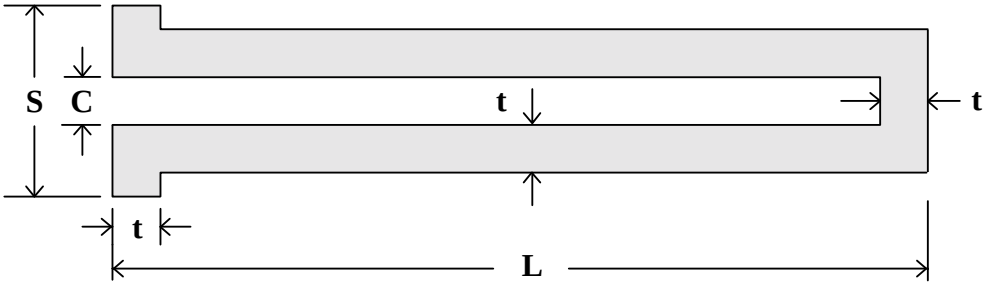

(a) Corrugated Unit Cell (CUC)

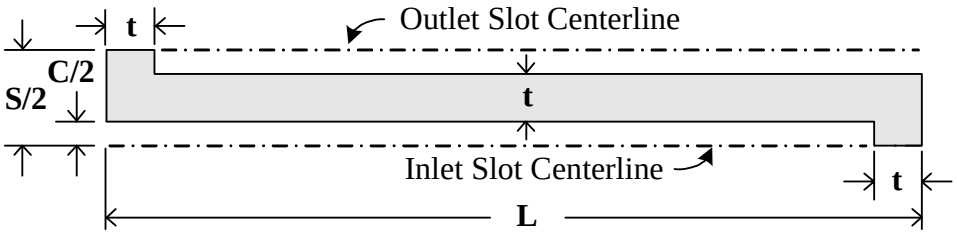

(b) Corrugated Half-Unit Cell (CHUC)

Figure 3.5. A top view (on the x-z plane) of Unit Cell and Half-Unit Cell used for modeling.

3. A corrugated unit cell (CUC) will encompass the full heat transfer and pressure-drop effects that occur in the heat exchanger.

4. A corrugated half-unit cell (CHUC) can be used to predict the performance of the symmetric CUC and allows for improved mesh quality.

5. Negligible pressure gradients exist in fluid region downstream of the CHUC.

3.2.2 Thermophysical Assumptions

Several thermophysical assumptions were made in the development of the appropriate model. First, the analysis focuses on the steady-state performance of the heat exchanger. Also, laminar flow was assumed because the significant flow resistance

imposed by graphite foam requires the use of low flowrates in order to ensure the practical application of the material. The working fluid in this analysis was water, whose properties do not change significantly in the temperature range expected. For simplicity, homogeneous, isotropic foam properties were assumed. Lastly, local thermal equilibrium in the foam-fluid matrix was assumed along with negligible thermal dispersion, and both of these assumptions will be explained in more detail in the following chapter. The thermophysical assumptions made are summarized as follows:

1. Steady, laminar flow
2. Constant fluid properties -- density (incompressible), dynamic viscosity, specific heat, thermal conductivity
3. Homogeneous, isotropic foam properties -- effective thermal conductivity (ETC), permeability, form coefficient
4. Local thermal equilibrium (LTE)
5. No thermal dispersion

Incorporated property values

Under the assumptions listed above, the list of constant properties used in the models are presented in Table 3.1. A reasonable reference temperature of 20^{o} C or 293.15 K was selected, and the water properties evaluated at this temperature were taken from Munson et al. (1998). The permeability and form coefficient of graphite foam were reported by Osgood (2001), and the effective thermal conductivity was reported by Klett et al. (2000).

Table 3.1: Thermophysical properties used in models.

Property	**Symbol**	**Value**	**Units**
Fluid*			
Density	ρ_f	998.2	kg/m^3
Molecular Viscosity	μ	0.001002	kg/m-s
Specific Heat	$(c_p)_f$	4182	J/kg-K
Thermal Conductivity	k_f	0.59	W/m-K
Matrix			
Permeability	K	1.4e-10	m^2
Form Coefficient	c_F	0.5243	
Effective Thermal Conductivity	k_m	150	W/m^2K

*Water properties are based on data from the *Handbook of Chemistry and Physics*, 69th Ed., CRC Press, 1998.

Chapter 4

Equations

4.1 Introduction

Now that the geometric parameters in the model have been established, the appropriate conservation equations are discussed below. The next section focuses on the history of the porous media momentum equation, and an appropriate form is suggested for the present study. Also, a Reynolds number that pertains to flow through porous media will be introduced. Then, several assumptions will be explained that were made to allow the use of the traditional energy equation to model heat transfer in both the fluid and porous regions of the 3D model. A method for predicting foam height for the 3D simulations will follow. Finally, definitions of the performance parameters will be made to allow for a comparison with previous studies.

4.2 Background of Porous Media Momentum Equation

The porous media momentum equation has evolved tremendously over the past one and one-half centuries, as explained by Lage (1998). This progress is most evident with the introduction and refinement of the individual terms that compose the equation. In particular, the viscous drag, the form drag, the boundary shear, and the convective inertia terms are discussed in this chapter in light of their history and relevance to the general equation that is accepted today.

4.2.1 Viscous Drag (Darcy) Term

History

The study of flow through porous media was pioneered by Henry Darcy in 1856 during his research on the water supply system for the city of Dijon, France. The Darcy equation was developed based on experiments in which water seepage through packed beds was induced by gravity. It was discovered that the pressure-drop of the fluid as it flowed through the medium was linearly proportional to the macroscopic velocity. The original form of the Darcy equation is:

$$k_H = U \frac{e}{|\Delta p|} \tag{4.1}$$

where k_H = Hydraulic conductivity
U = Macroscopic velocity
e = Porous flow length
p = Pressure

As explained by Lage (1998), in 1893, the temperature-dependence of the fluid was taken into account by Hazen, and the dynamic viscosity was explicitly introduced into the equation by Krüger in 1918. The common form of the Darcy equation is therefore

$$U = \left(\frac{K}{\mu} \right) \frac{|\Delta p|}{e} \tag{4.2}$$

where K is the specific permeability, in units of square-meters, and μ is the dynamic, or molecular, viscosity.

Relevance to Present Study

The Darcy term in the porous media momentum equation accounts for the viscous shear stress imposed on the fluid by the solid ligaments of the matrix. This term is dominant in the overall governing equation since graphite foam permeability is relatively low in magnitude, being on the order of 10^{-10} m^2 (Osgood, 2001). Therefore, the contribution of this term to pressure-drop, which is inversely proportional to the permeability, is significant. For flow that is predominantly viscous, the velocity profile is relatively uniform across the channel, resembling slug flow. The Darcy equation, however, cannot be satisfied by the no-slip condition imposed by the adjacent boundary.

4.2.2 Form Drag (Forchheimer) Term

History

Although Darcy had proven the linear relationship between pressure-drop and velocity based on extensive experimental data, Dupuit in 1863 was the first to use scientific principles to explain the physics of Darcy's Law, as explained by Lage (1998). He did so by comparing the flow through a permeable matrix with that of open channel flow with a uniform velocity profile. As a result, Dupuit proposed the following relationship:

$$0 = \frac{|\Delta p|}{\Delta x} - \alpha U - \beta U^2 \tag{4.3}$$

where the coefficients α and β were to be determined experimentally. Years later, Forchheimer was credited by Muskat (1937) and others for establishing the quadratic equation, hence the common referral in the literature to the "Darcy-Forchheimer"

equation. In reality Forchheimer's contribution to the field was his experimental data presented in 1901 that confirmed the use of a quadratic equation over the widely accepted Darcy equation. He extended this theory by suggesting that the dependence may even be third order at very high fluid velocities.

References to the "Ergun Equation" in the literature are due to an experimental study by Ergun (1952) focusing on gas flow through crushed porous solids that revealed a second-order pressure-drop equation that is commonly used for flow through packed beds. An extensive experimental study by Ward (1964) revealed a relationship of pressure-drop and velocity in the form

$$\frac{|dp|}{dl} = \frac{\mu v}{k} + \frac{c\rho v^2}{k^{1/2}} \tag{4.4}$$

where ρ is the fluid density and c is the form coefficient that was first (and incorrectly) thought to be equal to 0.550 and applicable to all porous media. Although there is no physical reasoning for the placement of $k^{-1/2}$ in the quadratic term, several studies have been performed since Ward's work to use experimental results to curve fit pressure-drop versus velocity data and calculate K and c for various porous media. A systematic method for simultaneously evaluating permeability and inertia (form) coefficient was reported by Beavers and Sparrow (1969) and verified for fibrous media by Hunt and Tien (1988), among others.

Relevance to Present Study

This term was added to the Darcy term of the momentum equation by a simple linear superposition. Its effect was noticed when fluid flow rates were relatively high.

Theorists have proposed that the cause of this exponential rise in pressure gradient is due to the form drag effect imposed by the solid ligaments. This effect can be described by the imbalance of pressure surrounding a blunt body in a fluid stream due to a wake that is formed on the downstream side of the obstacle. When the magnitude of the form drag is comparable to that of the viscous drag caused by the surface of the solid ligament, the quadratic term becomes important. Experimental findings of pressure-drop versus fluid velocity reveal a nonlinear curve that can be effectively modeled with proper knowledge of the Forchheimer (form) coefficient.

4.2.3 Viscous Shear (Brinkman) Term

History

In 1947, Brinkman introduced a new Laplacian term into the Darcy equation based on the influence of viscous shear stress placed on the fluid by the adjacent solid surface of a high-permeability porous medium. This effect, he argued, was in addition to the solid viscous drag force located at the fluid-solid interface that explained the existence of the Darcy term. The resulting equation with inertial terms omitted takes the form (Nield, 1999):

$$\nabla P = -\frac{\mu}{K}\mathbf{v} + \mu'\nabla^2\mathbf{v} \tag{4.5}$$

where μ' is the effective viscosity, which Brinkman simply set equal to the molecular viscosity, and $\mathbf{v}$ is the velocity vector. The inclusion of the Brinkman term is handled differently by various authors.

Relevance to Present Study

A scale analysis reveals the relative magnitude of the Brinkman term with respect to the Darcy term as $O(K/L^2)$, where L is the characteristic length of the macroscopic problem (Nield, 2002). Many authors have defined the Darcy number as $Da=K/L^2$, and therefore, the Brinkman term becomes increasingly important as $Da\rightarrow\infty$ and negligible as $Da\rightarrow 0$. Therefore, the effect of the Brinkman term is negligible for modeling pressure-drop across graphite foam. Typically, this term is included to satisfy the no-slip boundary condition at the impermeable walls surrounding the porous medium. The present 2D model, however, does not include a no-slip boundary condition.

4.2.4 Advective (Convective) Inertial Term

History

Nield (1999) explained that several authors have derived equations analogous to the Navier-Stokes equation that include an inertial term, such as:

$$\rho_f\left[\phi^{-1}\frac{\partial \mathbf{v}}{\partial t}+\phi^{-2}(\mathbf{v}\cdot\nabla)\mathbf{v}\right]=-\nabla p-\frac{\mu}{K}\mathbf{v} \tag{4.6}$$

where ρ_f = Density of fluid
ϕ = Porosity
$\mathbf{v}$ = Velocity vector
t = Time

The $(\mathbf{v}\cdot\nabla)\mathbf{v}$ term in the porous media momentum equation is identical to the convective term in the Navier-Stokes equation. The importance of this term for porous media is debated by several authors (Nield, 2002). Joseph et al. (1982) stated that since the inertial effects are incorporated by the Forchheimer term, the advective term is negligible.

Nield (1994) argued that only the irrotational part of the vector identity $(\mathbf{v}\cdot\nabla)\mathbf{v} = \nabla(\mathbf{v}^2/2) + \mathbf{v}\times(\nabla\times\mathbf{v})$ need be retained for modeling compressible fluids. Also, Nield suppressed the notions that the term is necessary for the formation of hydrodynamic boundary layers and for the prediction of entrance length.

Relevance to Present Study

In comparison with the Forchheimer drag term (which is already smaller in magnitude than the Darcy term for low to moderate flowrates), the advective term scales as O($\sqrt{K}/c_F\phi^2 L$), and since K is very low for graphite foam, this term can be neglected (Nield, 2002).

4.2.5 General and Applicable Porous Media Momentum Equations

The explanation of the history and relevance to the present study of the individual terms in the porous media momentum equation allows us now to state a generally accepted equation that includes non-Darcian effects, and to establish the form of the equation that will be accepted here as applicable to graphite foam.

Vafai and Tien (1981) combined the contributions of Brinkman (1947) and Muskat (1937) to establish local volume averaged differential balance laws that include boundary and inertial (form) effects in addition to the Darcy term in the momentum equation. Modern refinements have been made to the equation by Vafai and Kim (1990). The resulting volume-averaged momentum equation for porous media is the Brinkman-Forchheimer equation, restated by Nield (2002):

$$\rho\left[\frac{1}{\phi}\frac{\partial \mathbf{v}}{\partial t}+\frac{1}{\phi^2}\left(\mathbf{v}\cdot\nabla\mathbf{v}\right)\right]=-\nabla p+\mu_e\nabla^2\mathbf{v}-\frac{\mu}{K}\mathbf{v}-\frac{c_F\rho}{K^{1/2}}|\mathbf{v}|\mathbf{v} \tag{4.7}$$

where μ_e = Effective viscosity
c_F = Forchheimer (form) coefficient

In the present study, the appropriate equation for steady, fully developed flow through low permeability porous media has been derived by Joseph *et al.* (1982) and restated by Nield and Bejan (1999) as:

$$\nabla P=-\frac{\mu}{K}\mathbf{v}-c_F K^{-1/2}\rho_f|\mathbf{v}|\mathbf{v} \tag{4.8}$$

4.2.6 Porous Media Reynolds Number

The definition of Reynolds number for flow through porous media is a crucial issue in order to fully understand the effect that this parameter has on the pressure-drop performance. Traditionally, Reynolds number is defined as:

$$\mathrm{Re}=\frac{\rho UL}{\mu} \tag{4.9}$$

where U and L are some characteristic velocity and length, respectively. When the Navier-Stokes equations are applied to model a certain flow situation, the Reynolds number is an indication of the ratio of inertia to viscous forces in the fluid. When friction factors are determined as a function of Reynolds number, the interest is usually in the behavior of the flow in certain flow regimes: laminar, transitional, and turbulent. When a porous medium is inserted into the stream, the Brinkman-extended Darcy-Forchheimer equation governs the flow for that region. Since the pressure gradients are dramatically larger in the porous region, especially for low permeability media, the ratio of inertia to

viscous forces is no longer as important. Here, the ratio of form to viscous drag imposed by the porous matrix is more indicative of the flow regime under which a certain application lies. Therefore, several authors have introduced a porous media Reynolds number to explain the effects of this more pertinent ratio of forces on the frictional drag. The two parameters under question are the characteristic velocity and length. Philipse and Schram (1991) introduce the characteristic length equal to the permeability quotient, (k_1/k_2), where k_1 and k_2 are the Darcian (specific) and non-Darcian permeabilities, respectively, as defined in the equation

$$\frac{|\Delta P|}{\Delta x} = \frac{\mu}{k_1} U + \frac{\rho}{k_2} U^2 \tag{4.10}$$

The authors found that this ratio was linearly proportional to the pore size of the foams under consideration, thus justifying its role as the characteristic length. Moreover, the Reynolds number based on this length proved to be good indicator of the Darcian flow regime based on the experimental study.

According to Lage (1998), the Reynolds number should not even be used to characterize the Darcian and non-Darcian flow regimes since the ratio of inertia to viscous forces is irrelevant. However, the same concept is utilized by Lage. The so called Hazen-Dupuit-Darcy flow equation is proposed:

$$0 = \frac{|\Delta P|}{\Delta x} - \frac{\mu}{K} U - C_F \rho U^2 \tag{4.11}$$

where C_F is the form coefficient. From here, the physically meaningful ratio suggested is:

$$\frac{C_F \rho U^2}{\left(\frac{\mu}{K}\right)U} = \frac{\rho C_F K}{\mu} U \tag{4.12}$$

Note here that the form coefficient C_F is equivalent to $1/k_2$ from above. After some manipulation, it is easy to see that:

$$\frac{c_F}{\sqrt{K}} = C_F = \frac{1}{k_2} \tag{4.13}$$

Lage argues that C_F is preferable to $c_F/\sqrt{K}$ since c_F seems to have been defined based on the coincidence that C_F is of the order of O($K^{-1/2}$). In any event, it is obvious that:

$$\frac{\rho C_F K}{\mu} U = c_F \frac{\rho U \sqrt{K}}{\mu} = \frac{\rho U}{\mu}\left(\frac{k_1}{k_2}\right) \tag{4.14}$$

It can be concluded here that regardless of the terminology, the form to viscous drag ratio can be identically defined in various ways. In this study, the modified Reynolds number will be incorporated:

$$\mathrm{Re}_K^* \equiv c_F \frac{\rho U_0 \sqrt{K}}{\mu} \approx \frac{form\ drag}{viscous\ drag} \tag{4.15}$$

Where c_F is the form coefficient and U_0 is the frontal velocity. It is interesting to note that this expression is equivalent to the term $c\,\mathrm{Re}_K$ reported by Ward (1964). Experimental studies have shown that form drag becomes comparable to viscous drag at $\mathrm{Re}_K^* \geq 0.1$ (Philipse and Schram, 1991).

4.3 Background of Porous Media Energy Equation

4.3.1 Local Thermal Equilibrium

When modeling the flow and heat transfer in a porous matrix, the local thermal equilibrium (LTE) assumption is often incorporated so that both the solid and fluid components of the porous matrix are modeled as a single medium. Under this assumption, a single equation for the conservation of energy is derived using a local-volume-averaging technique, and effective matrix properties emerge. One motivation for the use of a single energy equation is that similarities can be deduced from solutions to problems involving only fluid flow (i.e., with no porous matrix present). Otherwise, under the local thermal non-equilibrium (LTNE) assumption, a model with two energy equations is used to simulate heat transfer in the solid and fluid phases separately, and a temperature distribution exists for each phase.

LTE is defined by Kaviany (1994) as:

$$\langle T \rangle = \langle T \rangle^{s}(x) = \langle T \rangle^{l}(x) = \langle T \rangle^{g}(x) \tag{4.16}$$

where s, l, and g denote solid, liquid, and gas respectively. In other words, the local-volume-averaged temperature of the effective single medium is equal to the local-volume-averaged temperature of each phase. Kaviany suggested the simple constraint for LTE (1994):

$$\Delta T_d << \Delta T_l << \Delta T_\delta \tag{4.17}$$

where the subscripts d, l, and δ, are the linear dimensions of the particle, representative elementary volume, and system, respectively. Here, the system temperature difference

$\Delta T_\delta = |T_s - T_\infty|$ is defined such that T_s is the temperature of the bounding surface and T_∞ is the temperature of the matrix far from the surface.

A comprehensive criterion for establishing LTE was reported by Kim and Jang (2002). The conditions were derived to encompass a broad range of flow situations that had previously been unreported. Using the general constraint stated by Kaviany, the authors arrived at the following criterion for the LTE assumption:

$$\frac{\dot{m} C_{p_f}}{h_{sf} a_{sf} V} << 1 \tag{4.18}$$

where
- $\dot{m}$ = Mass flow rate
- C_{p_f} = Specific heat of fluid
- h_{sf} = Interstitial convection coefficient per unit volume
- a_{sf} = Specific surface area
- V = system volume

This form of the criterion suggests that the LTE assumption is valid for cases where, among other things, the specific surface area between the solid and fluid is very large. This result was converted into a non-dimensional form consisting of important engineering parameters such as the Prandtl, Reynolds, Darcy, and Nusselt numbers:

$$\mathrm{Pr}_{eff,f}\ \mathrm{Re}_{d_p}\ Da^{1/2}\ \frac{\varepsilon}{Nu} << 1 \tag{4.19}$$

where

$$\mathrm{Pr}_{eff,f} \equiv \frac{(\rho C_p)_f \nu}{k_f \varepsilon}\ ;\ \mathrm{Re}_{d_p} \equiv \frac{u_p d_p}{\nu}\ ;\ Da \equiv \frac{{d_p}^2}{L^2}\ ;\ Nu \equiv \frac{h_{sf} d_p}{k_f} \tag{4.20}$$

where ε = Porosity
ν = Kinematic viscosity
k_f = Thermal conductivity of fluid
u_p = Pore velocity
d_p = Pore diameter
L = Characteristic length of system

Under this criterion, the LTE assumption is valid for Re→0 or Da→0. This implies that for relatively slow flow or for very small pore diameters, the LTE assumption is valid. Physically, this corresponds to the fluid particle temperature equaling that of its surrounding solid since the length scale inside the pore is relatively small. This result is consistent with the findings of Amiri and Vafai (1994), who established that the Darcy number (based on permeability) is the most important parameter in determining the validity of the LTE assumption and that the particle Reynolds number is also influential.

Since the pore diameter of graphite foam (roughly 350 microns) is relatively small compared to metal foams and other porous heat transfer media, the permeability (and corresponding Darcy number) is very low. Also, though a particular value is unknown at this time, the specific surface area is presumably high. Furthermore, the pressure-drop that occurs across low permeability media is rather significant, limiting most applications to relatively low fluid mass flowrates. As a result, most applications involving graphite foam will operate at low Reynolds numbers. Therefore, since flow through graphite foam can generally be characterized as having low Reynolds and Darcy numbers, and since the specific surface area of the foam is large, the LTE assumption is applicable and used in the present study.

Under this assumption, the heat transfer is governed by a single energy equation that treats both phases as one continuum. Therefore, the same equation is used for the fluid and porous regions, but the latter requires the use of an *effective* thermal conductivity (ETC) that represents the ability of the fluid-saturated porous medium to conduct heat.

4.3.2 Thermal Dispersion

Thermal dispersion is a heat transfer enhancement phenomenon that results from the intra-pore fluid mixing that occurs as a result of the tortuous path within a porous medium. Hunt ant Tien (1988) modeled thermal dispersion using a dispersion conductivity that is added to the stagnant conductivity in the effective thermal conductivity term of the energy equation(s). This term is used to capture enhanced heat transfer as fluid velocities are increased. However, Angirasa (2002) has shown that porous media with low permeability are typically exposed to low velocities where this phenomenon is absent. Therefore, no thermal dispersion effect was considered in the present study.

4.4 Height Estimation of the Corrugated Foam

In order to design graphite foam heat exchangers for compactness and to reduce the cross sectional area of flow, an estimate of the necessary foam height was made. In addition, for the three-dimensional simulations the number of nodes becomes quite large. Therefore, it is desirable to keep the height H of the corrugated foam to be sufficiently small to keep the computational domain and the associated number of nodes to a

necessary but manageable size. If thermal entrance conditions are maintained, the heat transfer coefficients will be higher than those in the thermally developed regime. Thus, for high heat transfer, H should be greater than or equal to the thermal boundary layer thickness at x=L for a force convection through a full foam block. The value of H can be estimated from the variation of the two-dimensional boundary layer thickness δ_T with x.

Using a scaling analysis, Nield (1999) has shown that for a semi-infinite porous medium, the thermal boundary layer thickness, δ_T, for both isothermal and constant heat flux boundaries scales with Peclet number, Pe_x, as

$$\delta_T \propto x\, Pe_x^{-1/2} \tag{4.21}$$

or

$$\frac{\delta_T}{x} \propto \sqrt{\frac{\alpha_m}{u_\infty x}} \tag{4.22}$$

where

$$\alpha_m \equiv \frac{k_m}{\rho_m Cp_m} \ . \tag{4.23}$$

Here, the subscript *m* denotes a matrix property.

Kaviany (1987), using an integral method, showed that for the Darcian flow regime with an isothermal boundary, the proportionality constant is $\sqrt{8}$. Thus,

$$\frac{\delta_T}{x} = \sqrt{\frac{8}{Pe_x}} = \sqrt{\frac{8\alpha_m}{u_\infty x}} \quad . \tag{4.24}$$

This may also be written as

$$\frac{\delta_T}{x} = 2.83\sqrt{\frac{\alpha_m}{u_\infty x}} \quad \text{where } T_W = \text{constant.} \tag{4.25}$$

For the case of constant heat flux at the boundary, the proportionality constant is not available in the literature, so its value was determined in this study. For the two-dimensional internal flow and heat transfer through a full block of graphite foam (i.e., no corrugations) with a uniform heat flux boundary, the proportionality constant is determined from numerical solutions in STAR-CD® for L=0.05 m and two values of Re_K^* (0.236 and 1.18) and a large value of H=L. From the temperature distribution results, the δ_T variation with x was obtained, and the proportionality constant was determined to be 2.73. Here, δ_T is determined as the distance normal to the heater surface where the local dimensionless temperature reaches 97 percent of its value far from the wall. Thus, thermal boundary layer thickness correlation becomes:

$$\frac{\delta_T}{x} = 2.73\sqrt{\frac{\alpha_m}{u_\infty x}} \qquad \text{where} \quad q'' = \text{constant} \tag{4.26}$$

The above result can be used for corrugated geometry of length L to determine its height H, the dimension of foam in the direction of the heat transfer. For a given length L, H can be taken to be thermal boundary thickness δ_T, and x replaced by L. Thus the estimate for H becomes:

$$\frac{H}{L} = 2.73\sqrt{\frac{\alpha_m}{u_\infty L}} \quad \text{where} \qquad q'' = \text{constant} \tag{4.27}$$

In this study, α_m for a water-graphite matrix was taken as 4.67e-5 m^2/s. For each of the three-dimensional simulations using STAR-CD® , H was set at a value near that calculated from equation (4.27).

4.5 Dimensionless Performance Parameters

4.5.1 Porous Media Friction Factor

Experimental findings by Ward (1964) revealed that when friction factor is defined as

$$f_K \equiv \frac{\Delta P_T}{(L/\sqrt{K})\rho U_o^2} \tag{4.28}$$

and Reynolds number as

$$\mathrm{Re}_K \equiv \frac{\rho U_0 \sqrt{K}}{\mu} = \frac{\mathrm{Re}_K^*}{c_F} \tag{4.29}$$

then, the pressure-drop results can be condensed in to one curve that is expressed by the equation

$$f_K = \frac{1}{\mathrm{Re}_K} + c_F \tag{4.30}$$

Note that equation (4.29) shows the relationship between two definitions of Reynolds number for porous media and that each has its own significance in the present study.

4.5.2 Heat Transfer Coefficient

In the present study, the average heat transfer coefficient is defined as

$$\bar{h} \equiv \frac{q''}{\left(\overline{T}_W - \frac{T_{b,in} + T_{b,out}}{2}\right)} \tag{4.31}$$

where q'' = Heat flux
$\overline{T}_W$ = Average heated wall temperature
$T_{b,in}$ = Inlet bulk temperature
$T_{b,out}$ = Outlet bulk temperature

Special care was taken to ensure that an energy balance was maintained by calculating the outlet bulk temperature based on the enthalpy flow rate balance. The definition of outlet bulk temperature used in this study is

$$T_{b,out} \equiv \frac{\sum_j (\rho U \Delta A)_j T_j}{\sum_j (\rho U \Delta A)_j} \tag{4.32}$$

where $(\rho U \Delta A)_j$ = Mass flowrate for each cell
j = Index of cell number

The average Nusselt number, or dimensionless heat transfer coefficient, is then defined as

$$\overline{Nu}_{Dh} \equiv \frac{\overline{h} D_h}{k_f}. \tag{4.33}$$

In this definition, the characteristic length is defined as the hydraulic diameter, $D_h \equiv 4 A_{cs} / P_w$; here, A_{cs} and P_w are the cross-sectional area and wetted perimeter of the of the flow passage. In the present study, the hydraulic diameter of the CHUC is

$$D_h \equiv \frac{2SH}{S+2H}. \tag{4.34}$$

Using the hydraulic diameter as the length scale, the Reynolds number can also be defined as

$$\mathrm{Re}_{D_h} = \frac{\rho U_o D_h}{\mu}. \tag{4.35}$$

4.5.3 Compact Heat Exchangers

A traditional method of evaluating performance of compact heat exchangers is by comparison of the Colburn-j, j_H, and friction factors as a function of Reynolds number. The friction factor based on hydraulic diameter is defined as

$$f \equiv \frac{\Delta P_T}{(L/D_h)\rho U_o^2}. \tag{4.36}$$

where ΔP_T is the total pressure-drop across the CHUC for minimum pressure-drop cases. Finally, the Colburn-j factor is defined as

$$j_H \equiv \frac{\bar{h}}{(\rho c_p)_f U_o} \mathrm{Pr}_f^{2/3}. \tag{4.37}$$

where Pr_f is the fluid Prandtl number.

Chapter 5

Software Implementation

5.1 Introduction

5.1.1 Governing Equations

The two-dimensional (2D) FEMLAB® and three-dimensional (3D) STAR-CD® models each consisted of two subdomains that were governed by separate momentum conservation equations. Upstream of the porous region, the Navier-Stokes momentum equation was used. In the porous region, a form of the quadratic porous media momentum equation was implemented. Each software has an inherent ability to model flow through porous media but requires a different method of manipulating the given porous media momentum equation to suit the current problem. An explanation of the required manipulation of the given porous media momentum equation in each software package will follow.

5.1.2 Boundary Conditions

A few boundary conditions are similar for both the 2D and 3D models. A constant inlet velocity is imposed since the lateral position of the corrugated unit cell within the full width is arbitrary. Although a parabolic velocity profile may be present over the full width (and over the height for that matter) of the device, that portion of the profile that approaches a particular unit cell is relatively uniform, and it differs from one unit cell to the next. A zero pressure boundary condition is imposed at the end of the foam length, which neglects the transport phenomena downstream of the foam. However, the most important heat transfer and flow behavior occurs before this downstream region.

Therefore, the value of static pressure at the inlet in the final solution is equal to the differential pressure across the unit cell. Finally, a symmetry boundary condition was imposed on each edge (2D) and face (3D) across which the unit cell mirrors itself with respect to the solution variables. Further explanation of the additional boundary conditions imposed for each model will follow in the appropriate section.

5.2 FEMLAB® Model

5.2.1 Governing Equations

Fluid Region

The incompressible, steady-state, constant viscosity form of the continuity and Navier-Stokes equations that are invoked by FEMLAB® were derived by Gresho and Sani (1998), and are reduced to (FEMLAB® User's Guide, 2002):

Mass: $$\nabla \cdot \mathbf{u} = 0 \tag{5.1}$$

Momentum: $$-\eta \nabla^2 \mathbf{u} + \rho(\mathbf{u} \cdot \nabla)\mathbf{u} + \nabla p = F \tag{5.2}$$

where $\mathbf{u}$ = Velocity vector
η = Dynamic (molecular) viscosity
ρ = Density
p = Pressure
F = Body force

Porous Region

In FEMLAB®, the two options for modeling flow through porous media are to use the Darcy or Brinkman equation provided. The Darcy equation in FEMLAB® does not

allow for the transverse components of the velocity vectors, i.e. multidirectional flow. However, the Brinkman equation in this software introduces the velocities in the spatial directions as dependent variables (FEMLAB® User's Guide, 2002). Therefore, although the effect of the Brinkman term is considered to be negligible in comparison with the Darcy and Forchheimer terms, it had to be included to incorporate multidimensional effects. In addition, the form drag effect must be implemented by manipulating the body force term, which will be described below.

In FEMLAB®, the steady-state, constant viscosity Brinkman equation is reduced to (FEMLAB® User's Guide, 2002):

$$-\eta\nabla^2\mathbf{u}+\frac{\eta}{k}\mathbf{u}+\nabla p=F \tag{5.3}$$

where k is the permeability of the porous medium. This equation resembles the Navier-Stokes equation (5.2), except the Darcy term is added as a flow resistance and the convective inertia term is dropped. In order to account for the quadratic term in the porous media momentum equation, the body force term, F, must be utilized. If we temporarily ignore the Brinkman (viscous) term in equation (5.3), the resulting equation is:

$$\nabla p=-\frac{\eta}{k}\mathbf{u}+F \tag{5.4}$$

The appropriate porous media momentum equation (4.7), with $\mathbf{u}$ as the velocity vector is restated here as:

$$\nabla P = -\frac{\mu}{K}\mathbf{u} - c_F K^{-1/2} \rho_f \left|\mathbf{u}\right| \mathbf{u} \tag{5.5}$$

We can see that the Forchheimer term must be added to the Brinkman equation by defining the body force term, F , as:

$$F \equiv -c_F K^{-1/2} \rho_f \left|\mathbf{u}\right| \mathbf{u} \tag{5.6}$$

5.2.2 Boundary Conditions

The boundary conditions for the 2D FEMLAB® model are shown in Figure 5.1, where the subscripts *p* and *f* designate the porous and fluid regions, respectively. The inlet velocity was set to a constant whose value was based on the Reynolds number of the particular run in the parametric study. Symmetric boundaries, in which the normal component of the velocity vector was set to zero, were imposed on the centerlines of the inlet and outlet slots. In FEMLAB® (unlike STAR-CD® ,which will be shown in the next section), the interfacial boundary conditions between the fluid and porous regions must be specified by designating the velocity on the entrance and the pressure on the exit of each region. Therefore, on the upstream end of the porous region, designated by the blue line in Figure 5.1, the fluid-side pressure was set equal to the porous-side pressure in order to satisfy the Navier-Stokes equations; and the porous-side velocity was set equal to the fluid-side velocity in order to satisfy the Brinkman equation. Likewise, on the downstream end of the porous region, designated by the red line in Figure 5.1, the porous-side pressure was set equal to the fluid-side pressure in order to satisfy the Brinkman equation; and the fluid-side velocity was set equal to porous-side velocity in

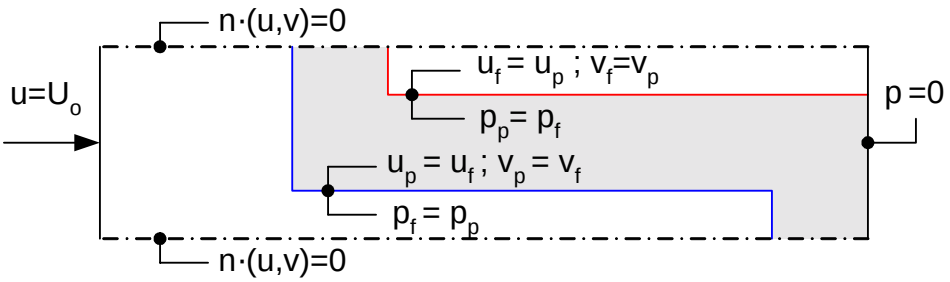

Figure 5.1. The boundary conditions of the FEMLAB® model.

order to satisfy the Navier-Stokes equation. Finally, the pressure was set equal to zero for both the fluid and porous regions at the outlet of the model.

5.2.3 Grid Considerations

The 2D FEMLAB® models were built with a mesh algorithm that concentrated nodes in certain locations where high velocity and pressure gradients were expected. An example is shown in Figure 5.2, which shows the finite element mesh for L=0.05 m, L/S=2, C/S=0.1. The corners at the inlet, the exit, and in the slots possessed the highest node concentration. In addition, an arc with length S/4 was placed before the inlet slot entrance in recognition of the large gradients expected due to the presence of the sudden contraction. Also, most of the edges in the model contained small cell lengths, especially those on the porous-fluid interface. The tolerance, or magnitude of the difference in solution for each variable between successive iterations, was set to 10^{-7}, and convergence was reached for all 2D simulations, whose results are reported in this thesis.

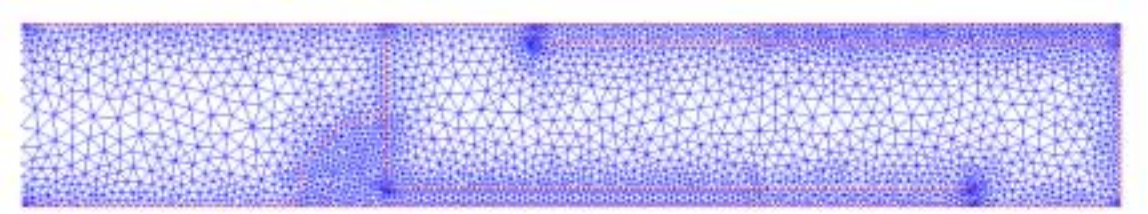

Figure 5.2. Example of mesh in the FEMLAB® model.

5.3 STAR-CD® Model

5.3.1 Governing Equations

Fluid Region

The steady-state form of the conservation equations in STAR-CD® for a homogeneous fluid were derived by Warsi (1980), and are reduced to (STAR-CD® Methodology, 2002):

Mass:
$$\frac{\partial}{\partial x_j}\left(\rho\tilde{u}_j\right)=0 \tag{5.7}$$

Momentum:
$$\frac{\partial}{\partial x_j}\left(\rho\tilde{u}_j u_i-\tau_{ij}\right)=-\frac{\partial p_p}{\partial x_i} \tag{5.8}$$

Energy:
$$\frac{\partial}{\partial x_j}\left(\rho\tilde{u}_j h_t-F_{h_t,j}\right)=\tilde{u}_j\frac{\partial p_p}{\partial x_j}+\tau_{ij}\frac{\partial u_i}{\partial x_j} \tag{5.9}$$

Here, the following terms are also defined:

$$h_t \equiv \bar{c}_p T \tag{5.10}$$

$$F_{h_t,j} = k\frac{\partial T}{\partial x_j} \tag{5.11}$$

$$\tau_{ij} = 2\mu s_{ij} - \frac{2}{3}\mu\frac{\partial u_k}{\partial x_k}\partial_{ij} \tag{5.12}$$

$$\partial_{ij} = \begin{cases} 1 & i = j \\ 0 & i \neq j \end{cases} \tag{5.13}$$

$$s_{ij} = \frac{1}{2}\left(\frac{\partial u_i}{\partial x_j} + \frac{\partial u_j}{\partial x_i}\right) \tag{5.14}$$

where x_i = Cartesian coordinate (i=1,2,3)

ρ = Density

$\tilde{u}_j$ = $u_j - u_{cj}$, relative velocity between fluid and local (moving) coordinate frame that moves with velocity u_{cj}

u_i = Absolute fluid velocity component in direction x_i

τ_{ij} = Stress tensor components

p_p = Piezometric pressure = $p_s - \rho_0 g_m x_m$ where p_s is static pressure, ρ_0 is reference density, the g_m are gravitational field components and the x_m are coordinates from a datum, where ρ_0 is defined.

h_t = Thermal enthalpy

$F_{h_t,j}$ = Diffusional thermal energy flux in direction x_j

k = Thermal conductivity

τ_{ij} = Stress tensor components

μ = Molecular viscosity

s_{ij} = Rate of strain tensor

∂_{ij} = Kronecker delta function

Porous Region

STAR-CD® allows the user to model a porous region as a "distributed resistance." In this region, the cells are designated as fluid cells in which there exists a local balance

between pressure and these "distributed resistance" forces. This balance is defined as (STAR-CD® Methodology, 2002):

$$-K_i u_i = \frac{\partial p_p}{\partial \zeta_i} \tag{5.15}$$

where $\zeta_i (i = 1,2,3)$ = The (mutually orthogonal) orthotropic directions
K_i = Permeability
u_i = Superficial velocity in direction ζ_i

Here, permeability is given in the form:

$$K_i = \alpha_i |\vec{v}| + \beta_i \tag{5.16}$$

It should be noted that the permeability, K_i, in STAR-CD® is not equivalent to the traditional permeability, K, which is actually embedded within the α_i and β_i terms in the above equation.

Combining equations (5.15) and (5.16) returns

$$\frac{\partial p_p}{\partial \zeta_i} = -(\alpha_i |\vec{v}| + \beta_i) u_i = -\beta_i u_i - \alpha_i |\vec{v}| u_i \tag{5.17}$$

Restating equation (4.7) here, with $\mathbf{v} = u_i$

$$\nabla P = -\frac{\mu}{K} u_i - c_F K^{-1/2} \rho_f |u_i| u_i \tag{5.18}$$

It can be seen that the following coefficients can be defined:

$$\alpha_i \equiv c_F K^{-1/2} \rho_f \tag{5.19}$$

$$\beta_i \equiv \frac{\mu}{K} \tag{5.20}$$

5.3.2 Boundary Conditions

The boundary conditions for the STAR-CD® model are shown in Figure 5.3. The inlet boundary condition consisted of a uniform velocity and an inlet temperature of 20°C, or 293.15 K, at which the constant fluid properties were evaluated, while the outlet boundary condition was set at zero piezometric pressure. Symmetric boundaries were placed on the mid-planes of the inlet and outlet slots. The symmetry boundary condition in STAR-CD® means that the normal velocity and normal gradients of all other variables are set to zero (STAR-CD® Methodology, 2002). A no-slip, constant flux condition of 12 W/cm^2 was imposed to simulate the heat source that extends the entire length of foam. This heat flux value was the same as that used by Osgood (2001). The remaining boundaries were adiabatic, no-slip walls located on the bottom surface and on the top region upstream of the foam.

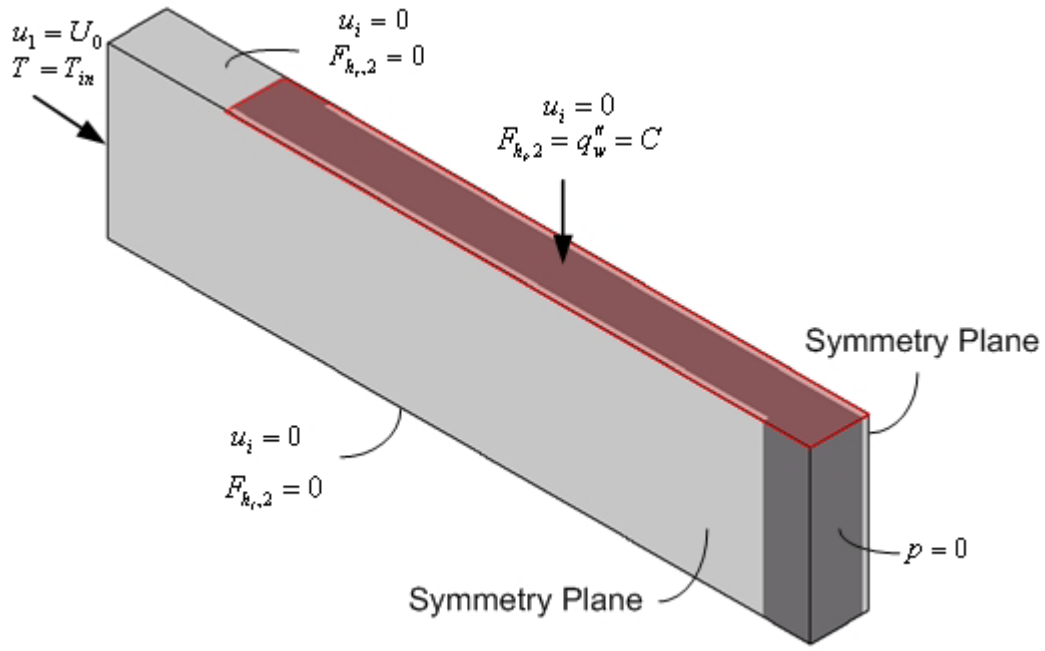

Figure 5.3. The boundary conditions of the STAR-CD® model.

5.3.3 Grid Considerations

The 3D STAR-CD® models were built with a structured mesh consisting of hexahedra that were most concentrated at the heated surface and grew in size in the height direction. In addition, in every case at least four cells were located in the slots of the CHUC. A study was conducted to determine the influence of grid refinement and tolerance of STAR-CD® models. The results of this study are shown in Appendix A.

Chapter 6

Results

6.1 Two-dimensional Hydrodynamic Results

The cases that were investigated included CHUC lengths of 0.05, 0.075, and 0.10 m. At each length, the geometric parameters L/S and C/S were varied from 2 to 10 and 0.075 to 0.0175, respectively. Furthermore, these cases were run at modified Reynolds numbers, Re_K^*, ranging from 0.01 to 1.

The porous media friction factor, defined by equation (4.28), of each configuration in the parametric study was plotted for a fixed Reynolds number in order to determine the relative importance of L/S and C/S, as shown in Figure 6.1 (a) and (b) for the cases of L=0.05 m and Re_K^* =0.1 and Re_K^* =1, respectively. Similar plots showing the results for the remaining lengths and Reynolds numbers are presented in Appendix B. In addition, a list of the optimal configurations based on the minimum total friction factor is shown in Table 6.1, which can be used as a reference for design work. Figure 6.1 (a) shows that for a fixed C/S, a minimum value of friction factor exists at a certain L/S value. Furthermore, the L/S value at which this occurs increases with C/S. For each C/S curve, increasing L/S initially results in a dramatic decrease in friction factor before reaching the minimum point. At this point, any further increase in L/S results in a gradual rise of friction factor. For fixed L/S, an increase in C/S reduces the friction factor. For higher L/S values, this friction factor reduction becomes more dramatic.

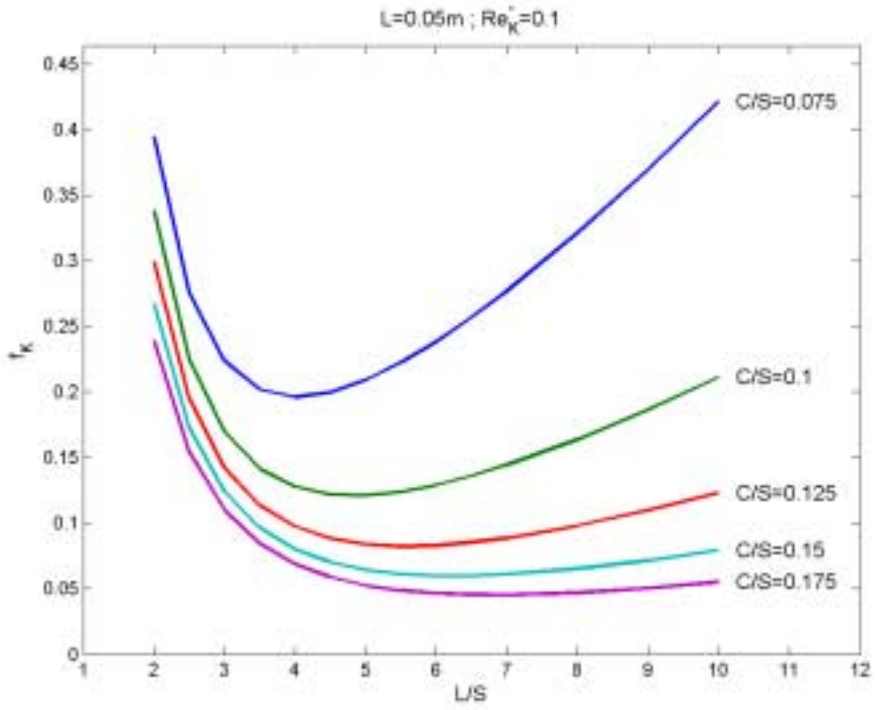

(a)

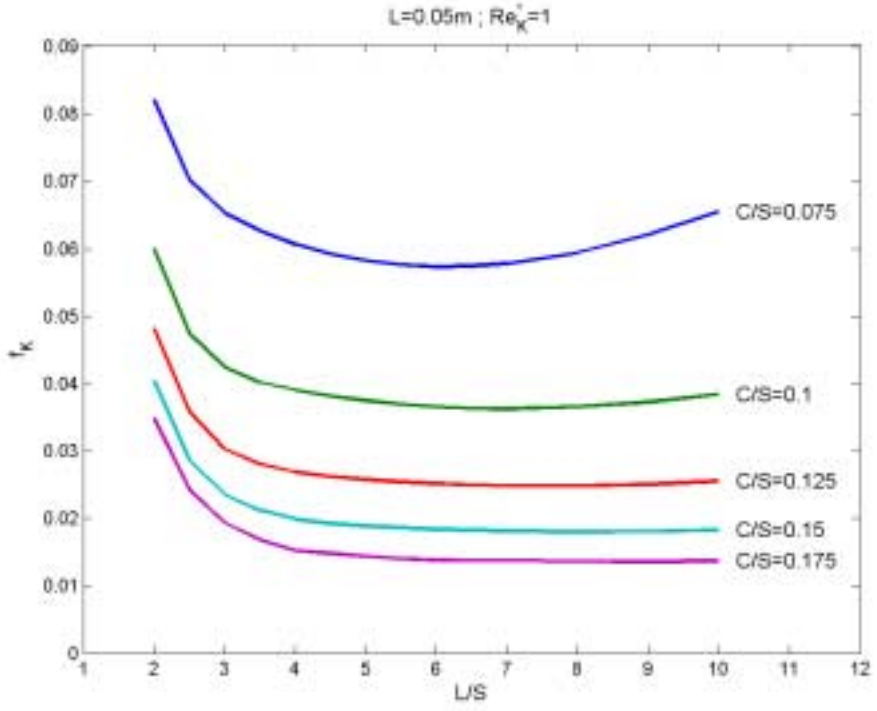

(b)

Figure 6.1. Porous media friction factor variation with L/S for several values of C/S, for L=0.05 m , and (a) Re_K^* =0.1 and (b) Re_K^* =1.

Table 6.1 Optimal Geometric Configurations and the Friction Factors

$Re^*_K = 0.01$								
L = 0.050 m			L = 0.075 m			L = 0.100 m		
C/S	L/S	f_K	C/S	L/S	f_K	C/S	L/S	f_K
0.075	4	1.638	0.075	5	1.096	0.075	5.5	0.8211
0.1	5	1.024	0.1	6	0.683	0.1	6.5	0.5133
0.125	5.5	0.7039	0.125	7	0.4704	0.125	8	0.353
0.15	6	0.5157	0.15	8	0.3454	0.15	9	0.258
0.175	7	0.3918	0.175	8	0.2623	0.175	10	0.1969
$Re^*_K = 0.050$								
L = 0.050 m			L = 0.075 m			L = 0.100 m		
C/S	L/S	f_K	C/S	L/S	f_K	C/S	L/S	f_K
0.075	4	0.3545	0.075	5	0.238	0.075	5.5	0.1787
0.1	5	0.2205	0.1	6	0.1474	0.1	6.5	0.1109
0.125	5.5	0.1508	0.125	7	0.1011	0.125	8	0.07587
0.15	6	0.1101	0.15	8	0.07389	0.15	9	0.05534
0.175	7	0.08351	0.175	8	0.056	0.175	10	0.04211
$Re^*_K = 0.100$								
L = 0.050 m			L = 0.075 m			L = 0.100 m		
C/S	L/S	f_K	C/S	L/S	f_K	C/S	L/S	f_K
0.075	4	0.1961	0.075	5	0.1323	0.075	5.5	0.09972
0.1	5	0.1211	0.1	6	0.08129	0.1	6.5	0.06123
0.125	5.5	0.08243	0.125	6.5	0.0554	0.125	8	0.0417
0.15	6	0.05995	0.15	8	0.04032	0.15	9	0.03025
0.175	7	0.0454	0.175	8	0.03048	0.175	10	0.02295
$Re^*_K = 0.200$								
L = 0.050 m			L = 0.075 m			L = 0.100 m		
C/S	L/S	f_K	C/S	L/S	f_K	C/S	L/S	f_K
0.075	4	0.1198	0.075	5	0.08164	0.075	5.5	0.06186
0.1	5	0.0732	0.1	6	0.04942	0.1	6.5	0.03739
0.125	5.5	0.04928	0.125	6.5	0.03332	0.125	8	0.02522
0.15	6	0.03559	0.15	8	0.02406	0.15	9	0.0181
0.175	7	0.02684	0.175	8	0.01808	0.175	10	0.01364

Table 6.1. Continued.

Re^*_K = 0.300									
L = 0.050 m			L = 0.075 m			L = 0.100 m			
C/S	L/S	f_K	C/S	L/S	f_K	C/S	L/S	f_K
0.075	4	0.09559	0.075	5	0.06578	0.075	5.5	0.05016
0.1	5	0.05816	0.1	6	0.0395	0.1	7	0.03002
0.125	5.5	0.03887	0.125	6.5	0.02644	0.125	8	0.02012
0.15	6.5	0.02796	0.15	8	0.01897	0.15	9	0.01431
0.175	6.5	0.02098	0.175	8	0.01419	0.175	10	0.01073
Re^*_K = 0.400									
L = 0.050 m			L = 0.075 m			L = 0.100 m			
C/S	L/S	f_K	C/S	L/S	f_K	C/S	L/S	f_K
0.075	4	0.08379	0.075	5	0.05812	0.075	5.5	0.04461
0.1	5	0.05096	0.1	6	0.03482	0.1	7	0.02657
0.125	5.5	0.03396	0.125	6.5	0.02323	0.125	7	0.01769
0.15	6.5	0.02432	0.15	8	0.01658	0.15	8	0.01255
0.175	6.5	0.01824	0.175	8	0.01238	0.175	10	0.00938
Re^*_K = 0.500									
L = 0.050 m			L = 0.075 m			L = 0.100 m			
C/S	L/S	f_K	C/S	L/S	f_K	C/S	L/S	f_K
0.075	4.5	0.07627	0.075	5	0.05331	0.075	5.5	0.04133
0.1	5	0.04668	0.1	6	0.03211	0.1	7	0.02457
0.125	5.5	0.03113	0.125	6.5	0.02121	0.125	6.5	0.01632
0.15	6	0.02234	0.15	7	0.01529	0.15	8	0.01155
0.175	6.5	0.01669	0.175	8	0.01139	0.175	10	0.00861
Re^*_K = 1.000									
L = 0.050 m			L = 0.075 m			L = 0.100 m			
C/S	L/S	f_K	C/S	L/S	f_K	C/S	L/S	f_K
0.075	6	0.05734	0.075	7	0.04128	0.075	8	0.03241
0.1	7	0.03627	0.1	8	0.02578	0.1	10	0.02006
0.125	8	0.02484	0.125	10	0.01744	0.125	10	0.01346
0.15	8	0.01804	0.15	10	0.01257	0.15	9	0.00967
0.175	9	0.01357	0.175	10	0.00937	0.175	10	0.0072

Figure 6.1 (b) shows that as Reynolds number is increased to 1.0, the curves for each C/S value become less parabolic compared to Figure 6.1 (a). This means that the range of L/S at which the friction factor is within a small percentage of the minimum is increased. In addition, while the magnitude of Reynolds number increases by a factor of 10 from Figure 6.1 (a) to 6.1 (b), the pressure-drop magnitudes (which must be calculated from friction factor) increased by a factor of approximately 30. This can be explained by the Forchheimer effect that becomes significant at high Reynolds number.

An explanation of the various effects described above can be found by analyzing the individual contributions that C/S, L/S, and Re_K^* have on the overall results. In order to illustrate the detailed physics of flow that contribute to the overall pressure-drop, the velocity vectors and pressure contours from the 2D models were explored. In addition, the static pressure distribution along the symmetry axes of the inlet and outlet slots was analyzed. Figure 6.2 (a) shows the overlay of both velocity vectors and corresponding pressure contours for the case of L=0.05 m, L/S=5, C/S=0.1, Re_K^* =0.1. The blue and red centerlines in Figure 6.2 (a) designate the slot locations at which static pressure was displayed in Figure 6.2 (b).

As shown in Figure 6.2 (a) and (b), the flow accelerates as it enters the inlet slot, and the static pressure drops dramatically in the entrance region. This behavior is similar to that of flow at a sudden contraction, where the increase in inertial forces from fluid acceleration causes a steep reduction in static pressure. In addition, some of the flow

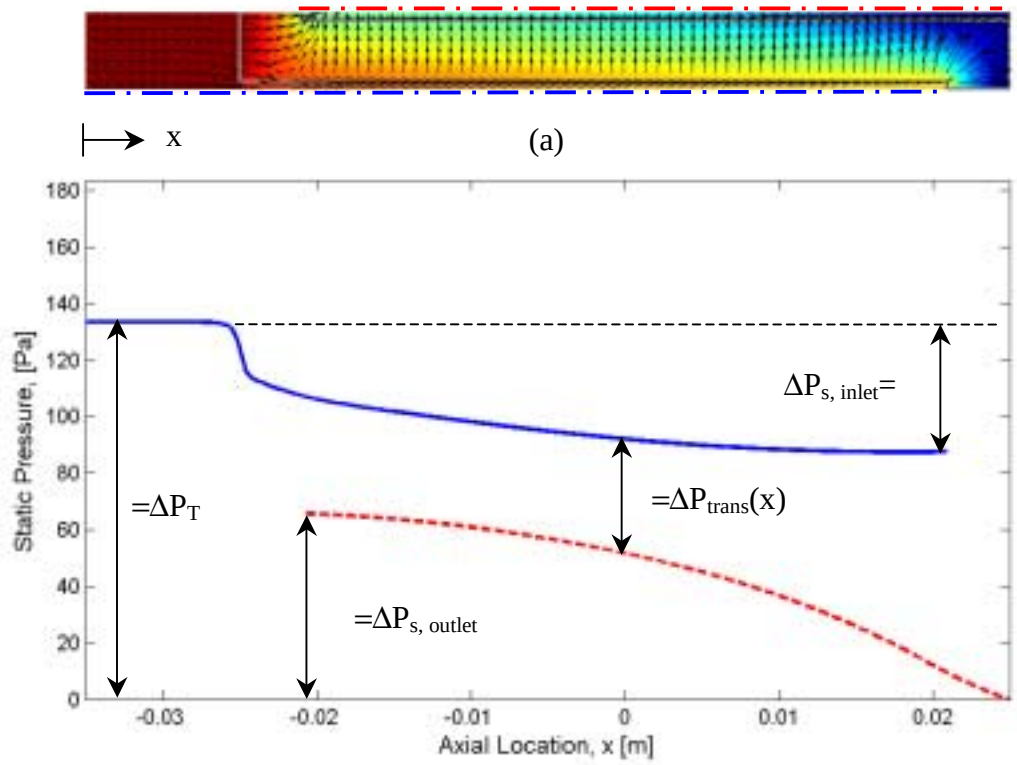

Figure 6.2. The velocity vectors and pressure contours (a) and the slot static pressure (b) for L=0.05 m, L/S=5, C/S=0.1, $Re_K^* = 0.1$.

enters the frontal face of the foam. Most of the flow that enters the foam at this location proceeds to the beginning of the outlet slot, and a small portion returns to the inlet slot after briefly crossing through the sharp corner of foam at the slot entrance. After its initial drop, the pressure continues to fall until the end of the inlet slot. This continuous pressure loss is attributed to viscous effects resulting from fluid layer shear stress, similar to flow along a duct. The total pressure-drop from the entrance of the inlet slot to the end of the inlet slot, $\Delta P_{s,\,inlet}$, is shown in Figure 6.2 (b).

It should be noted that there are some cases in which the static pressure actually rises just prior to the end of the inlet slot. When this is the case, a stagnation effect causes the fluid to accumulate at the end of the inlet slot . As a result, the high pressure propagates upstream, and the location of minimum pressure point in the inlet slot occurs upstream of the slot end.

As the fluid travels down the inlet slot, some of the fluid flows transversely across the foam in the z-direction to the outlet slot. The transverse flow is relatively uniform along the length of the inlet slot, which is reflected in the velocity vector distribution and the slot pressure curves in Figure 6.2. The transverse pressure-drop, $\Delta P_{trans}(x)$, from the inlet to the outlet slot is a function of axial location and represents an approximation of the pressure-drop that occurs across the foam in the z-direction. Uniform flow distribution in this direction occurs when the slot pressure curves are separated by a relatively equal difference in pressure. This pressure difference is larger at the end of the inlet slot, where the velocity vectors are larger in magnitude.

After the fluid passes through the foam, the pressure decreases in the outlet slot until its final location beyond the corrugated unit. This pressure-drop is attributed to the acceleration of the fluid as a gradual gain of fluid from transverse flow occurs along the outlet slot. The pressure reaches zero at the end of the outlet slot, satisfying the boundary condition imposed at this location. The total pressure-drop from the entrance of the outlet slot to the end of the outlet slot, $\Delta P_{s,\,outlet}$, is shown in Figure 6.2 (b).

6.1.1 Effect of L/S

For fixed L, holding C/S constant allows one to see the effect of varying only L/S by decreasing S. A constant C/S has an important implication regarding heat transfer. Specifically, a constant C/S is equivalent to a fixed t/S, which means that the total relative contact area between the heat source and the corrugated foam remains the same with increasing L/S.

A decrease in S results in a smaller foam thickness, which was one of the initial motivations for corrugating the foam. However, decreasing S also decreases slot width, and further analysis was necessary to determine the contribution this effect has on total pressure-drop. Recall from Figure 6.1 (a) that for each C/S value there is a minimum in total pressure-drop as L/S increases, and that for C/S=0.1, this occurs at L/S=5. This can be designated the design point for C/S=0.1. To determine the cause of the occurrence of a minimum pressure-drop, the relative effects of $\Delta P_{trans}(x)$, $\Delta P_{s,\,in}$, and $\Delta P_{s,\,out}$ were analyzed. Figure 6.3 shows the distribution of static pressure along the inlet and outlet slots as L/S was increased from 3 to 7 for L = 0.05 m, $Re_K^* = 0.1$, and C/S = 0.1. In this figure, the pressure-drop prior to the entrance edge of the inlet slot is not shown.

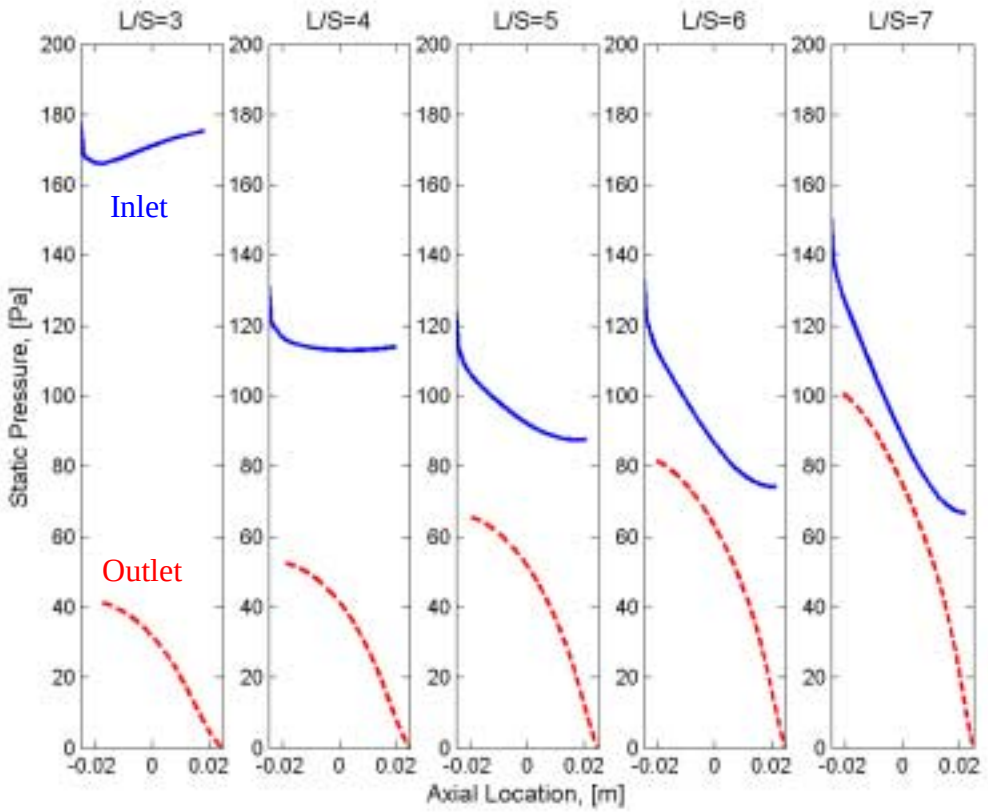

Figure 6.3. Static pressure along inlet and outlet slots for L=0.05m, Re_K^* =0.1, C/S=0.1.

Here, it is shown that as L/S increases from 3 to 5 (where 5 represents the configuration with minimum ΔP_T , or the design point), $\Delta P_{trans}(x)$ decreases as a consequence of the foam thickness reduction, as can be seen by the narrowing of the pressure difference between the two curves, and ΔP_T decreases accordingly. As L/S is increased beyond the design point, $\Delta P_{trans}(x)$ continues to decrease, but the ΔP_T actually increases. This increase in ΔP_T for L/S values greater than the design point is primarily due to the contribution of pressure-drop in both slots as the slot width decreases. When ΔP_T is dominated by the slot pressure-drop effect, as shown in this Figure 6.3 for L/S=7, the

transverse flow is significantly reduced, which results in a non-uniform flow distribution across the foam. The existence of flow uniformity can be seen in Figure 6.4, which shows the velocity vectors and pressure contours for the corresponding cases. Here it is shown that ΔP_T is increased by changing L/S from 5 to either 4 or 6; however, a more uniform flow distribution occurs at L/S=4. This effect suggests that if the L/S value that produces a minimum pressure-drop can not be implemented due to additional design or manufacturing limitations, it is more desirable to seek a reasonable value of L/S that is lower than the initial design point. Such a case would result in ΔP_T somewhat higher than optimal. L/S values higher than the design point will result in non-uniform flow across the foam, which is highly undesirable for heat transfer.

Therefore, for each C/S curve in Figure 6.1 (a), a minimum total pressure-drop occurs at certain L/S values because a balance exists between the reduction of flow resistance caused by decreasing foam thickness and an increase in slot pressure caused by decreasing slot width. Furthermore, when L/S is higher than the design point, the total pressure-drop is dominated by the slot pressure-drop effect, and the flow across the foam becomes less uniform, which adversely affects heat transfer.

6.1.2 Effect of C/S

For a fixed L/S, C/S was varied to examine its role in the reduction of total pressure-drop. From Figure 6.1 (a), it was seen that for a fixed L/S, increasing C/S reduces ΔP_T dramatically. Figure 6.5, which shows slot pressure as C/S varies from 0.075 to 0.175 in increments of 0.025 for the cases of L=0.05m, $\mathrm{Re}_K^* = 0.1$, L/S=5, displays the relative contributions that transverse flow and slot flow have on ΔP_T. As

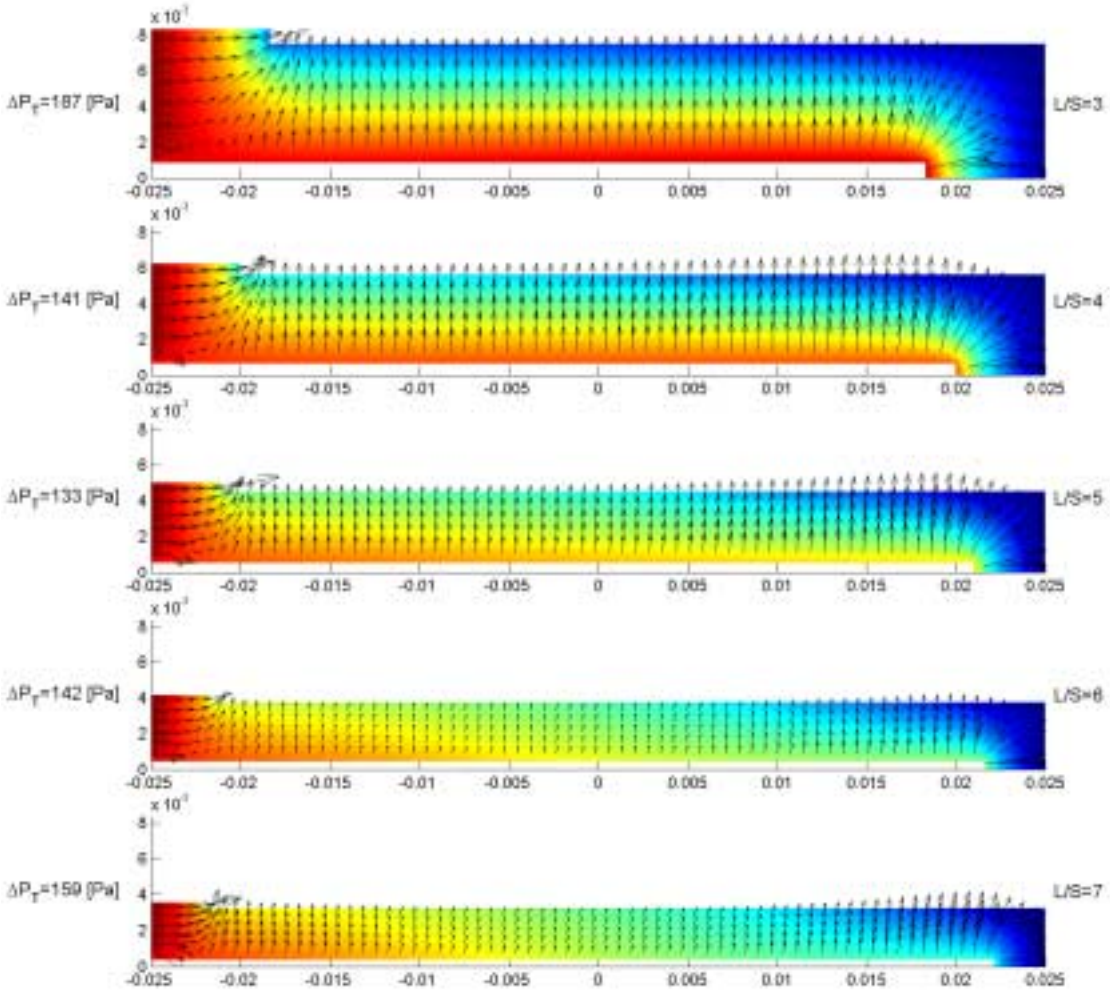

Figure 6.4. Effect of L/S on velocity vectors, pressure contours, and ΔP_T for L=0.05m, $\mathrm{Re}_K^* = 0.1$, C/S=0.1.

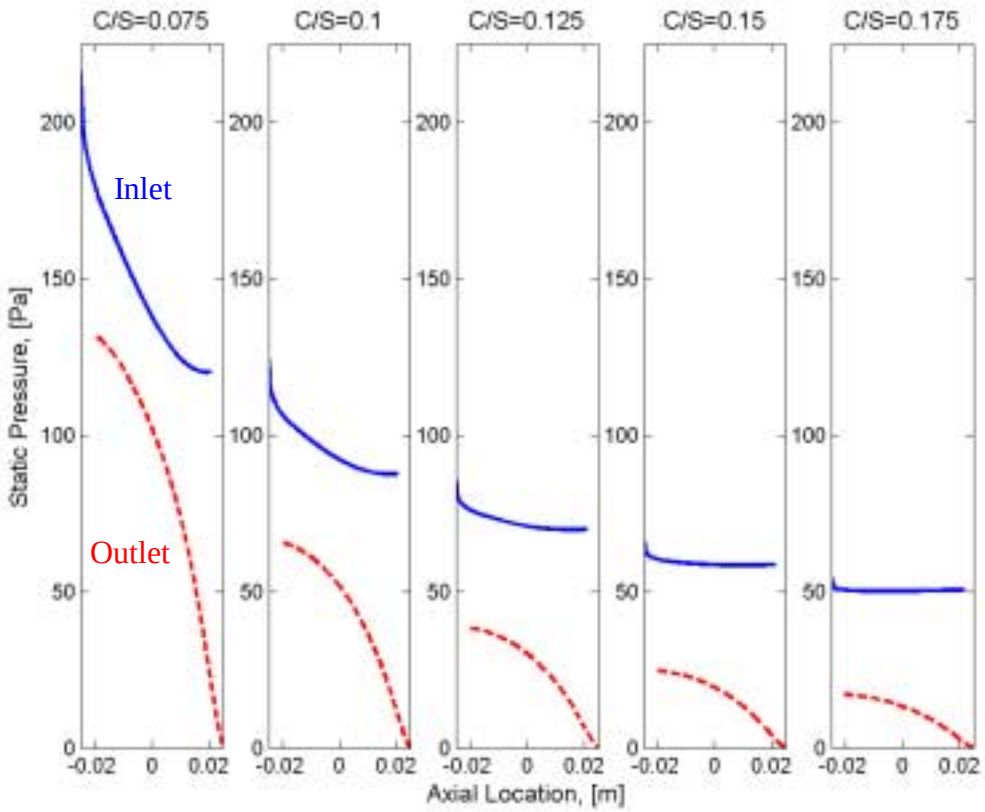

Figure 6.5. Effect of C/S on static pressure along inlet and outlet slots for L=0.05m, $Re_K^* = 0.1$, L/S=5.

C/S increases, the foam thickness decreases, so $\Delta P_{trans}(x)$ decreases as a result. However, it is shown here that for fixed L/S, decreasing the foam thickness has a relatively small effect on the reduction of ΔP_T in comparison with the slot pressure-drop effect, which is most apparent in this figure for the case of C/S=0.075. Here, C is relatively small, so the fluid accelerates dramatically in both slots, and the momentum of the fluid prevents a substantial amount of transverse flow across the foam. As a result, the pressure-drop within the slots outweighs that across the foam, and this slot pressure-drop is very sensitive to increasing C/S for relatively small slot widths.

Further, as C/S increases, the velocity vector and pressure gradient distribution across the foam becomes more uniform. This effect is shown in Figure 6.6, which shows the velocity vectors and pressure contours while C/S varies from 0.075 to 0.175 in increments of 0.025 for the case of L=0.05m, $Re_K^* = 0.1$, L/S=5. Although a large C/S is beneficial to both the reduction in total pressure-drop and the increase of flow uniformity, the contact area between the foam and the heat source is reduced, resulting in lower heat transfer. As will be shown later, hot spots occur at the locations at which no foam is in contact with the heat source, and this effect must be minimized.

6.1.3 Reynolds Number Effect

In Figure 6.7, velocity vectors and pressure contours are plotted for $Re_K^* = 0.01$, 0.05, 0.1, 0.5, and 1.0 where L=0.05 m, C/S=0.1, L/S =5. It is evident from this figure that a non-uniform flow distribution across the foam is prevalent for relatively high Reynolds numbers. The transition from relatively uniform to non-uniform flow distribution across the foam appears to occur around $Re_K^* = 0.1$ For cases in which flow is faster than this, the predominant flow across the foam occurs at the leading and trailing sections of the corrugated geometry.

For relatively high Reynolds number flows, the ratio of inertia to viscous forces in the fluid region and the ratio of form to viscous drag imposed by the porous region are increased. As a result, the ability of the fluid to change direction diminishes. Therefore, the fluid velocity component in the primary flow direction (parallel to the slots)

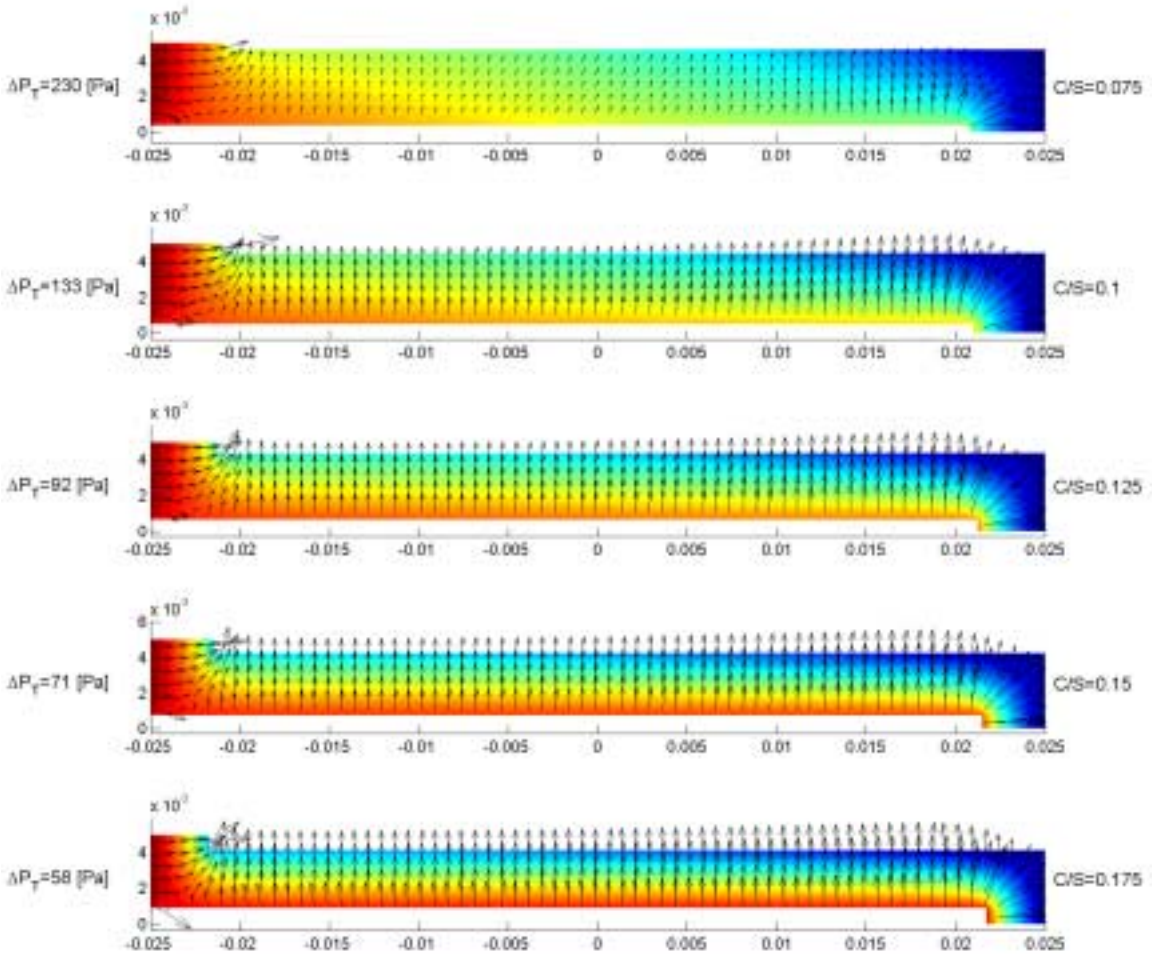

Figure 6.6. Effect of C/S on velocity vectors, pressure contours, and ΔP_T for L=0.05m, Re_K^* =0.1, L/S=5.

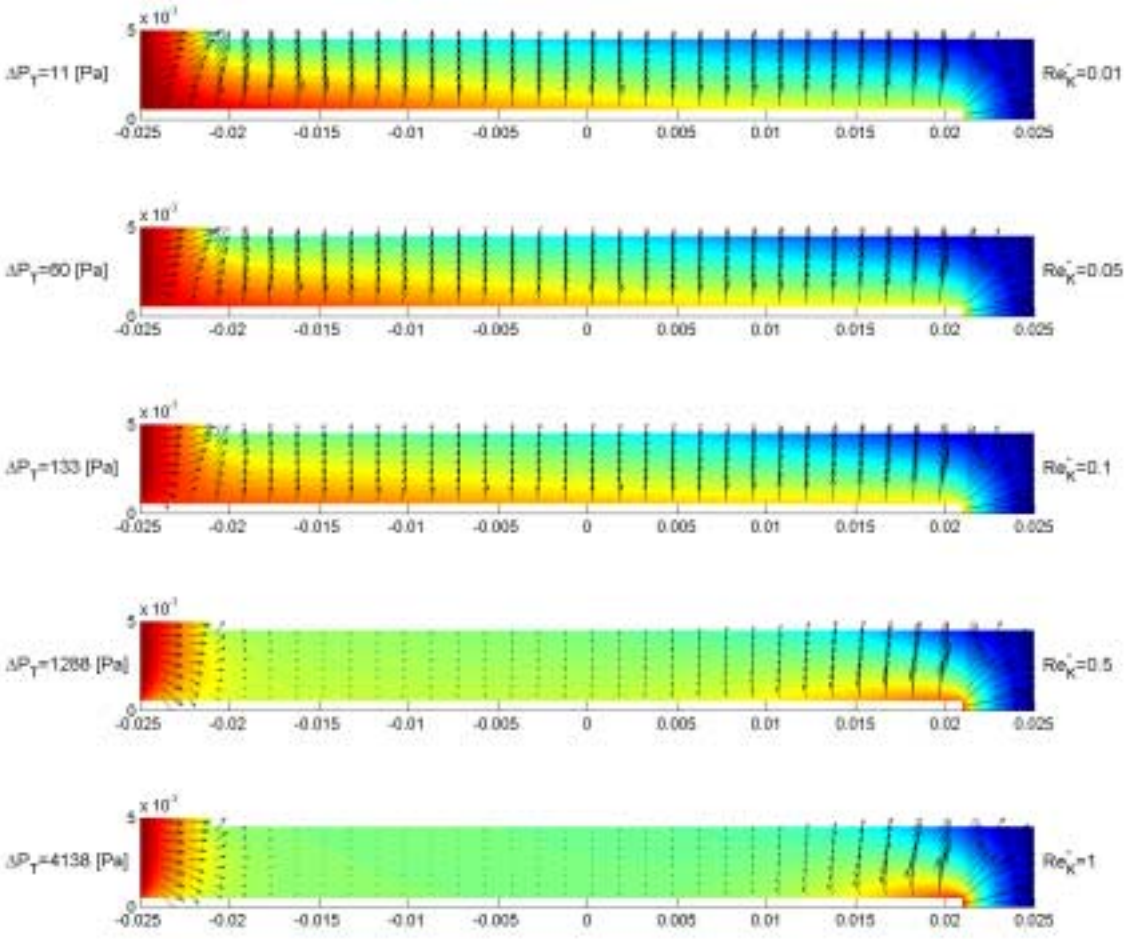

Figure 6.7. Effect of Re_K^* on velocity vectors, pressure contours, and ΔP_T for L=0.05m, L/S=5, C/S=0.1.

dominates that in the transverse direction. Since the relative magnitudes of the transverse component of the velocity vectors are reduced as Reynolds number increases, the transverse section of the foam becomes less effective. Therefore, high Reynolds number flows should be avoided if possible.

6.2 Three-dimensional Results

Reducing the pressure-drop is of utmost importance for porous heat exchangers, so the 2D FEMLAB® results were used to identify minimum pressure-drop configurations that were referred to as the optimal configurations. These configurations should be competitive with conventional compact heat exchangers. It was necessary to determine the heat transfer performance in only these optimal configurations. The heat transfer problem is three-dimensional, as previously indicated. To conduct 3D simulations in STAR-CD® , the height dimension based on equation (4.27) was used.

In order to simplify the mesh generation process in STAR-CD®, slight variations from the optimal values (yet preserving uniform transversal flow with values of L/S slightly lower than optimal values) of the geometric parameters had to be used for some of the optimal configurations. In the mesh generation process, a fixed minimum cell length was used for all cases having same L, and as a result, L/S and C/S values could not exactly correspond with the desired values for the 2D results. However, the case of L/S=5 and C/S=0.1 matched the 2D configuration so that a comparison of 2D and 3D results could be made.

6.2.1 3D Pressure Distributions

Three-dimensional plots of static pressure for a CHUC are shown in Figure 6.8 for the cases of $\mathrm{Re}_K^* = 0.1$ (a) and $\mathrm{Re}_K^* = 0.5$ (b) for L=0.05m, C/S=0.100, L/S=5.00. This figure shows that the dominant pressure-drop effects occur in the plane perpendicular to the slot mid-planes, indicating that the pressure distribution is 2D. Therefore, the calculation of pressure-drop using the 2D model is well justified. In addition, flow uniformity is represented in Figure 6.8 (a) by relatively constant width pressure contours along the transverse section of the foam. In Figure 6.8 (b) the absence of uniform width of the pressure contours indicates that the flow distribution is non-uniform at higher Reynolds numbers. These observations are consistent with the 2D results.

When the results were compared for the case where L=0.05m, C/S=0.100, L/S=5.00, the 3D pressure-drop results were about 10 % below the 2D results, indicating that the FEMLAB® simulations were more conservative approximations than those of STAR-CD® . This difference is likely due to the limitation imposed on the mesh quality within the slots of the 3D model. In order to keep the total number of nodes from exceeding about one million, no more than five cells were used within each of the half-slots in the transverse direction.

6.2.2 Effectiveness of Corrugations

Ward (1964) determined that plotting friction factor based on a length scale of $\sqrt{K}$ versus Re_K for flow through a channel filled with a porous medium condensed all experimental results into a single curve. A similar curve for graphite foam using equation (4.30) is shown in Figure 6.9, labeled as “Full Block” in the legend. The

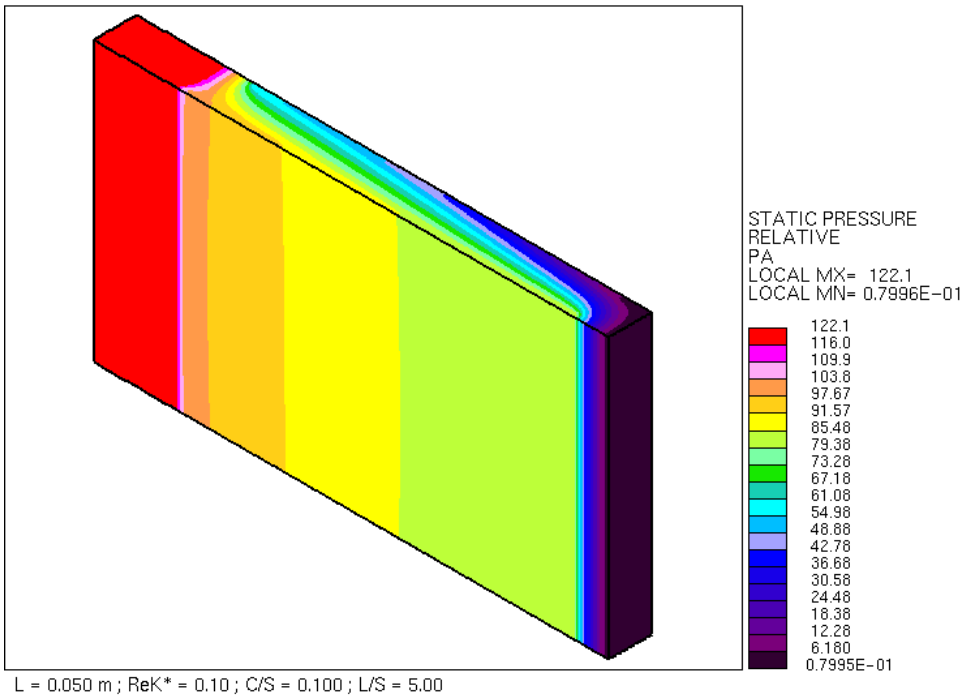

(a)

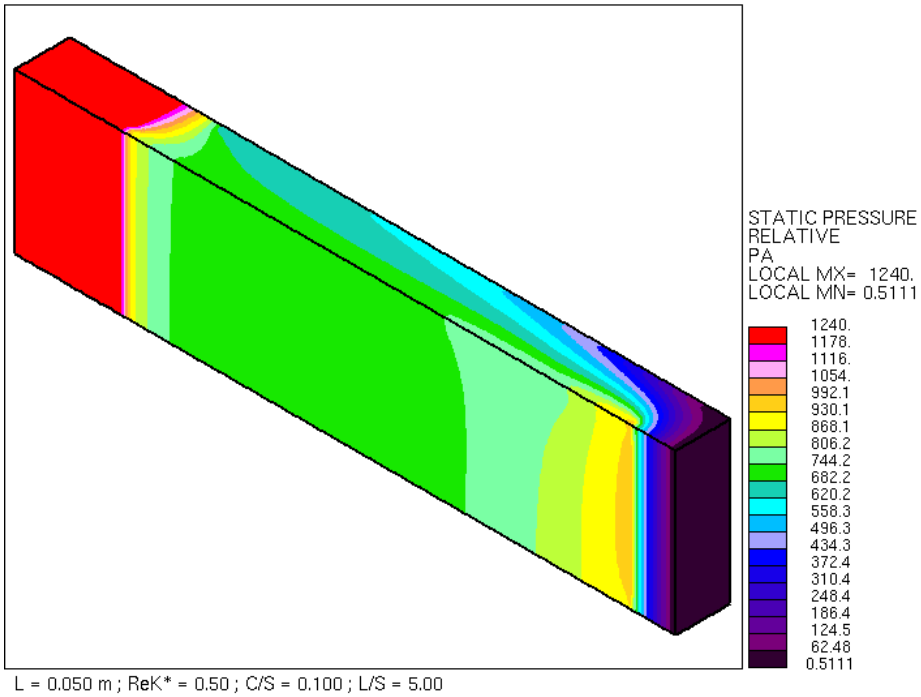

(b)

Figure 6.8. Three-dimensional static pressure for L=0.05m, C/S=0.100, L/S=5.00, and Re_K^* =0.10 (a) and Re_K^* =0.50 (b).

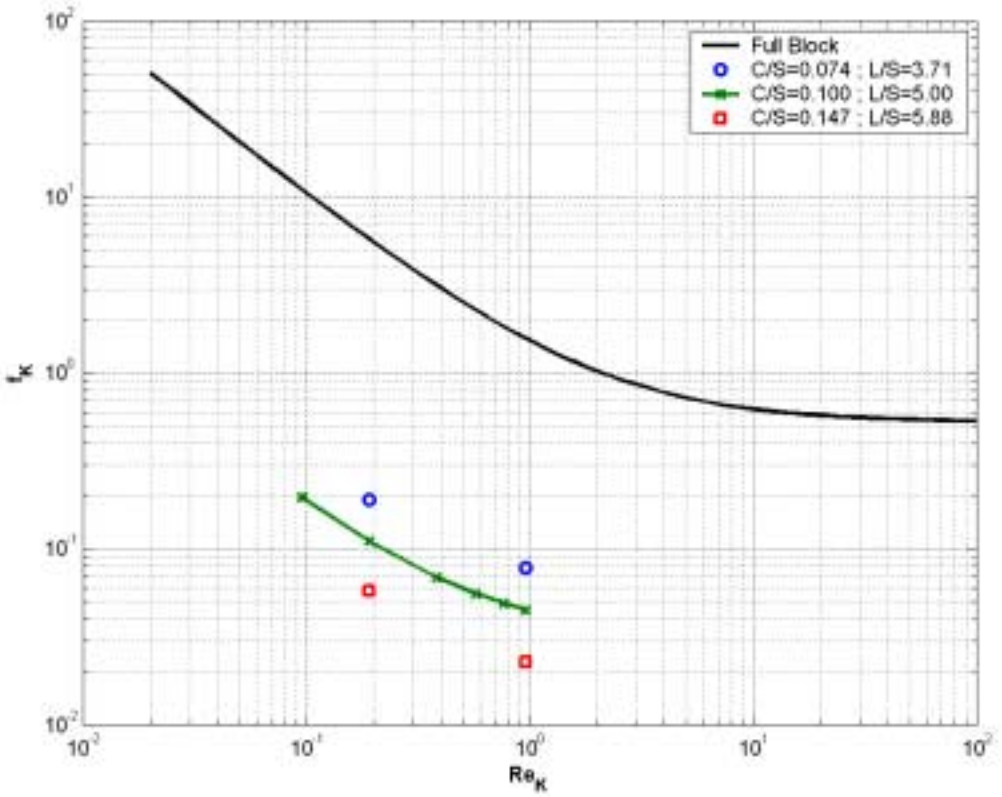

Figure 6.9. Comparison of friction factors for optimal corrugated geometries to an uncorrugated (full) block of graphite foam.

friction factors based on the 3D STAR-CD® calculations for corrugated graphite foam heat exchangers are compared to those for an uncorrugated, or full block, of graphite foam. By corrugating, the friction factors for the cases investigated were reduced to approximately 1/35 to 1/50 of those for a full block, which is a significant reduction.

6.2.3 3D Temperature Distributions

Three-dimensional plots of temperature for a CHUC are shown in Figure 6.10 for the cases of $Re_K^* = 0.1$ (a) and $Re_K^* = 0.5$ (b) for L=0.05m, C/S=0.100, L/S=5.00. It should be pointed out that the temperature scales for these figures were selected to show the details of the first 20 K of temperature rise, and all temperatures higher than that are

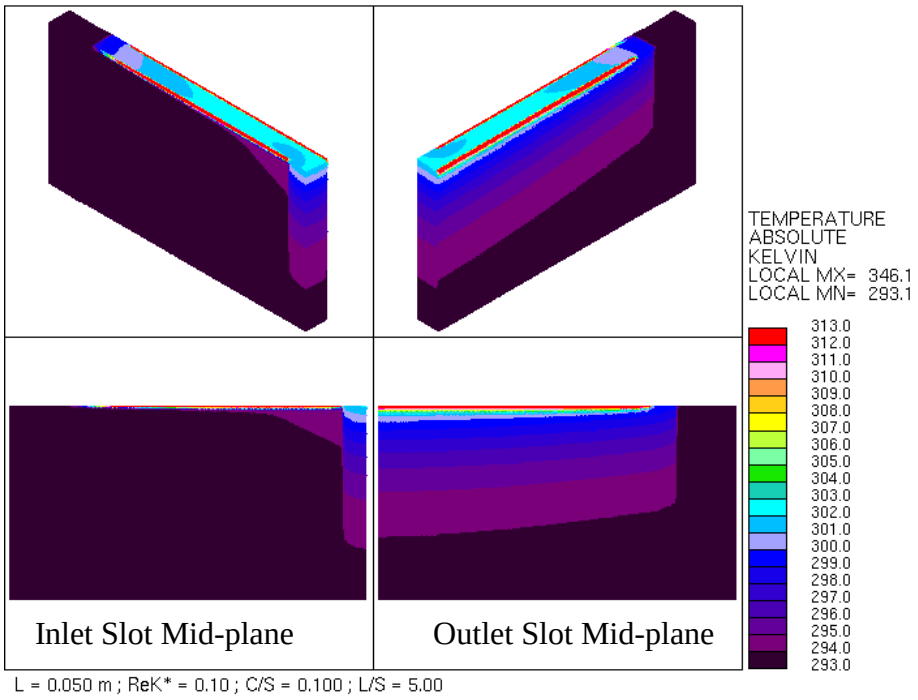

(a)

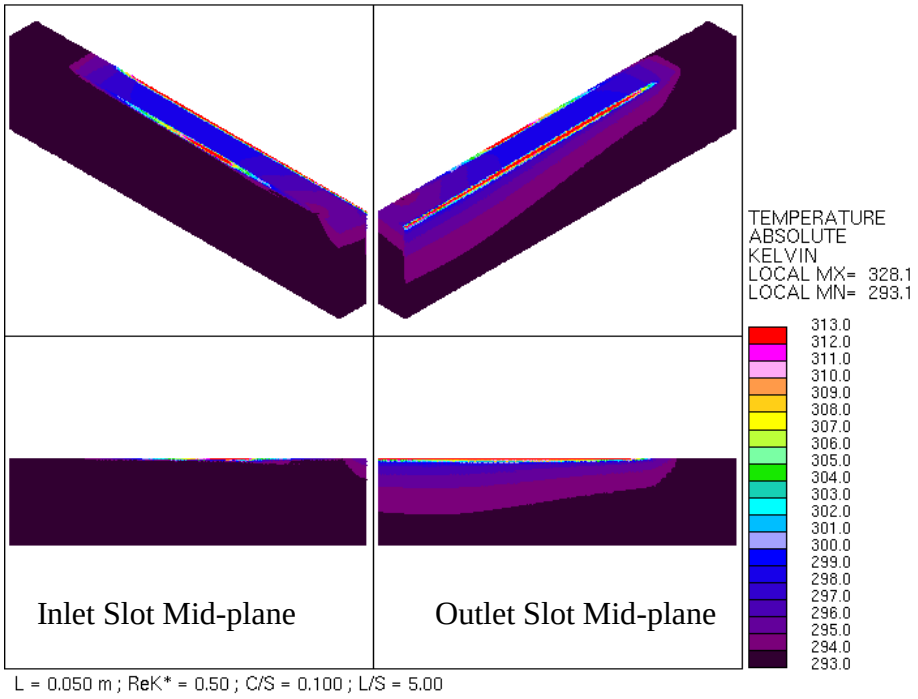

(b)

Figure 6.10. Three-dimensional temperature contours for L=0.05m, C/S=0.100, L/S=5.00, Re_K^* =0.10 (a) and Re_K^* =0.50 (b).

embedded in the red zone. However, the numerical value of the maximum temperature of the heated surface is shown above the color scale.

As shown in Figure 6.10 (a), for the fluid in the inlet slot, very little heat penetration occurs until the fluid enters the trailing foam section. In other words, the incoming cold fluid gets heated very little. In subsequent flow through the foam, the temperature penetration in the height direction is much more significant. This is clearly attributable to the high thermal conductivity of the matrix, which is roughly 300 times that of the fluid. In addition, *hot spots* occur along the inlet slot, where only fluid comes directly in contact with the heat source. These hot spots are relatively worse for lower Reynolds number flow, as can be seen by comparing Figures 6.10 (a) and (b).

The temperatures in the porous region in contact with the heat source are on average significantly lower than those in the slots. The outlet slot contains the *peak* temperatures in each model. The temperature contours in the outlet slot reveal that the fluid gains a substantial amount of heat as it passes through the foam, and it enters the outlet slot at elevated temperatures. Further, the hot fluid region that is directly in contact with the heated surface is also subjected to the constant heat flux boundary condition as it flows through the outlet slot, resulting in the highest temperatures. For these reasons, in general, the outlet channel temperatures are higher than those in the inlet channel, as can be seen in Figure 6.10(b). Although not obvious due to the temperature scales used, the same effect is also present in Figure 6.10 (a).

6.2.4 Heat Transfer Results

Until now, results have been based on a length scale equal to the porous media Reynolds number. To compare performance results of the present study to those of

conventional compact heat exchangers, the hydraulic diameter of the CHUC is used as the length scale. In Figure 6.11, Nusselt number was plotted as a function of Re_{Dh} for the selected cases of L=0.05 m, and C/S=0.074, L/S=3.71; C/S=0.100, L/S=5.00; and C/S=0.147, L/S=5.88. The case of C/S=0.100, L/S=5.00 was simulated at additional Reynolds numbers in order to determine performance at intermediate flowrates. This figure shows that heat transfer coefficients, represented by the Nusselt numbers, are increased with increasing Reynolds number and decreasing C/S values. Recall that lower C/S values represent higher relative values of contact area between the foam and the heat source, resulting in higher heat transfer. In addition, lower C/S values result in narrower regions of hot spots in both inlet and outlet slots. In general, a heat spreader or bonding material used to mount the foam heat exchanger to its heat source will tend to reduce the peak temperatures and the regions of hot spots by conjugate conduction.

A traditional form of presenting compact heat exchanger performance is used in Figure 6.12, which shows the variation of j_H and f as a function of Re_{Dh} for the same configurations as above. Lower C/S values result in higher j_H, but the friction factors are correspondingly higher. In other words, with the higher heat transfer rates come higher pumping power requirements. Typically, for compact heat exchangers used in the automotive industry, friction factors are approximately 3 to 5 times higher than j_H (Cowell and Achaichia, 1997). For corrugated graphite foam heat exchangers, the friction factors are two orders of magnitude higher than j_H factors, which is quite substantial.

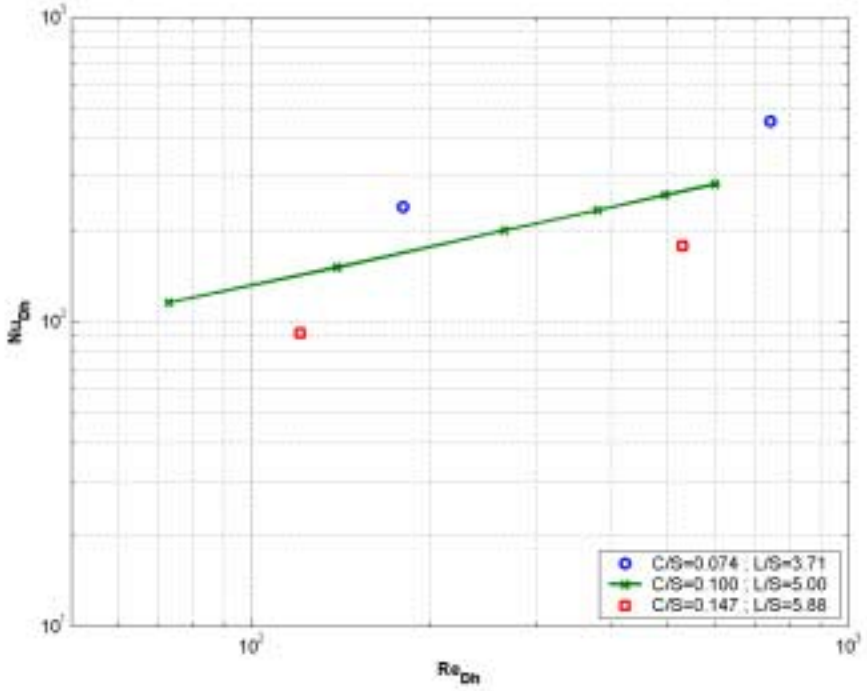

Figure 6.11. Nusselt number as a function of Reynolds number for optimal cases.

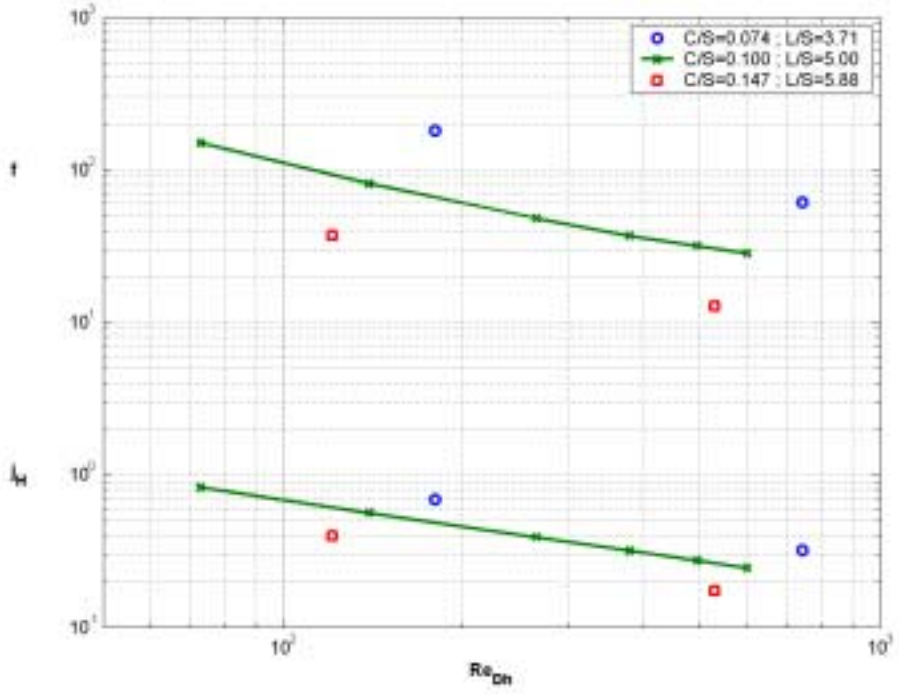

Figure 6.12. Colburn-j and friction factor as a function of Reynolds number for optimal cases.

Traditional methods also present compact heat exchanger performance in the form of j_H versus f plots. In Figure 6.13, the results of the present study are compared with typical automotive heat exchangers, as reported by Cowell and Achaichia (1997) and with Reynolds analogy. The automotive values plotted represent a variety of state-of-the-art heat exchange surfaces developed and improved over 30 years. It can be seen that the heat transfer performance of corrugated graphite foam heat exchangers is an order of magnitude higher than that of conventional compact heat exchangers in the automotive industry. As a matter of fact, the j_H values represent a new realm of heat transfer performance. However, the pumping power requirements are also quite substantial.

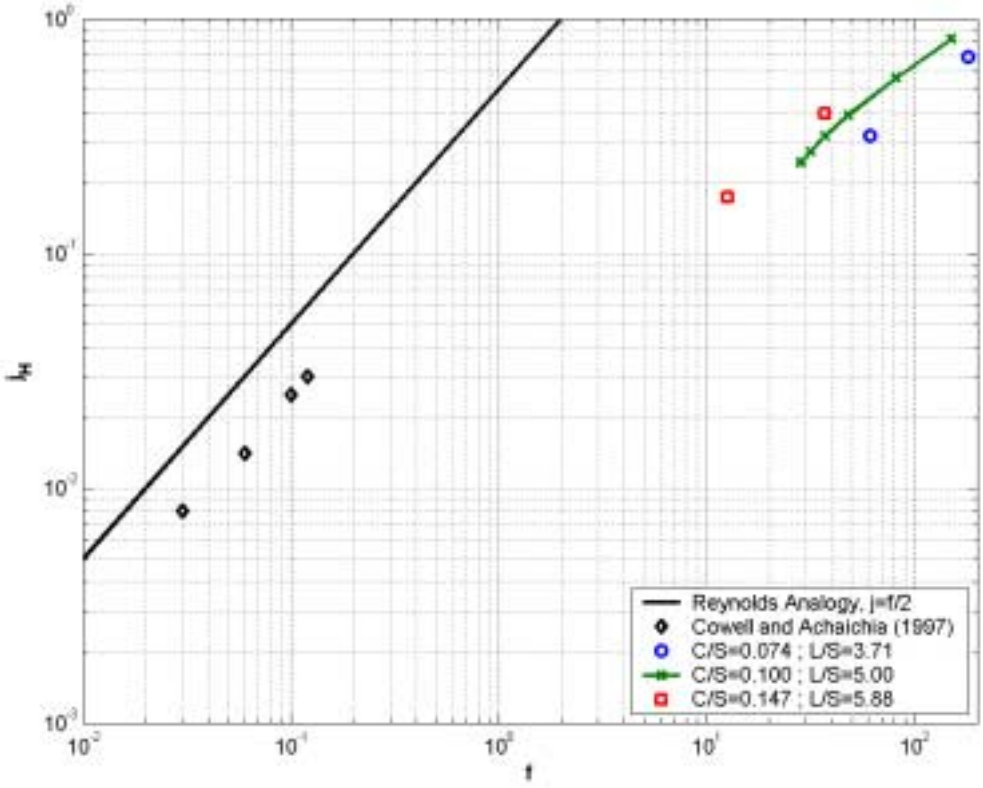

Figure 6.13. Colburn-j vs. friction factor for optimal cases.

Chapter 7

Conclusions and Recommendations

7.1 Conclusions

An extensive parametric study for two-dimensional pressure-drop was conducted that showed that certain configurations of a corrugated graphite foam heat exchanger can be selected as optimal cases in which the pressure-drop is reduced by nearly two orders of magnitude when compared to a full graphite foam block. These optimal cases are characterized by relatively uniform flow in the transverse direction across the foam. Flow uniformity was found to be severely reduced by slot widths that are too long and narrow and by flowrates that are too high. The configurations that yield the highest heat transfer coefficients contain a relatively large fraction of contact area between the foam and the heated surface. In addition, the heater surface regions that are in direct contact with the fluid contain hot spots that are detrimental in applications such as power electronics.

The heat transfer results for the optimal configurations showed that Colburn-j factors that are an order of magnitude higher than those for conventional compact heat exchangers are achievable. The friction factors, however, are higher by two orders of magnitude relative to those of the same heat exchangers.

7.2 Recommendations

Based on the results of this study, it is recommended that

1. while some experimental data is available, more experimental research be conducted in the area of graphite foam property determination (specifically, permeability, form coefficient, and effective conductivity) to validate the existing computational models and to establish the full range of possible graphite foam properties;
2. the entrance to the inlet slot be rounded to reduce the entrance loss associated with the sharp corners of the present model;
3. the slots not be cut the full distance of foam height, such that fluid does not come in direct contact (without going through foam) with the heated surface;
4. further investigation be conducted regarding the conjugate heat transfer problem that includes a layer of solid material that distributes the heat in the plane perpendicular to the direction if the heat flux.

References

Amiri, A. and Vafai, K. (1994), "Analysis of Dispersion Effects and Non-thermal Equilibrium, Non-Darcian, Variable Porosity Incompressible Flow Through Porous Media," *International Journal of Heat and Mass Transfer*, Vol. 37, No. 6, pp. 939-954.

Angirasa, D. (2002), “Forced Convective Heat Transfer in Metallic Fibrous Materials,” *Journal of Heat Transfer*, Vol. 124, pp. 739-745.

Bartlett, R. F. and Viskanta, R. (1996), "Enhancement of Forced Convection in an Asymmetrically Heated Duct Filled With High Thermal Conductivity Porous Media," *Journal of Enhanced Heat Transfer*, Vol. 3, No. 4, pp. 291-299.

Beavers, G. S. and Sparrow, E.M. (1969), "Non-Darcy Flow Through Fibrous Porous Media," *ASME Journal of Applied Mechanics*, Vol. 36, pp. 711-714.

Brinkman, H. C. (1947), “A Calculation of the Viscous Force Exerted by a Flowing Fluid on a Dense Swarm of Particles,” *Applied Scientific Research*, Vol. A1, pp.27-34.

Calmidi, V. V. Mahajan, R. L. (2000), "Forced Convection in High Porosity Metal Foams," *Journal of Heat Transfer*, Vol. 122, pp. 557-565.

Cowell, T, and Achaichia, N. (1997), “Compact Heat Exchangers in the Automobile Industry,” *Proceedings of the International Conference on Compact Heat Exchangers for the Process Industries*, Snowbird, pp. 11-28.

Ergun, S. (1952), “Fluid Flow Through Packed Columns,” *Chemical Engineering Progress*, Vol. 48, No. 2, pp. 89-94.

FEMLAB® User’s Guide, v2.3, (2002).

Gallego, N. and Klett, J. (2003), “Carbon Foams for Thermal Management,” *Carbon*, Vol. 41, pp. 1461-1466.

Gresho, P. M. and Sani, R. L. (1998), *Incompressible Flow and the Finite Element Method*, John Wiley and Sons, Chichester.

Hadim, A (1994), "Forced Convection in a Porous Channel With Localized Heat Sources," *Journal of Heat Transfer*, Vol. 116, pp.465-472.

Handbook of Chemistry and Physics (1998), 69th Ed., CRC Press.

Hunt, M. L. and Tien, C. L. (1988), "Effects of Thermal Dispersion on Forced Convection in Fibrous Media," *International Journal of Heat and Mass Transfer*, Vol. 31, No. 2, pp. 301-309.

Hwang, G.-J. and Chao, C.-H. (1994), "Heat Transfer Measurement and Analysis for Sintered Porous Channels," *Journal of Heat Transfer*, Vol. 116, pp. 456-464.

Hwang, J.-J., Hwang, G.-J., Yeh, R.-H. and Chao, C.-H. (2002), "Measurement of Interstitial Convective Heat Transfer and Frictional Drag for Flow Across Metal Foams," *Journal of Heat Transfer*, Vol. 124, pp. 120-129.

Jones, W. P. (1980), "Models for Turbulent Flows with Variable Density and Combustion," *Prediction Methods for Turbulent Flows*, Ed. Kollman W., Hemisphere, Washington.

Kaviany, M. (1985), "Laminar Flow Through a Porous Channel Bounded by Isothermal Parallel Plates," *International Journal of Heat and Mass Transfer*, Vol. 28, No. 4, pp. 851-858.

Kaviany, M. (1995), *Principles of Heat Transfer in Porous Media*, Springer-Verlag, New York.

Kaviany, M. (1987), "Boundary Layer Treatment of Forced Convection Heat Transfer From a Semi-Infinite Flat Plate Embedded in Porous Media," *Journal of Heat Transfer*, Vol. 109, pp. 345-349.

Kays, W. and London, A. (1984), *Compact Heat Exchangers*, 3rd Ed., McGraw-Hill, New York.

Kim, S. J. and Jang, S. P. (2002), "Effects of the Darcy Number, the Prandtl Number, and the Reynolds Number on Local Thermal Non-Equilibrium," *International Journal of Heat and Mass Transfer*, Vol. 45, pp. 3885-3896.

Kim, S. Y., Kang, B. H. and Kim, J.-H. (2001), "Forced Convection from Aluminum Foam Materials in an Asymmetrically Heated Channel," *International Journal of Heat and Mass Transfer*, Vol. 44, pp.1451-1454.

Kim, S. Y., Paek, J. W. and Kang, B. H. (2000), "Flow and Heat Transfer Correlations for a Porous Fin in a Plate-Fin Heat Exchanger," *Journal of Heat Transfer*, Vol. 122, pp.572-578.

Klett, J. (2000), "Process For Making Carbon Foam," *United States Patent and Trademark Office*, Patent No. 6,033,506, www.uspto.com.

Klett, J., Hardy, R., Romine, E., Walls, C. and Burchell, T. (2000), "High-Thermal-Conductivity, Mesophase-Pitch-Derived Carbon Foams: Effect of Precursor on Structure and Properties," *Carbon*, Vol. 38, pp. 953-973.

Koh, J. C. Y. and Colony, R. (1974), "Analysis of Cooling Effectiveness for Porous Material in a Coolant Passage," *Journal of Heat Transfer*, Vol. 96, pp. 324-330.

Lage, J. L. (1998), "The Fundamental Theory of Flow Through Permeable Media From Darcy to Turbulence," *Transport Phenomena in Porous Media* (eds. D. B. Ingham and I. Pop), pp.1-30, Pergamon, Oxford.

Munson, B., Young, D., and Okiishi, T. (1998), *Fundamentals of Fluid Mechanics*, Third Ed., John Wiley and Sons, New York.

Muskat, M. (1937), *Flow of Homogeneous Fluids Through Porous Media*, McGraw-Hill, New York.

Nield, D. A. (2002), "Modelling Fluid Flow in Saturated Porous Media and at Interfaces," *Transport Phenomena in Porous Media* (eds. D. B. Ingham and I. Pop), pp.1-19, Pergamon, Oxford.

Nield, D. A. and Bejan A. (1999), *Convection in Porous Media*, Second Ed., Springer, New York.

Osgood, S. J. (2001), *Heat Transfer in Carbon Foam*, Thesis, Rensselaer Polytechnic Institute.

Philipse, A. P. and Schram, H. L. (1991), "Non-Darcian Airflow through Ceramic Foams," *Journal of American Ceramic Society*, Vol. 74, No. 4, pp. 728-732.

Poulikakos, D. and Renken, K. (1987), “Forced Convection in a Channel Filled With Porous Medium, Including the effects of Flow Inertia, Variable Porosity, and Brinkman Friction,” *Journal of Heat Transfer*, Vol. 109, pp. 880-888.

Scheidegger, A. E. (1974), *The Physics of Flow Through Porous Media*, Third Ed., University of Toronto Press, Toronto.

Schumann, T. E. W. (1929), “Heat Transfer: A Liquid Flowing Through a Porous Prism,” *Journal of the Franklin Institute*, Vol. 208, pp. 405-416.

STAR-CD® Methodology, v3.15, (2001).

Tee, C. C. (2000), *Modeling of Thermal Conductivity and Pressure Drop, and Thermal/Mechanical Testing of Carbon Foam-Based Materials*, Thesis, University of Tennessee, Knoxville.

Vafai, K. and Amiri, A. (1998), "Non-Darcian Effects in Confined Forced Convective Flows," *Transport Phenomena in Porous Media* (eds. D. B. Ingham and I. Pop), pp. 313-329, Pergamon, Oxford.

Vafai, K. and Kim, S. J. (1989), "Forced Convection in a Channel Filled With a Porous Medium: An Exact Solution," *Journal of Heat Transfer*, Vol. 111, pp.1103-1106.

Vafai, K. and Kim, S. J. (1990), “Fluid Mechanics of an Interface Region Between a Porous Medium and a Fluid Layer – An Exact Solution," *International Journal of Heat and Mass Transfer*, Vol. 11, pp. 254-256.

Vafai, K. and Sozen, M. (1990), "Analysis of Energy and Momentum Transport for Fluid Flow Through a Porous Bed," *Journal of Heat Transfer*, Vol. 122, pp. 690-699.

Vafai, K. and Tien, C. L. (1981), "Boundary and Inertia Effects on Flow and Heat Transfer in Porous Media," *International Journal of Heat and Mass Transfer*, Vol. 24, pp. 195-203.

Ward, J. C. (1964), "Turbulent Flow in Porous Media," *Journal of the Hydraulics Division (ASCE)*, Vol. 90, pp. 1-12.

Warsi, Z. U. A. (1981), "Conservations Form of the Navier-Stokes Equations in General Nonsteady Coordinates," *AIAA Journal*, Vol. 19, No. 2, pp. 240-242.

Younis L. B. and Viskanta R. (1993), "Experimental Determination of the Volumetric Heat Transfer Coefficient between Stream of Air and Ceramic Foam," *International Journal of Heat and Mass Transfer*, Vol. 36, No. 6, pp. 1425-1434.

Appendices

Appendix A

Influence of grid refinement and tolerance on the accuracy of STAR-CD® models

A study was conducted to determine the influence of grid refinement and tolerance on the accuracy of STAR-CD® models. For this study, flow and heat transfer through a full block of porous medium was modeled using the same thermophysical properties as used for all the corrugated models. From an initial uniform fine mesh (1:1:1), the mesh was refined by doubling the number of nodes in the flow and the heat transfer directions (2:2:1) and then the mesh was further refined by tripling from the initial uniform mesh (3:3:1). For each of these meshed cases, three solutions with tolerances of 10^{-3}, 10^{-5}, 10^{-7} were obtained. The resulting temperature distributions are shown in the following figure. The percent error values in overall energy balances are shown in table to follow.

With a tolerances of 10^{-3}, for all three meshes, the temperature distributions indicate abnormal thermal boundary growth in the flow direction and the percent error in overall energy balances is unacceptably high. With a tolerances of 10^{-5}, the (1:1:1) and (2:2:1) meshes indicate normal thermal boundary growth and the percent error in overall energy balances although reduced is still high, and abnormal thermal boundary growth is indicated by the (3:3:1) mesh with an increased error in overall energy balance. However, with a tolerance of 10^{-7}, all three meshes indicate normal thermal boundary growth in the flow direction and with less than 0.15 percent overall energy balance error. Based on this study, a tolerance value of 10^{-7} was used in all reported corrugated simulations.

Mesh Refinement

Tolerance	1:1:1	2:2:1	3:3:1
10^{-3}	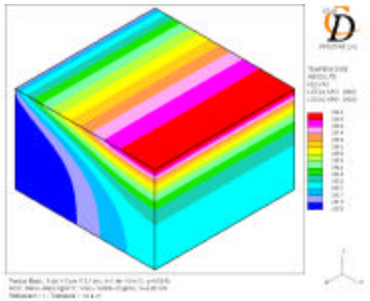	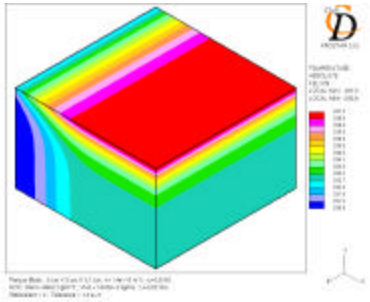	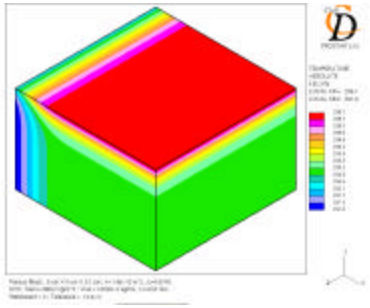
10^{-5}	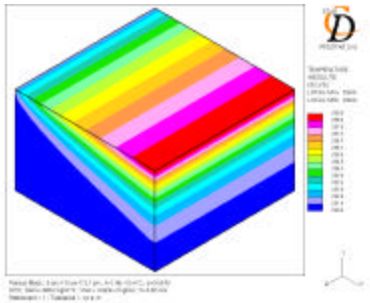	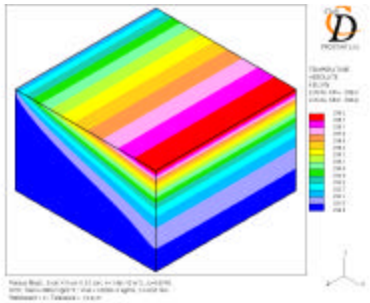	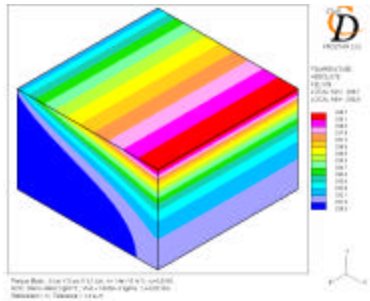
10^{-7}	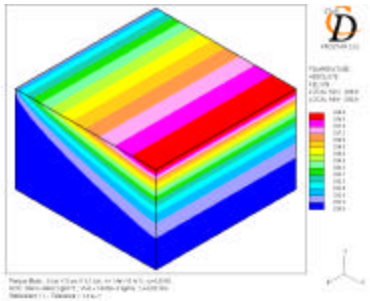	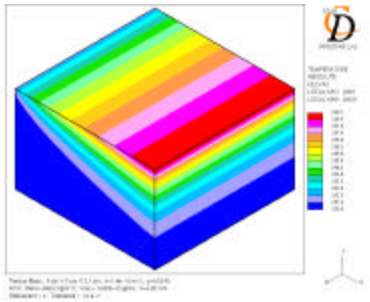	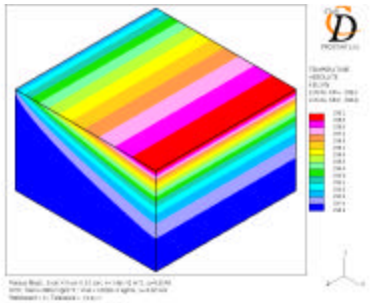

Percent Error on Energy Balance

Tolerance	Mesh Refinement 1:1:1	2:2:1	3:3:1
10^{-3}	47.51	17.70	4.97
10^{-5}	4.23	13.77	29.78
10^{-7}	0.08	0.11	0.15

Appendix B

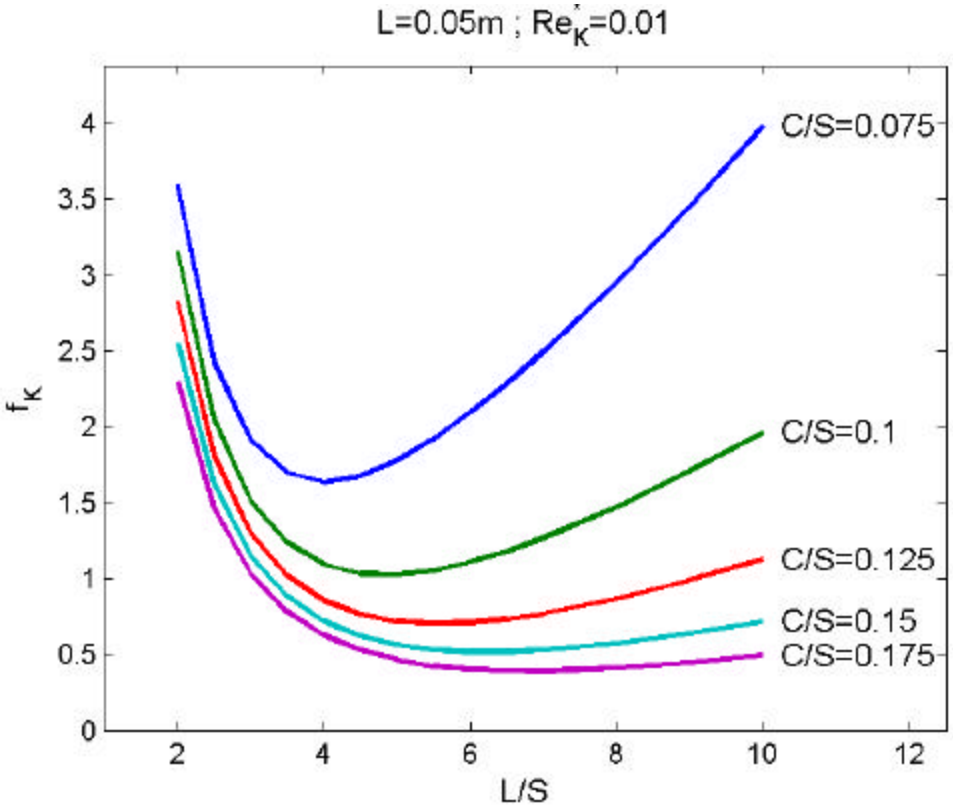
L=0.05m ; Re*K=0.01
C/S=0.075
C/S=0.1
C/S=0.125
C/S=0.15
C/S=0.175
fK
L/S
0
0.5
1
1.5
2
2.5
3
3.5
4
2
4
6
8
10
12

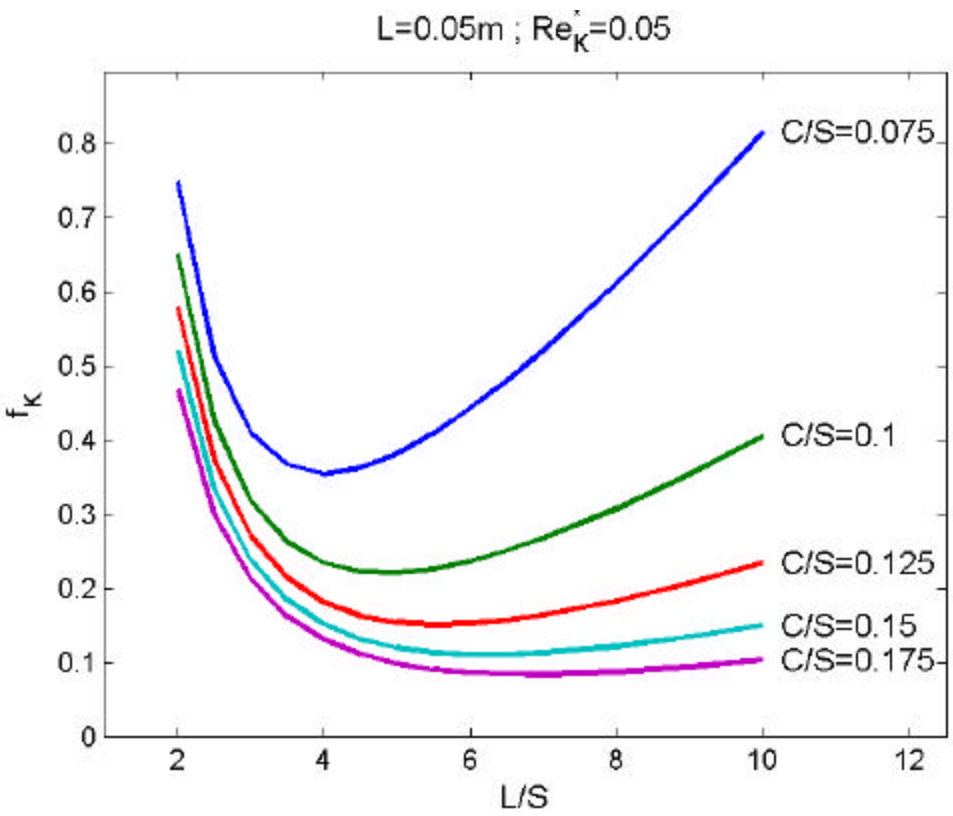
L=0.05m ; Re*K=0.05
C/S=0.075
C/S=0.1
C/S=0.125
C/S=0.15
C/S=0.175
fK
L/S
0
0.1
0.2
0.3
0.4
0.5
0.6
0.7
0.8
2
4
6
8
10
12

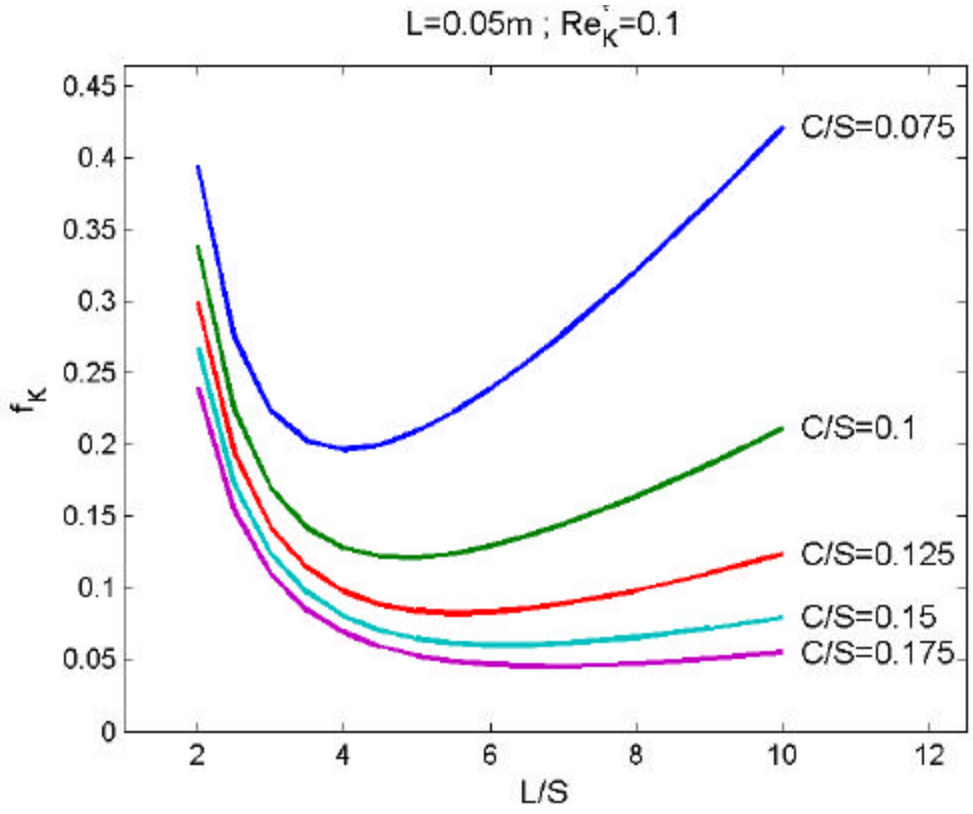
L=0.05m ; Re_K^*=0.1
0.45
0.4
0.35
0.3
0.25
0.2
0.15
0.1
0.05
0
f_K
2
4
6
8
10
12
L/S
C/S=0.075
C/S=0.1
C/S=0.125
C/S=0.15
C/S=0.175

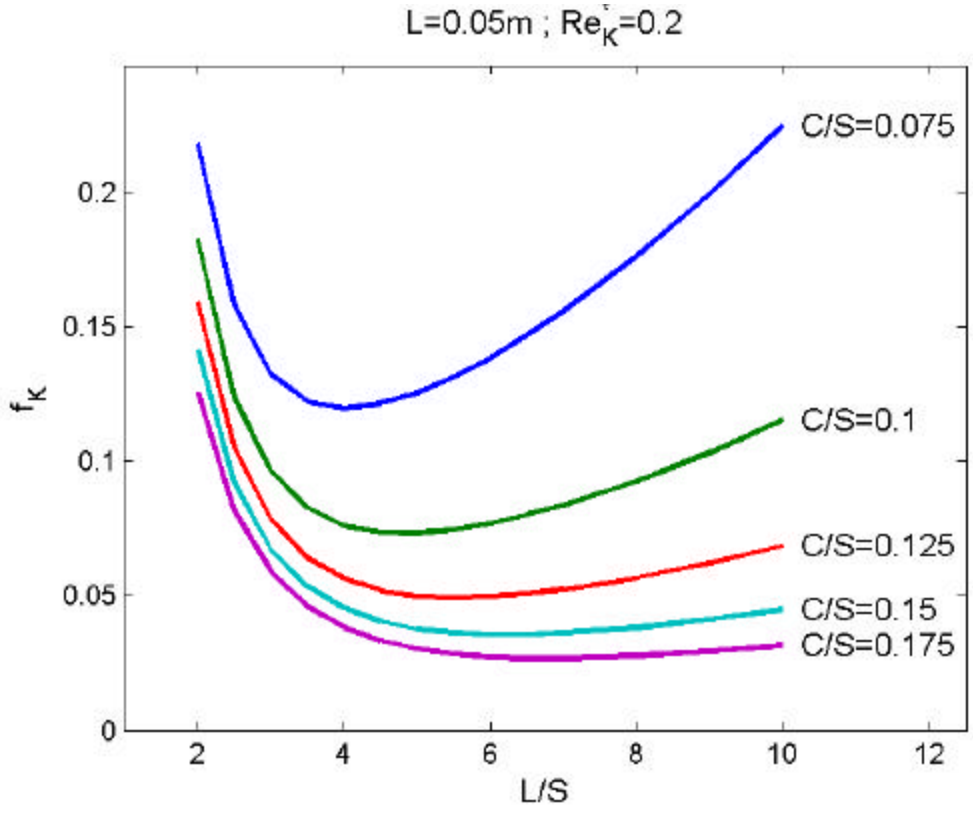
L=0.05m ; Re_K^*=0.2
0.2
0.15
0.1
0.05
0
f_K
2
4
6
8
10
12
L/S
C/S=0.075
C/S=0.1
C/S=0.125
C/S=0.15
C/S=0.175

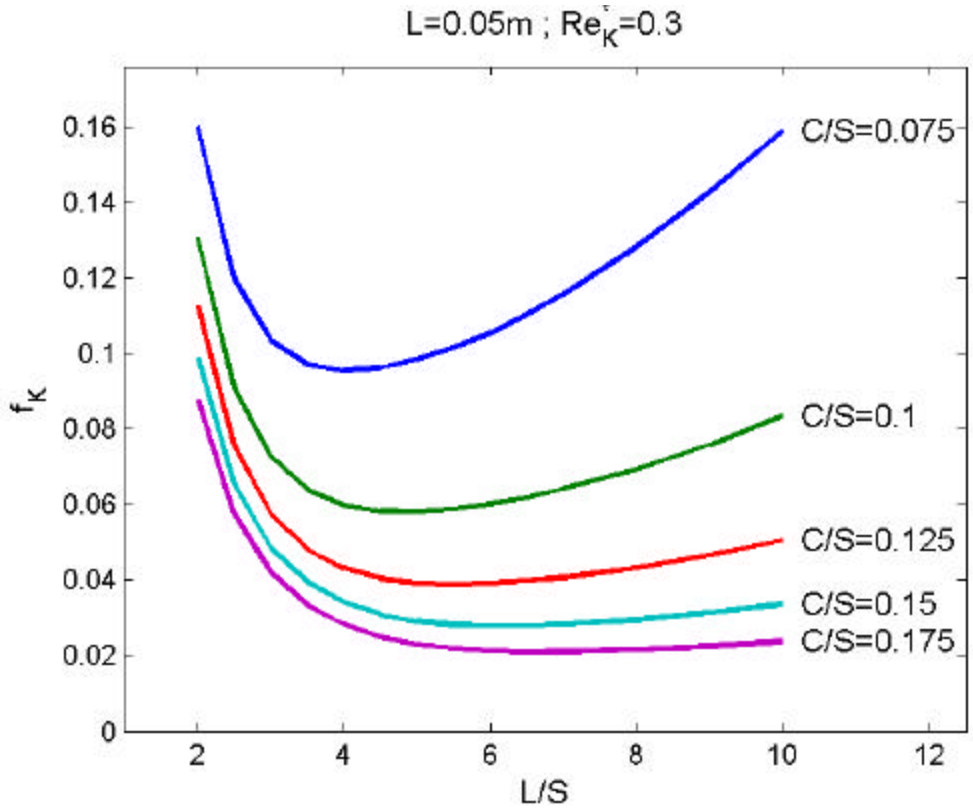
L=0.05m ; Re_K^*=0.3
f_K
L/S
C/S=0.075
C/S=0.1
C/S=0.125
C/S=0.15
C/S=0.175
0
0.02
0.04
0.06
0.08
0.1
0.12
0.14
0.16
2
4
6
8
10
12

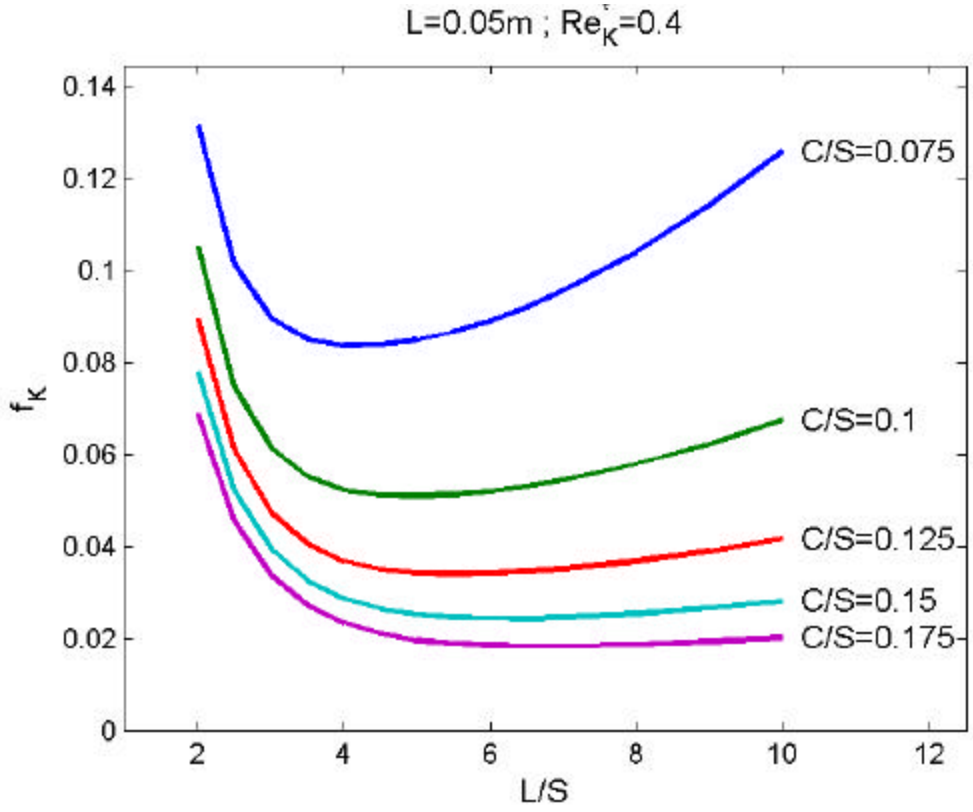
L=0.05m ; Re_K^*=0.4
f_K
L/S
C/S=0.075
C/S=0.1
C/S=0.125
C/S=0.15
C/S=0.175
0
0.02
0.04
0.06
0.08
0.1
0.12
0.14
2
4
6
8
10
12

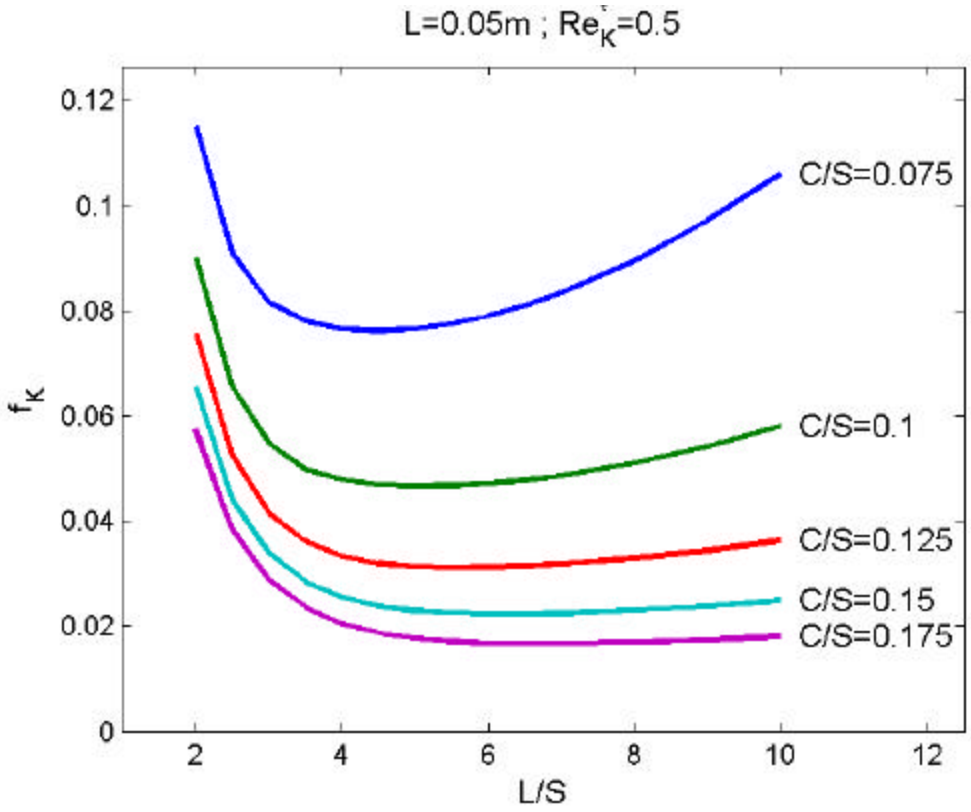
L=0.05m ; Re*K=0.5
0.12
0.1
0.08
0.06
0.04
0.02
0
fK
2
4
6
8
10
12
L/S
C/S=0.075
C/S=0.1
C/S=0.125
C/S=0.15
C/S=0.175

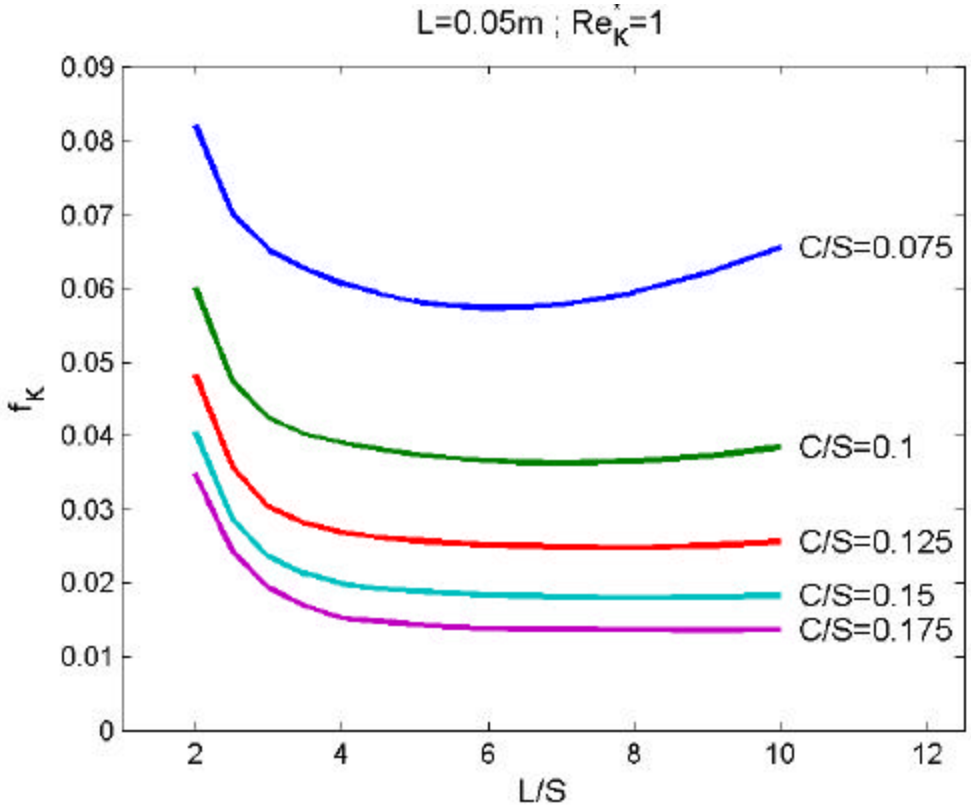
L=0.05m ; Re*K=1
0.09
0.08
0.07
0.06
0.05
0.04
0.03
0.02
0.01
0
fK
2
4
6
8
10
12
L/S
C/S=0.075
C/S=0.1
C/S=0.125
C/S=0.15
C/S=0.175

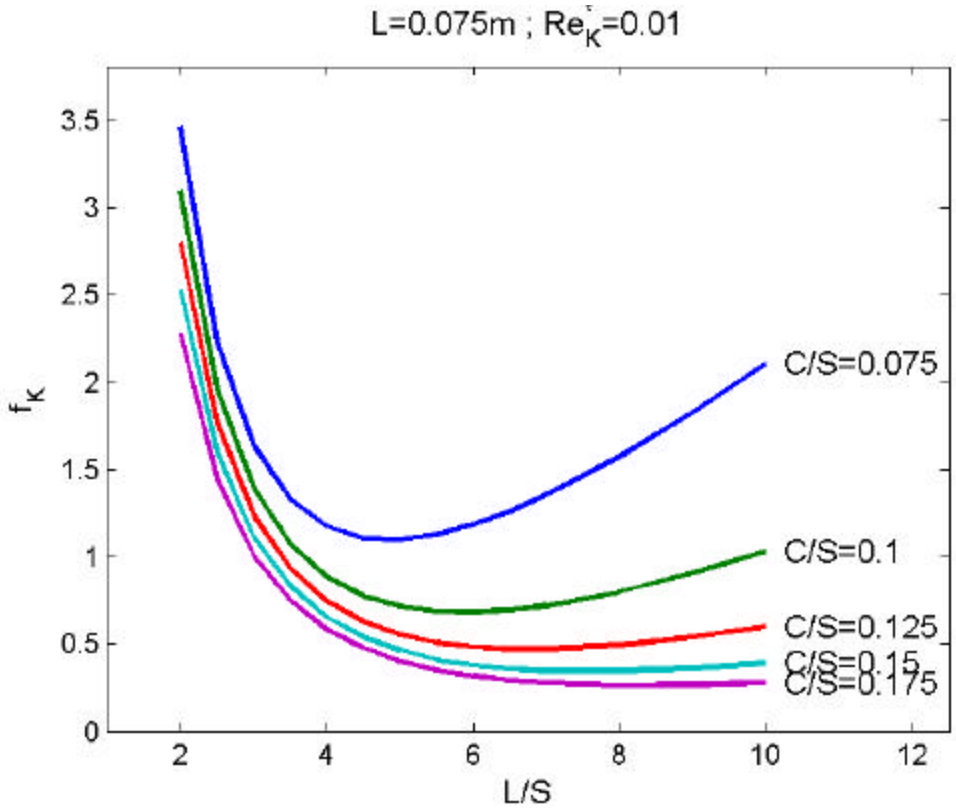
L=0.075m ; Re_K^*=0.01
f_K
L/S
C/S=0.075
C/S=0.1
C/S=0.125
C/S=0.15
C/S=0.175

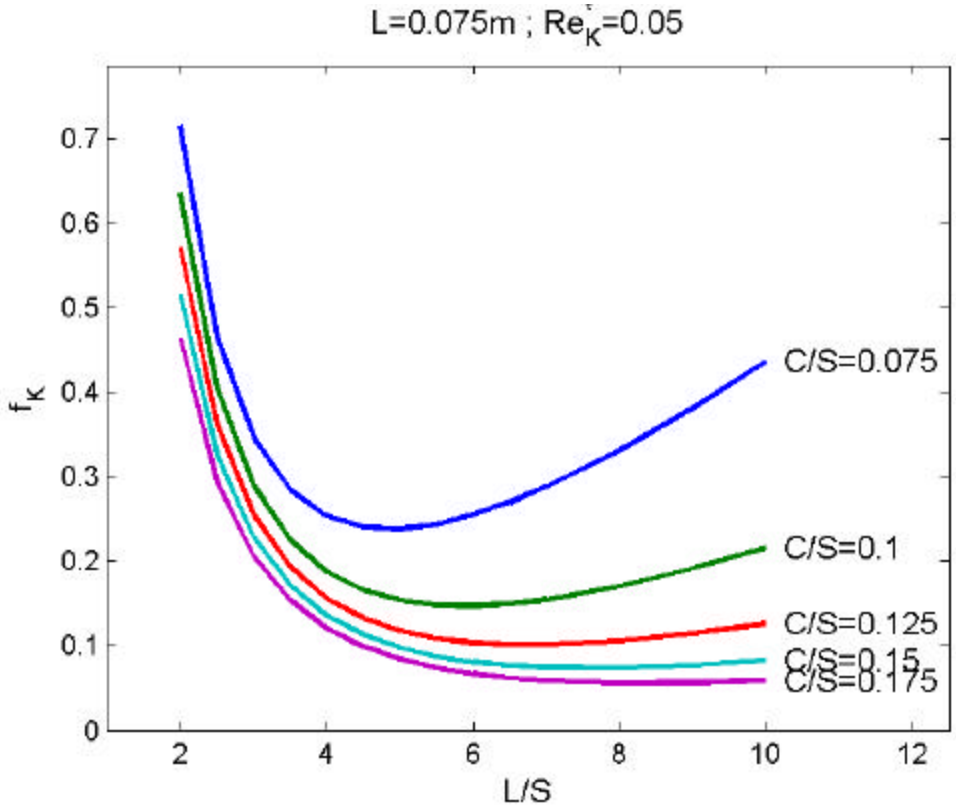
L=0.075m ; Re_K^*=0.05
f_K
L/S
C/S=0.075
C/S=0.1
C/S=0.125
C/S=0.15
C/S=0.175

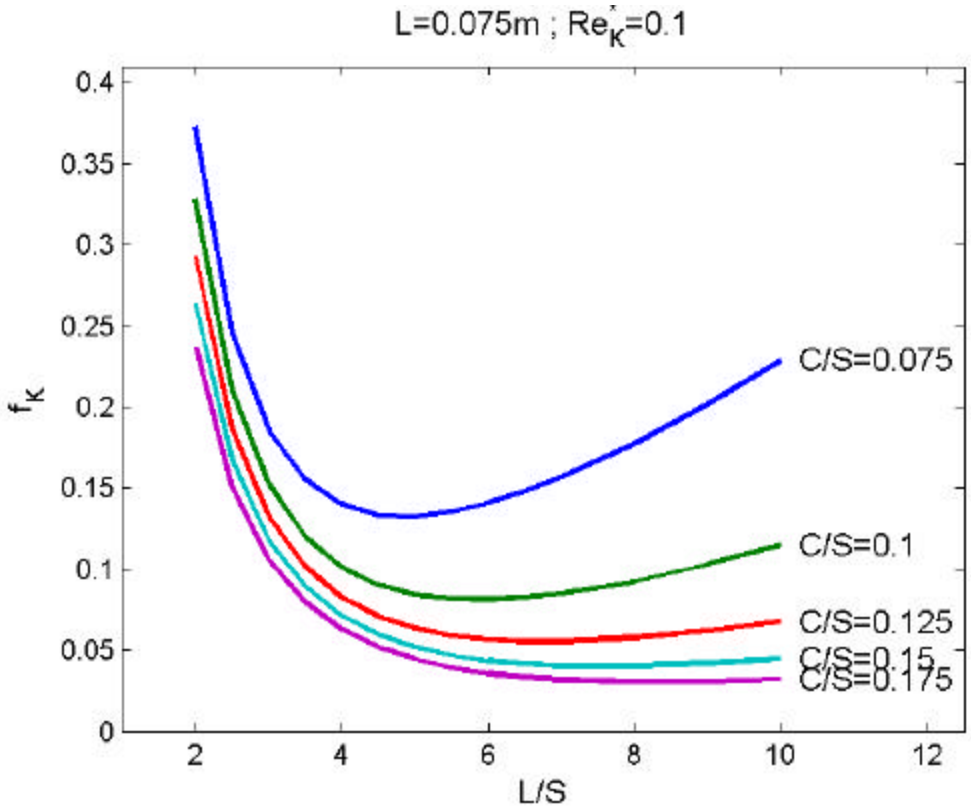
L=0.075m ; Re*K=0.1
fK
L/S
C/S=0.075
C/S=0.1
C/S=0.125
C/S=0.15
C/S=0.175

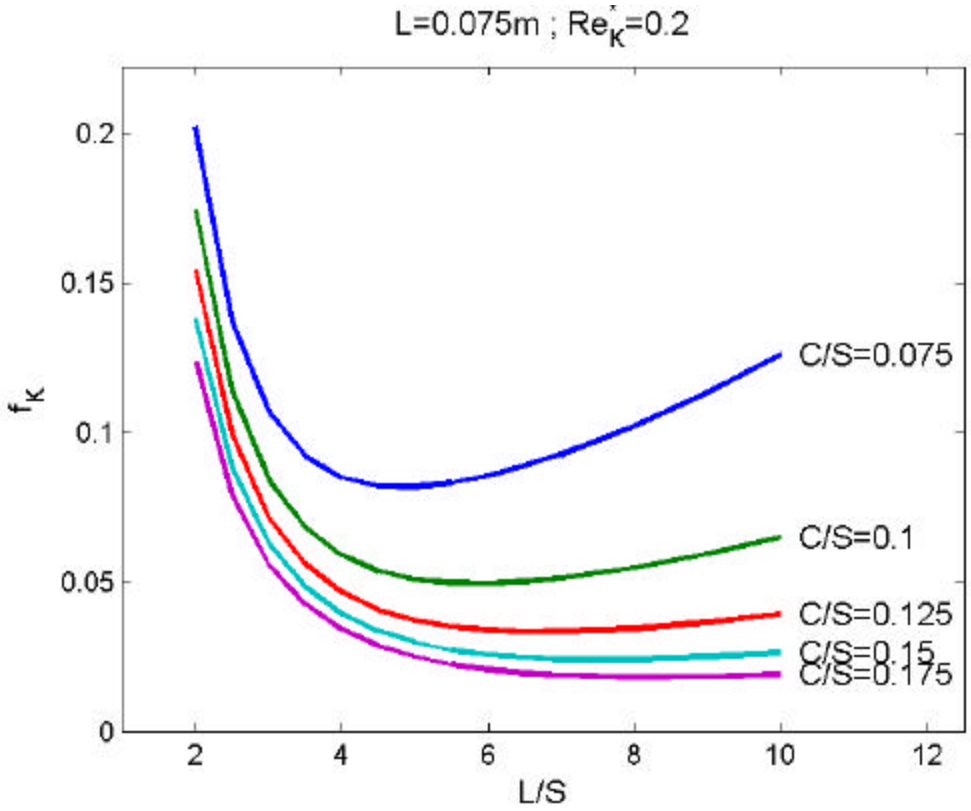
L=0.075m ; Re*K=0.2
fK
L/S
C/S=0.075
C/S=0.1
C/S=0.125
C/S=0.15
C/S=0.175

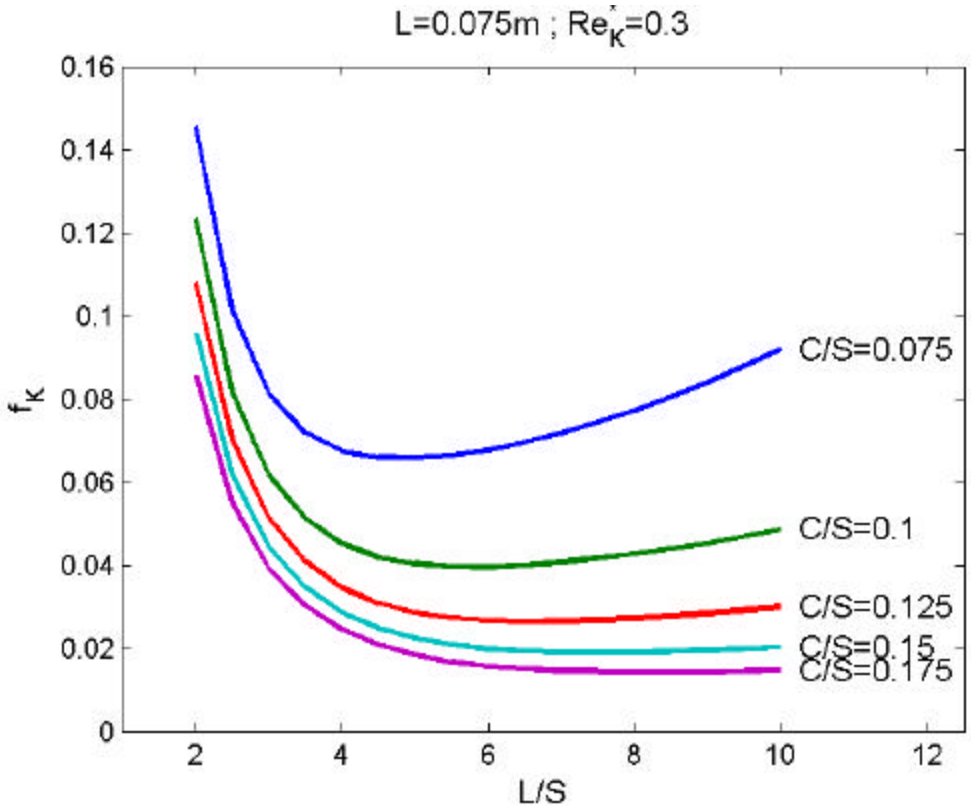
L=0.075m ; Re*K=0.3
fK
L/S
C/S=0.075
C/S=0.1
C/S=0.125
C/S=0.15
C/S=0.175

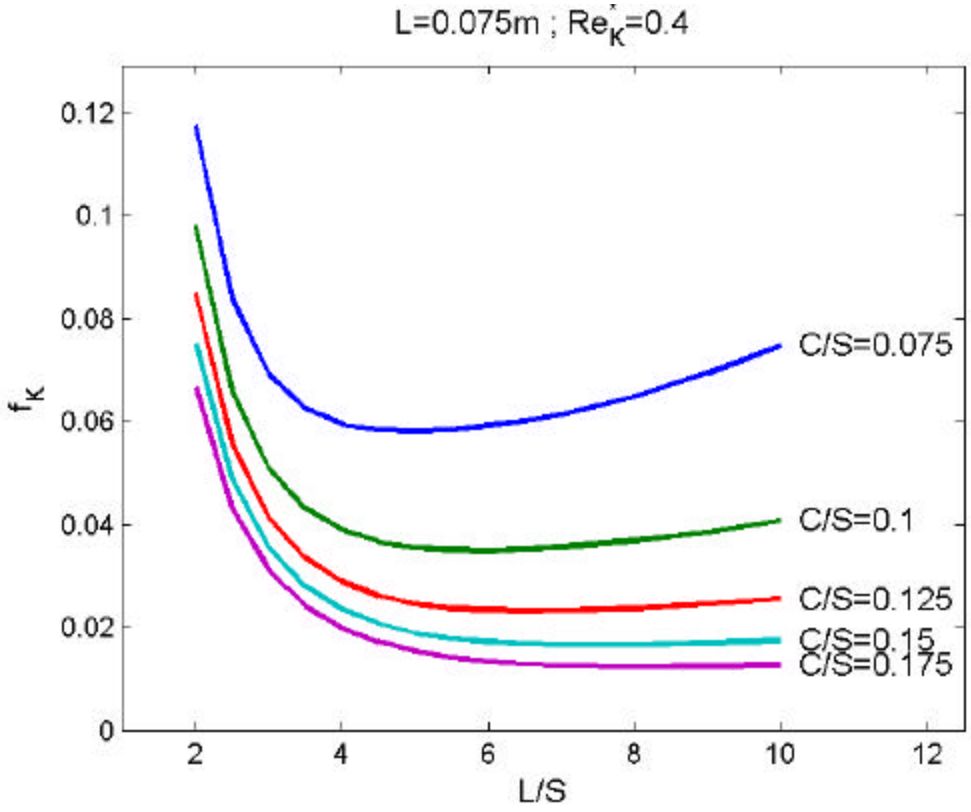
L=0.075m ; Re*K=0.4
fK
L/S
C/S=0.075
C/S=0.1
C/S=0.125
C/S=0.15
C/S=0.175

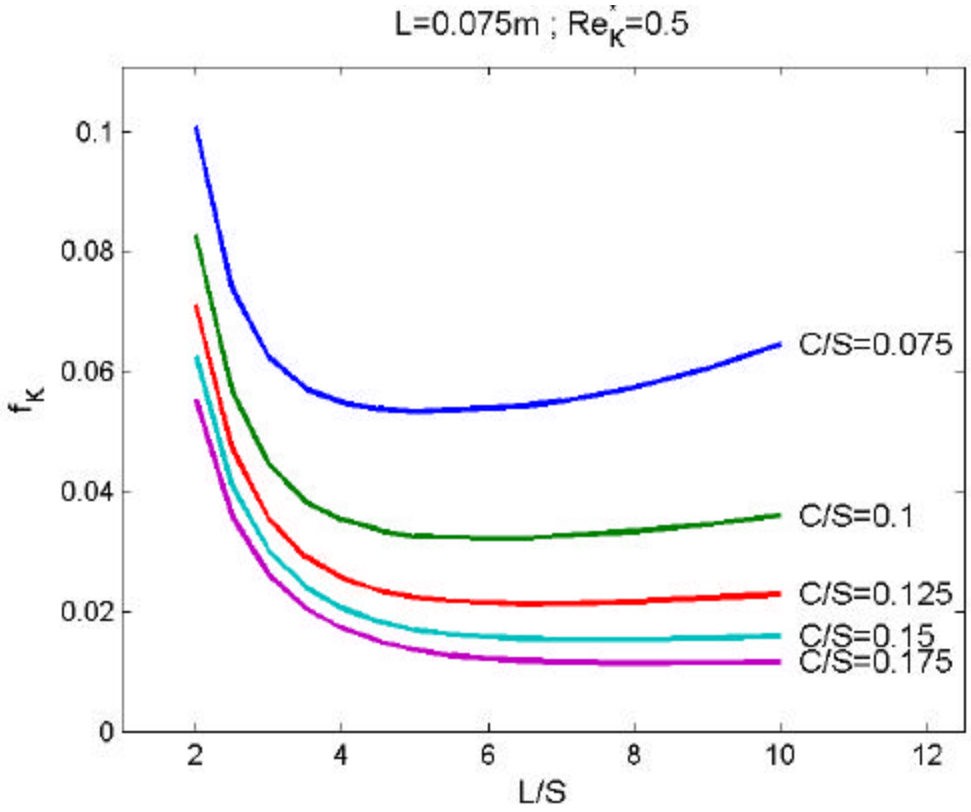
L=0.075m ; Re*K=0.5
fK
L/S
C/S=0.075
C/S=0.1
C/S=0.125
C/S=0.15
C/S=0.175
0
0.02
0.04
0.06
0.08
0.1
2
4
6
8
10
12

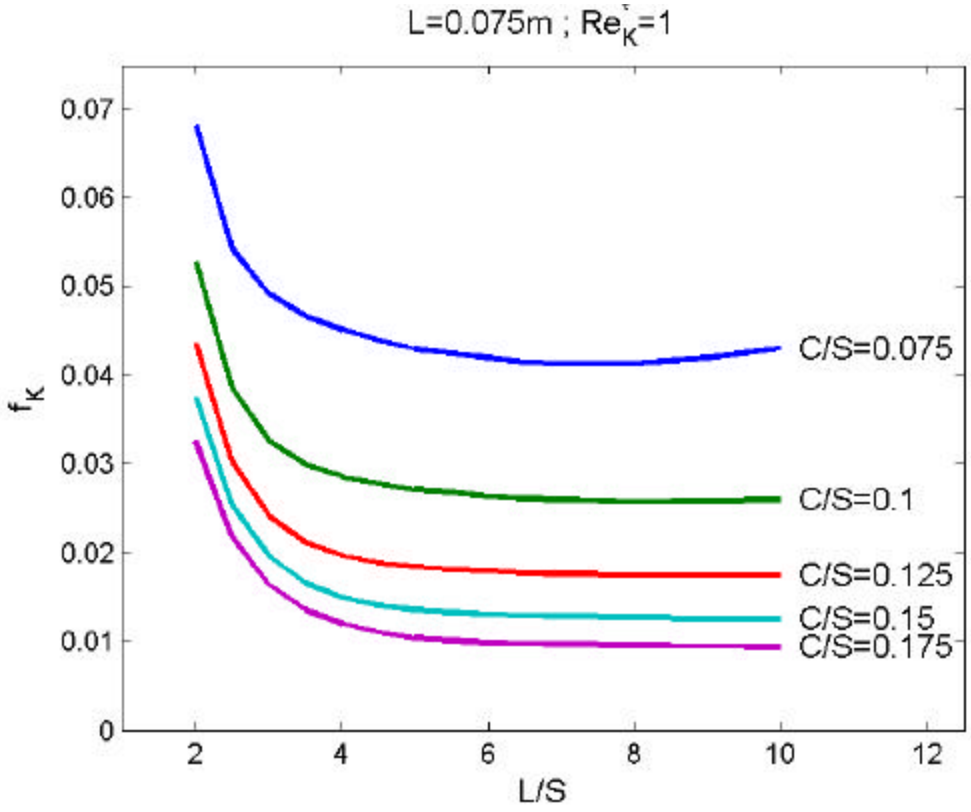
L=0.075m ; Re*K=1
fK
L/S
C/S=0.075
C/S=0.1
C/S=0.125
C/S=0.15
C/S=0.175
0
0.01
0.02
0.03
0.04
0.05
0.06
0.07
2
4
6
8
10
12

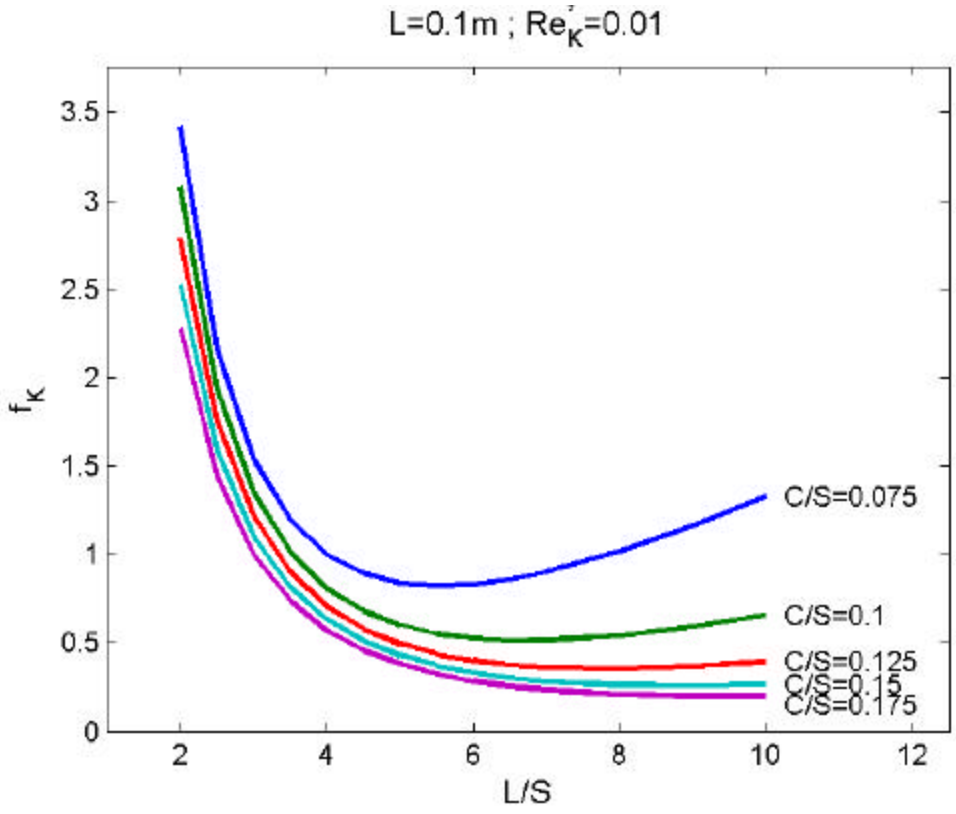
L=0.1m ; Re'K=0.01
fK
L/S
C/S=0.075
C/S=0.1
C/S=0.125
C/S=0.15
C/S=0.175

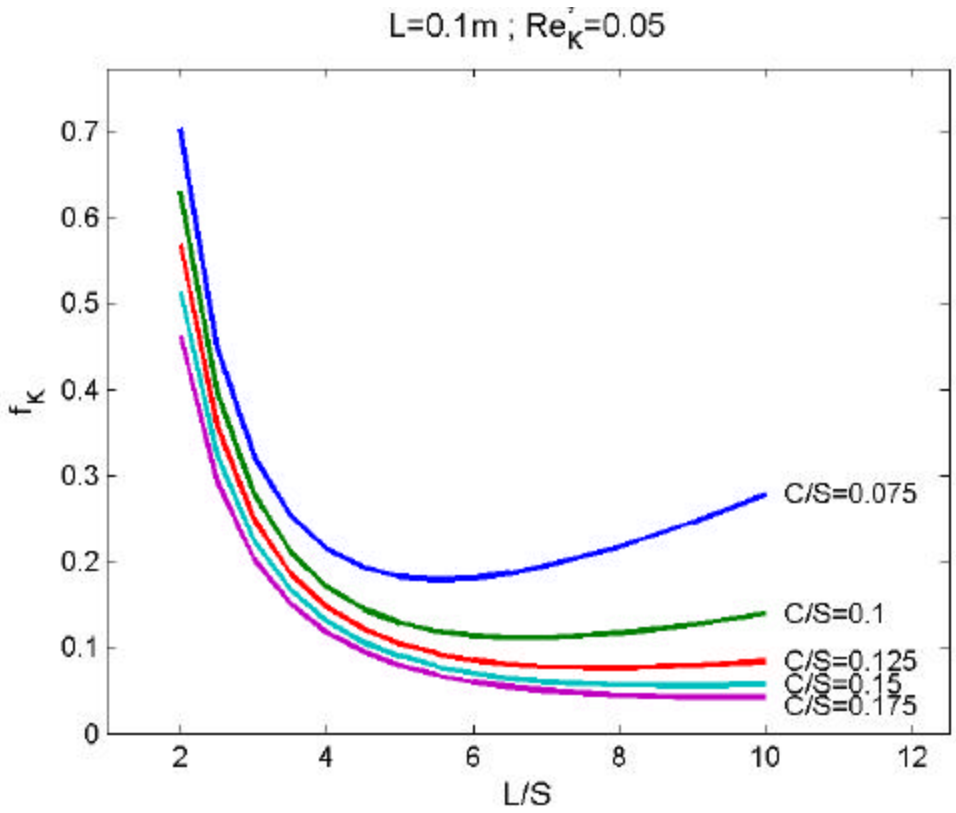
L=0.1m ; Re'K=0.05
fK
L/S
C/S=0.075
C/S=0.1
C/S=0.125
C/S=0.15
C/S=0.175

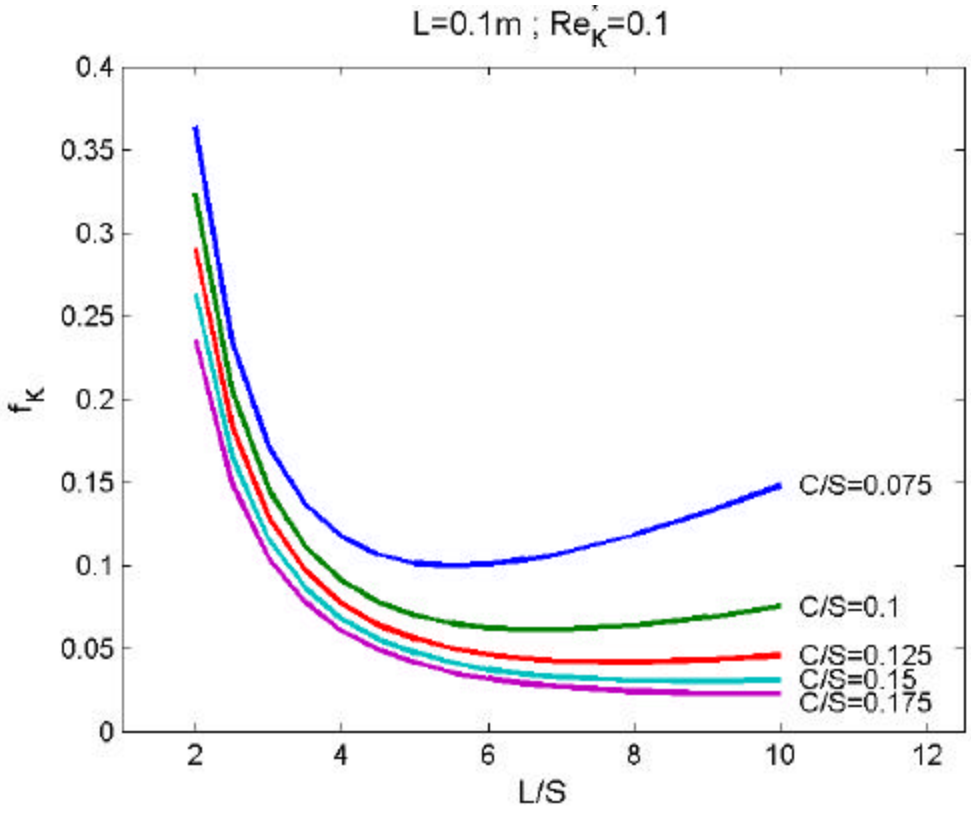
L=0.1m ; Re*K=0.1
fK
L/S
C/S=0.075
C/S=0.1
C/S=0.125
C/S=0.15
C/S=0.175

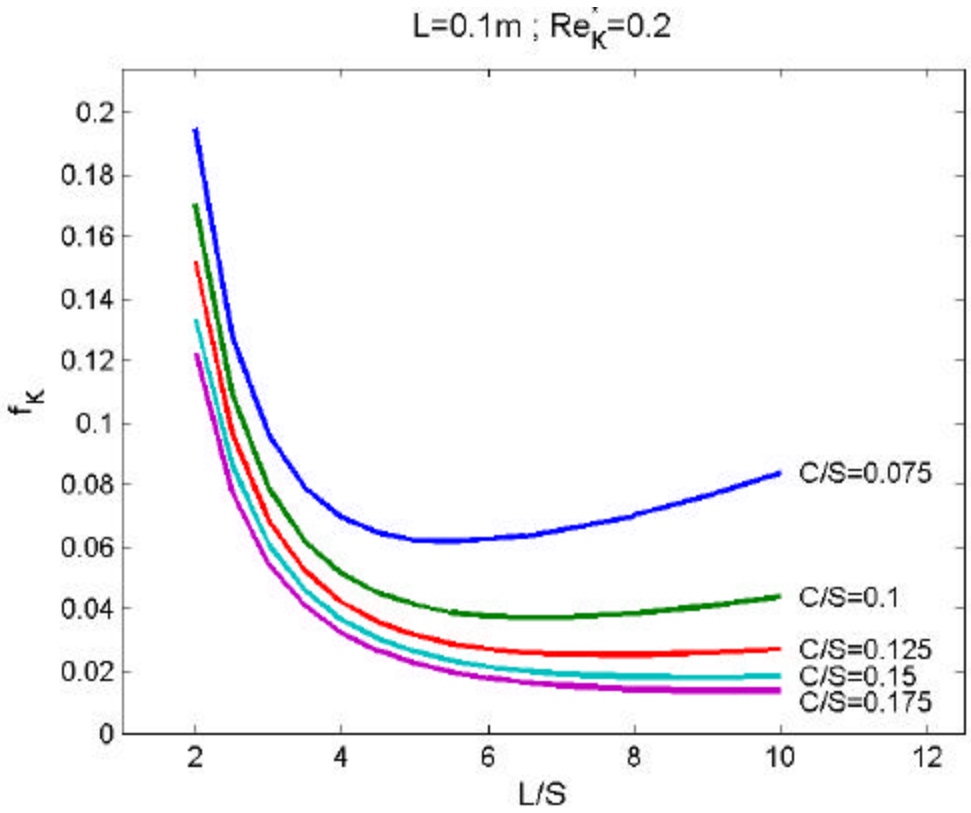
L=0.1m ; Re*K=0.2
fK
L/S
C/S=0.075
C/S=0.1
C/S=0.125
C/S=0.15
C/S=0.175

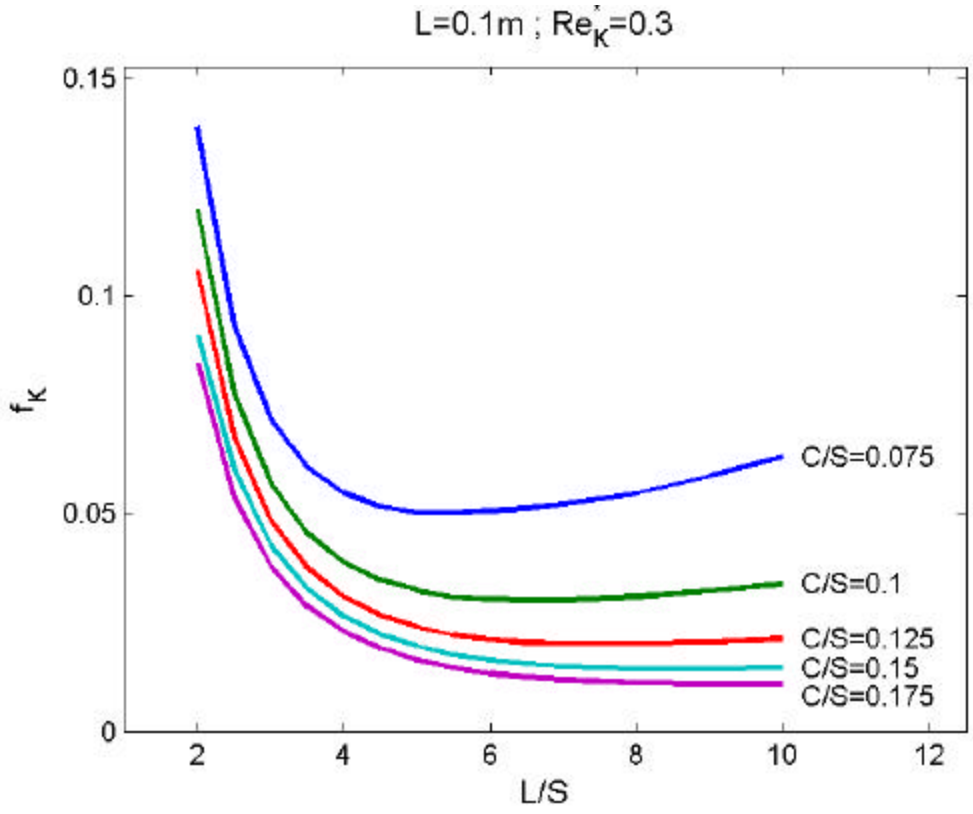
L=0.1m ; Re_K^*=0.3
0.15
0.1
0.05
0
f_K
2
4
6
8
10
12
L/S
C/S=0.075
C/S=0.1
C/S=0.125
C/S=0.15
C/S=0.175

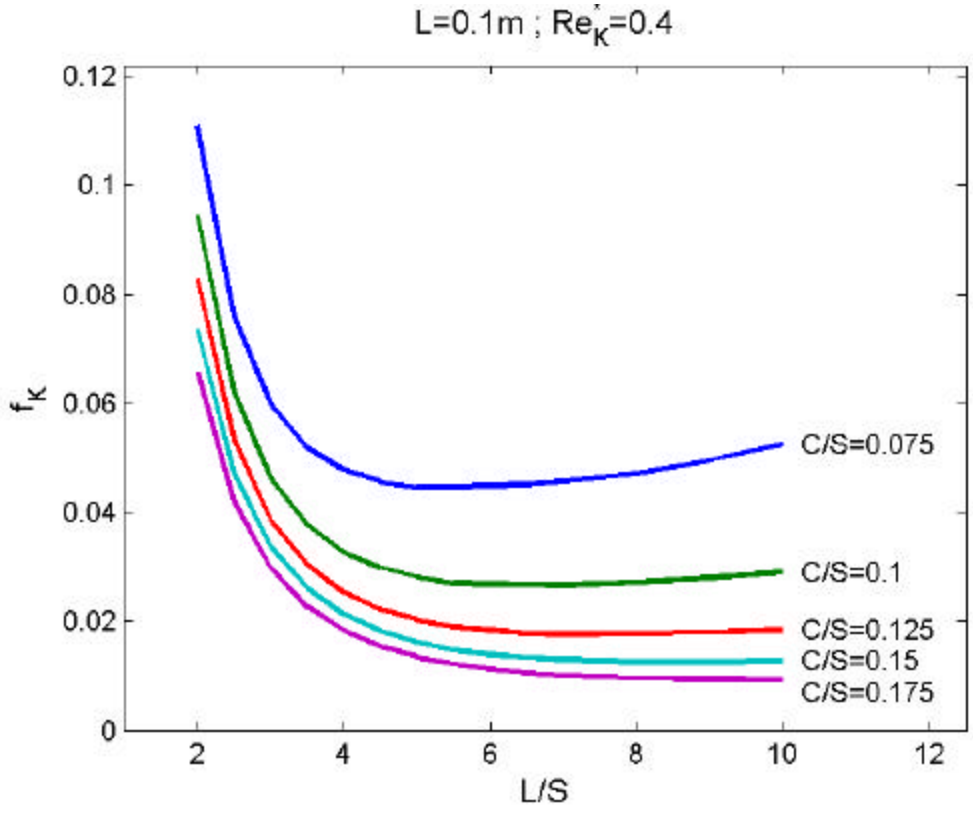
L=0.1m ; Re_K^*=0.4
0.12
0.1
0.08
0.06
0.04
0.02
0
f_K
2
4
6
8
10
12
L/S
C/S=0.075
C/S=0.1
C/S=0.125
C/S=0.15
C/S=0.175

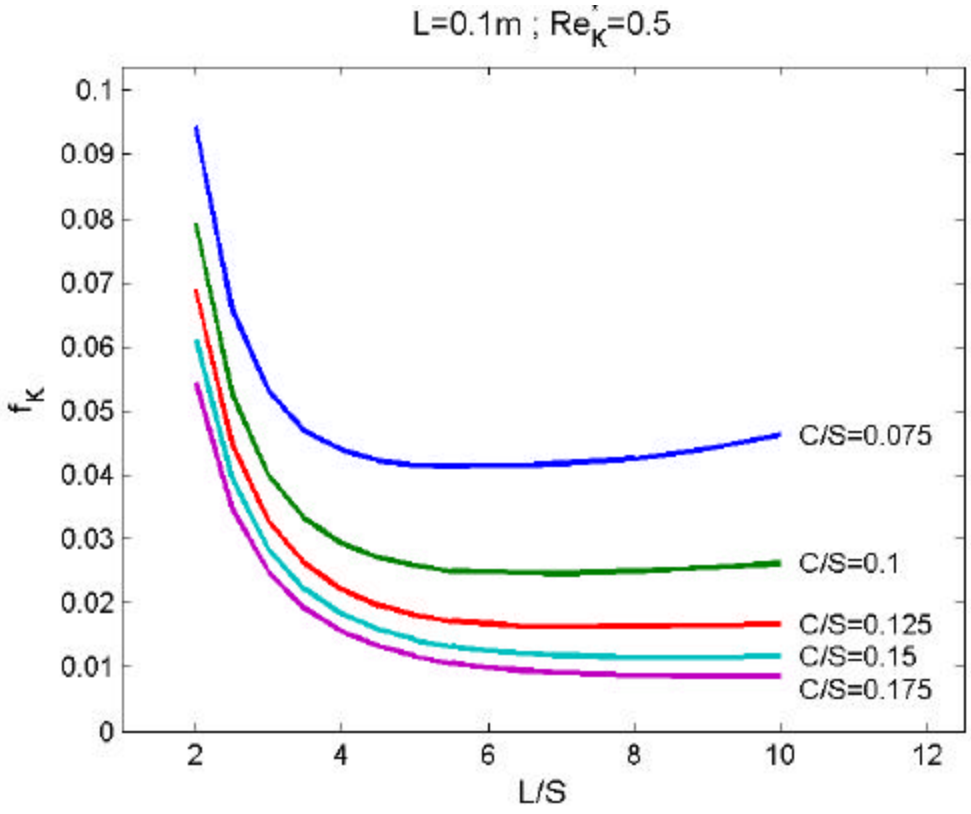
L=0.1m ; Re*K=0.5
fK
L/S
C/S=0.075
C/S=0.1
C/S=0.125
C/S=0.15
C/S=0.175

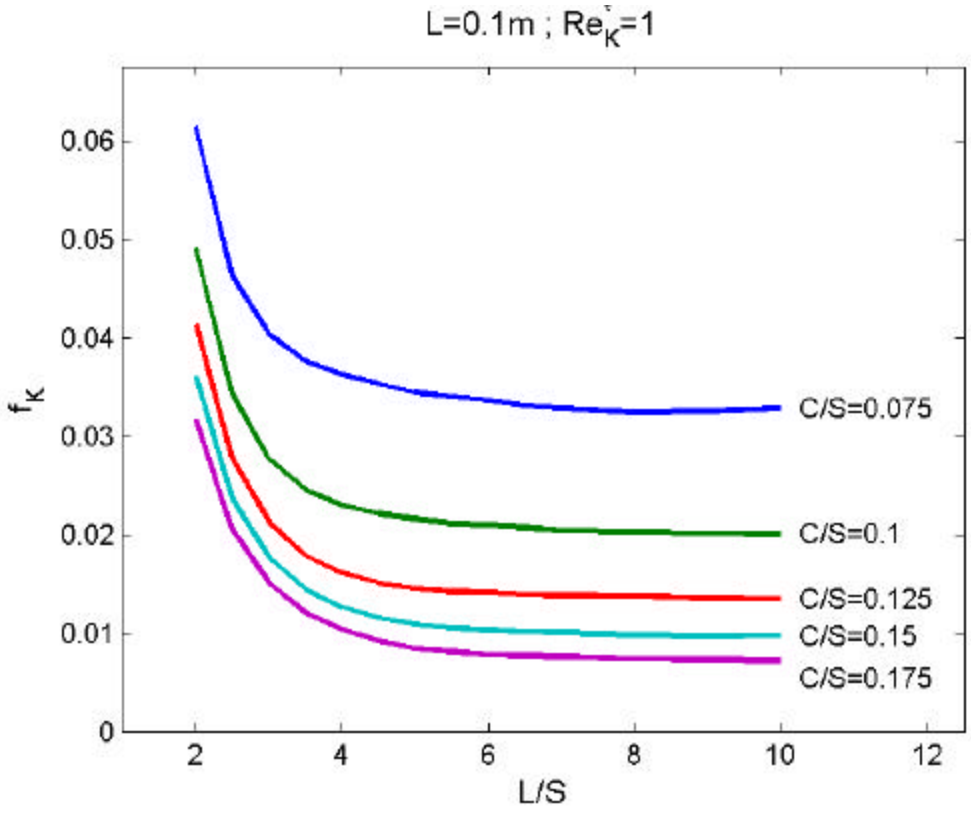
L=0.1m ; Re*K=1
fK
L/S
C/S=0.075
C/S=0.1
C/S=0.125
C/S=0.15
C/S=0.175

Vita

Timothy Henry Norton, Jr. was born in New Orleans, LA, on June 3, 1978 to Timothy Henry and Debra Dane Norton. He attended both Trinity Episcopal and Holy Name of Jesus elementary schools, and then he graduated from Jesuit High School in 1996. He then attended the University of Tennessee, Knoxville (UTK), where he received his Bachelor of Science in Mechanical Engineering in the fall of 2000. He then continued his education at UTK to pursue his Master of Science degree in Mechanical Engineering, which he will receive in the fall of 2003.